The role of nitric oxide controlling intracellular pathogen, a link between proliferation inhibition and permissive host cell recruitment

Thesis

for the degree of

doctor rerum naturalium
(Dr. rer. nat.)

Approved by the Faculty of Natural Sciences of Otto von Guericke University Magdeburg

by: M. Eng. Mohamad Alabdullah
born on 01.01.1986 in Damassuburb (Syria)

1. Examiner: Prof. Dr. Andreas Müller
2. Examiner: Prof. Dr. med. vet. Anca Dorhoi

submitted on: 25.04.2022, defended on 28.11.2022

Abstract

Nitric Oxide (NO), which is produced by the inducible NO synthase (iNOS), has a well-established antimicrobial effects mediated by multiple mechanisms, such as direct killing, or inhibition of pathogen growth. Besides these cellular defense function, NO can prevent unnecessary tissue damage by shutting down the recruitment of monocyte-derived phagocytes. Intracellular pathogens such as *Leishmania major* (*L. major*) can hijack these cells as a niche for replication. Thus, NO might contain intracellular pathogens by restricting the availability of the cellular niche required for efficient pathogen proliferation. Whether pathogen growth is directly inhibited by NO, or whether this is a consequence of the lack of proliferation-permissive host cells had however remained unclear.

In order to define the exact mode of action of NO on *L. major* containment, we fitted our experimental data on the course of infection with ordinary differential equation (ODE) models, which predicted that killing of the pathogen, and not immediate proliferation inhibition, is the dominant mechanism exerted directly by iNOS on the pathogen.

Using an *in vivo* proliferation reporter *L. major* strain, we were however able to show iNOS inhibition effect on the proliferation, which could be reversed by antibody-dependent blocking of monocyte recruitment. This shows that iNOS inhibition increases pathogen growth indirectly due to higher monocyte recruitment. Moreover, injection of monocytes to a site of infection, but not neutrophil recruitment, increased pathogen burden, indicating that depending on the phenotype of an inflammation, late-stage persistent infections with *L. major* can be reactivated through phagocyte recruitment. Therefore, NO fulfills two distinct functions for *L. major* containment: direct killing and restriction of a supply of proliferation-permissive host cells.

In a second part of the thesis, we investigated the time course of, and impact of iNOS inhibition on, the expression of coinhibitory receptors by effector and regulatory T cells populations.

Zusammenfassung

Stickstoffmonoxid (NO), das von der induzierbaren NO-Synthase (iNOS) produziert wird, hat eine antimikrobielle Wirkung, die durch mehrere Mechanismen vermittelt wird, beispielsweise durch direkte Abtötung oder Hemmung des Erregerwachstums. Neben dieser zellulären Abwehrfunktion kann NO unnötige Gewebeschäden verhindern, indem es die Rekrutierung von Monozyten an eine infektionsstelle hemmt. Intrazelluläre Krankheitserreger wie *Leishmania major* (*L. major*) können diese Zellen als Nische für ihre Vermehrung nutzen. NO könnte also intrazelluläre Pathogene eindämmen, indem es die Verfügbarkeit der zellulären Nische einschränkt, die für eine effiziente Pathogenvermehrung erforderlich ist. Ob das Wachstum von Pathogenen direkt durch NO gehemmt wird oder ob dies eine Folge der Reduktion von Wirtszellen ist, in denen *L. major* proliferieren kann, blieb jedoch unklar.

Um die genaue Wirkungsweise von NO bei der Kontrolle von *L. major* zu bestimmen, haben wir unsere experimentellen Daten zum Infektionsverlauf mit Differentialgleichungsmodellen abgeglichen, die vorhersagen, dass die Abtötung des Erregers und nicht die unmittelbare Proliferationshemmung der dominierende Mechanismus ist, der direkt von iNOS auf den Erreger ausgeübt wird.

Unter Verwendung eines in-vivo-Proliferationsreporterstammes von *L. major* konnten wir jedoch eine iNOS-hemmende Wirkung auf die Proliferation nachweisen, die durch eine antikörperabhängige Blockierung der Monozytenrekrutierung aufgehoben werden konnte. Dies zeigt, dass eine Hemmung von iNOS das Erregerwachstum indirekt durch eine höhere Monozytenrekrutierung erhöht. Darüber hinaus erhöhte die Injektion von Monozyten an eine Infektionsstelle, nicht aber die Rekrutierung von Neutrophilen, die Erregerlast, was darauf hindeutet, dass je nach Phänotyp einer Entzündung persistierende Infektionen mit *L. major* im Spätstadium durch die Rekrutierung von Phagozyten reaktiviert werden können. NO erfüllt also zwei unterschiedliche Funktionen bei der Eindämmung von *L. major*: Eine direkte Abtötung des Pathogens einerseits, und Einschränkung der verfügbaren Wirtszellen, die Proliferation erlauben, andererseits.

In einem zweiten Teil der Arbeit untersuchten wir den zeitlichen Verlauf und die Auswirkungen einer Hemmung von iNOS auf die Expression von koinhibitorischen Rezeptoren bei Effektor- und regulatorischen T-Zellpopulationen.

Table of contents

Abbreviations

AP-1	activator protein 1
AD	anno domini
AF	alexa Fluor
AICc	akaike information criterion with correction
APCs	antigen-presenting cells
BrdU	5-bromo-2′-deoxyuridine
CCL	chemokine C-C motif ligand
CD	cluster of differentiation
CFP	cyan fluorescent protein
CNS	central nervous system
CTLA-4	cytotoxic T lymphocyte antigen 4
CXCL	chemokine C-X-C motif ligand
Cy	cyanine dye
DCs	dendritic cells
DNA	deoxyribonucleic acid
DNFB	2,4-dinitrofluorobenezene
FVS	fixable viability stain
ICAM	intercellular adhesion molecule
IgG	immunoglobulin G
IL	interleukin
INF-γ	interferon gamma
LCMV	lymphocytic choriomeningitis virus
LDA	Limiting dilution assay
L. major	*Leishmania major*
LFA-1	lymphocyte function associated antigen 1
L-NIL	L-N6-(1-Iminoethyl)-lysine
LNs	lymph nodes
LPS	lipopolysaccharides
mAb	monoclonal antibodies
Mac-1	macrophage-1 antigen

NETs	neutrophil extracellular traps
NF-kB	nuclear factor kappa-light-chain-enhancer of activated B cells
NLRP3	NLR family pyrin domain containing 3
NO	nitric oxide
NOS	NO synthases
ODEs	ordinary differential equations
PAMPs	pathogen associated molecular patterns
PD-1	programmed cell death protein 1
PD-L1	programmed cell death 1 ligand 1
pH	potential of hydrogen
PRRs	pattern recognition receptors
PSGL-1	P-selectin glycoprotein ligand-1
RNA	ribonucleic acid
ROS	reactive oxygen species
SHG	second harmonic generation
TCR	T cell receptor
Teff	effector T cells
Th	T-helper
TIGIT	T cell immunoreceptor with Ig and ITIM domains
TIM3	T cell immunoglobulin and mucin-domain containing-3
TNF-α	tumor necrosis factor alpha
Treg	regulatory T cells
VCAM	vascular cell adhesion molecule
WHO	world health organization

1. Introduction

1.1 Immune responses

The immune system is responsible for the protection of our body, containment and clearance of “non-self” or transformed threats, which include pathogens, toxins and malignant cells. In order to do so, the immune system utilizes two major types of immunity, called innate and adaptive Klimov (2019).

The innate immunity is the first defense line. Its mechanisms include physical and chemical barriers, uptake of material by specialized cells called phagocytes, and acute phase proteins. Once an invader manages to break the physical barriers imposed by for example the skin or mucosa through an insect bite or a wound, conserved molecular structures of pathogens or toxins, so-called pathogen-associated molecular patterns (PAMPs), are recognized by the pattern recognition receptors (PRRs). This binding and subsequent production of inflammatory signal molecules (such as cytokines and chemokines) will lead to the recruitment of a variety of cells of the immune system. In many cases however, the innate immune response alone is not sufficient to efficiently fight the threat, and collaboration between the innate and adaptive immune responses is needed (Suresh and Mosser 2013); (Klimov 2019).

A few days after the induction of the innate immune response, the adaptive immune response can be launched. The adaptive immunity is capable of differentiating self and foreign structures, and also develops immune memory of such antigenic structures of the invading pathogen. The adaptive immunity is carried out by B cell-mediated (humoral) responses or T cell-mediated responses. B cell-mediated responses with the aid of T-helper (Th) cells include the maturation of the B cells into plasma cells, antibody class switching and production of memory cells. T cell-mediated responses act against different pathogens in a manner tailored to the specific infectious threat. T cells rely on the presentation of antigen on antigen-presenting cells (APCs) in order to become activated. This antigen consists of processed protein fragments of cytoplasmic material for cytotoxic T cells, or phagocytosed material for Th cells. Cytotoxic T cells cluster of differentiation 8 (CD8+) with the aid of T-helper 1 (Th1) exert killing against cells harboring viruses or cytoplasmic pathogens, as well as against malignantly transformed tumor cells. In contrast, helminth parasite infection and several allergic inflammatory conditions, including atopic dermatitis, allergic rhinitis and asthma are dominated by the T-helper 2 (Th2) and its associated cytokines interleukin-4 (IL-4), IL-5 and IL-13. T-helper 17 (Th17)-dominated immunity, with its key effector cytokine IL-17 is implicated in the protection against fungi and extracellular bacterial infections by the massive recruitment of neutrophilic granulocytes. Response against intracellular

pathogens competent in surviving phagocytosis by macrophages is usually Th1-mediated alongside with its associated cytokines interferon gamma (INF-γ) and tumor necrosis factor alpha (TNF-α), effector Th1 cells are capable of activating phagocytes to produce reactive oxygen species (ROS) and/or nitric oxide (NO) to contain the pathogen (Luckheeram, Zhou et al. 2012); (Klimov 2019).

1.1.1 Phagocytes

Several types of phagocytes are involved in the immune response triggered by intracellular pathogens.

Neutrophils are among the first responders to an infection. Neutrophils can exert an oxidative burst which leads to the production of ROS, which ,in turn, can act against phagocytosed pathogens (Boyle, Gyori et al. 2011). They are also capable to control the extracellular parasite via neutrophil extracellular traps (NETs). NETs are DNA structures covered by antimicrobial molecules which could facilitate parasite killing (Guimarães-Costa, Nascimento et al. 2009).

Also, among the first cells which take up the pathogen are resident dermal macrophages and dermal dendritic cells (DCs). Dermal macrophages are F4/80+ and characterized as Ly6C-CCR2-CX3CR1-, whereas dermal DCs are mainly characterized as CD64-Ly6C- (Romano, Carneiro et al. 2017).

Subsequent recruitment of monocytes from the blood stream takes place within days after infection, followed by monocytes differentiation into monocyte-derived macrophages and monocyte-derived DCs. Although macrophages can also be found in the draining lymph nodes, DCs are most competent in antigen presentation (León, López-Bravo et al. 2007). However, macrophages are, upon activation in a Th1 response, the most efficient cells killing phagocytosed pathogens (Sacks and Noben-Trauth 2002).

1.1.2 NO function in the immune response

NO, one of the most important effector molecules against intracellular pathogens infecting phagocytes, has a variety of different functions. It is produced by three different NO synthases (NOS), neuronal (nNOS, or NOS1), inducible (iNOS, or NOS2) and endothelial (eNOS, or NOS3). While the three isoforms catalyze the same reaction, they differ in the regulation and the duration of NO production. nNOS and eNOS usually exist as constitutively expressed proteins in the cell. nNOS is constitutively expressed in central and peripheral neurons and some other cell types.

Its functions include synaptic plasticity in the central nervous system (CNS), central regulation of blood pressure, smooth muscle relaxation, and vasodilatation via peripheral nitrergic nerves (Förstermann, Closs et al. 1994). eNOS is mostly expressed in endothelial cells. It keeps blood vessels dilated, controls blood pressure, and has numerous other vasoprotective and anti-atherosclerotic effects (Melikian, Seddon et al. 2009). However, iNOS operates in phagocytes upon activation (Förstermann and Sessa 2012); (Bogdan 2001). iNOS is not detectable in healthy tissue but is expressed after immunologic challenge or injury (Dillman, Dawson et al. 2001).

NO is shown to be involved in the pathogenesis and control of infectious diseases at many stages, with a diverse spectrum of activity. For example, sandfly saliva might enhance the initial survival of the transmitted pathogen by inhibiting the production of NO and a consequent lack of killing of *Leishmania* by host phagocytes (Hall and Titus 1995).

Moreover, within host organisms, NO was shown to have diverse functions. An antimicrobial role of NO has been observed for all groups of infectious pathogens (viruses, bacteria, protozoa, helminths, fungi), with a broad spectrum of host and effector cells such as monocytes and macrophages, microglia, neutrophils, eosinophils, fibroblasts, hepatocytes, endothelial cells, epithelial cells, and astroglia (Bogdan 1997); (Fang 1997); (Bogdan 2000). In term of anti-tumor function, various mechanisms were identified by which NO might cause death (apoptosis) of tumor cells (Hung, Hayashi et al. 1998); (Xie, Dong et al. 1996). Also a regulatory function of NO was reported, via regulation of proliferation, apoptosis and survival, and cytotoxic activity of lymphocytes (Albina, Abate et al. 1991); (Hoffman, Langrehr et al. 1990), modulation of cytokine response (Kim, Talanian et al. 1998); (Diefenbach, Schindler et al. 1998), or others (Bogdan 2000).

The interaction of NO is not limited to a single defined receptor, in fact, it can react with other inorganic molecules, structures in DNA or proteins. Many NO targets are themselves regulatory molecules (Bogdan 2001). For example, transcription factors like nuclear factor kappa-light-chain-enhancer of activated B cells (NF-KB) and activator protein 1 (AP-1), which is important with regard to the redox sensitivity of many transcription factors (Hierholzer, Harbrecht et al. 1998); (Haby, Lisovoski et al. 1994). In addition, the NO effect is strongly influenced by concentration, and not restricted to the site of infection (Olekhnovitch, Ryffel et al. 2014); (Bogdan 2001).

The diversity in pathogen-adapted responses is connected to a specific signature of the metabolism of immune cells, as both phagocytes and T cells may alter their

metabolic state to fulfill their response needs. For example, Th1 IFNγ-mediated activation of the monocyte-derived cells shows a metabolic shift toward the anaerobic glycolytic pathway, while Th2 IL-4-mediated activation shows lower tendency in this direction. NO is capable of modifying this metabolism signature. Importantly, one mode of action of NO during inflammation seems to be the metabolism-related dampening of inflammatory response counteract overshooting immunopathology (Everts, Amiel et al. 2012); (Postat, Olekhnovitch et al. 2018); (Formaglio, Alabdullah et al. 2021).

1.1.3 Recruitment mechanisms of monocytes into the tissue

Monocyte recruitment into the inflamed tissue starts with tethering of free flowing cells to the vessel wall followed by rolling, adhesion to endothelial cells, postadhesion strengthening, crawling, and finally transmigration. Different sets of integrins and selectins will be activated during different steps (Herter and Zarbock 2013).

Monocytes can adhere to and move across the apical surfaces of endothelial cells, integrins (which are αβ heterodimers) play a crucial role in monocyte recruitment (see figure 1). Monocytes encounter chemokines and other stimuli that activate them to bind firmly to the endothelial cell through CD11a-CD18 and CD11b-CD18 integrins interact with endothelial intercellular adhesion molecule 1 (ICAM-1) and ICAM-2, and CD49d-CD29 integrins interact with endothelial vascular cell adhesion molecule 1 (VCAM-1) (Schenkel, Mamdouh et al. 2004). In the rolling stage, integrin VLA-4 (CD49d-CD29) expressed on the monocytes mediates the interaction with the endothelium, which expresses the required ligands for this interaction upon activation in inflamed tissues. Subsequent post-adhesion steps strengthen the binding to the vessel wall and crawling of the monocytes across the endothelium are mediated by CD49d and β2 (known also as CD18) integrins, as well as lymphocyte function-associated antigen 1 (LFA-1) and macrophage-1 antigen (Mac-1) integrins (Herter and Zarbock 2013).

The leukocyte adhesion cascade is not only achieved by integrins, selectins and their respective ligands, but also by chemokines and chemokine receptors. Activated endothelial cells are capable of producing chemoattractants, proteolytic cleavage in activated mast cells and platelets is another source of chemoattractants. Platelets for example deposit chemokine (C-C motif) ligand 5 (CCL5), C-X-C motif chemokine 4 (CXCL4) and CXCL5 onto the inflamed endothelium (Ley, Laudanna et al. 2007). These mechanisms ultimately result in the entry of the monocytes from the blood vessel into the inflamed tissue. Figure 2 shows the role of integrin in monocytes recruitment.

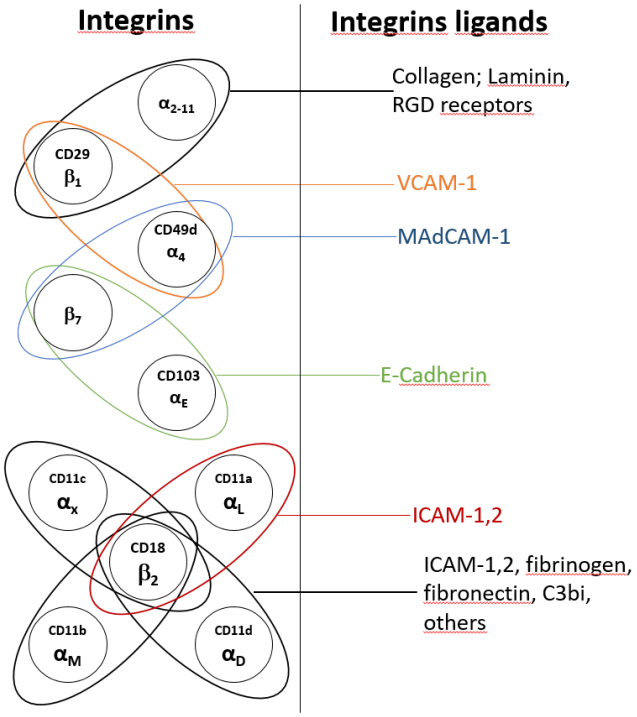

Figure 1: Integrin molecules consist of α and β heterodimers (shown in circles). Adapted from (Bamias, Rivera-Nieves et al. 2018).

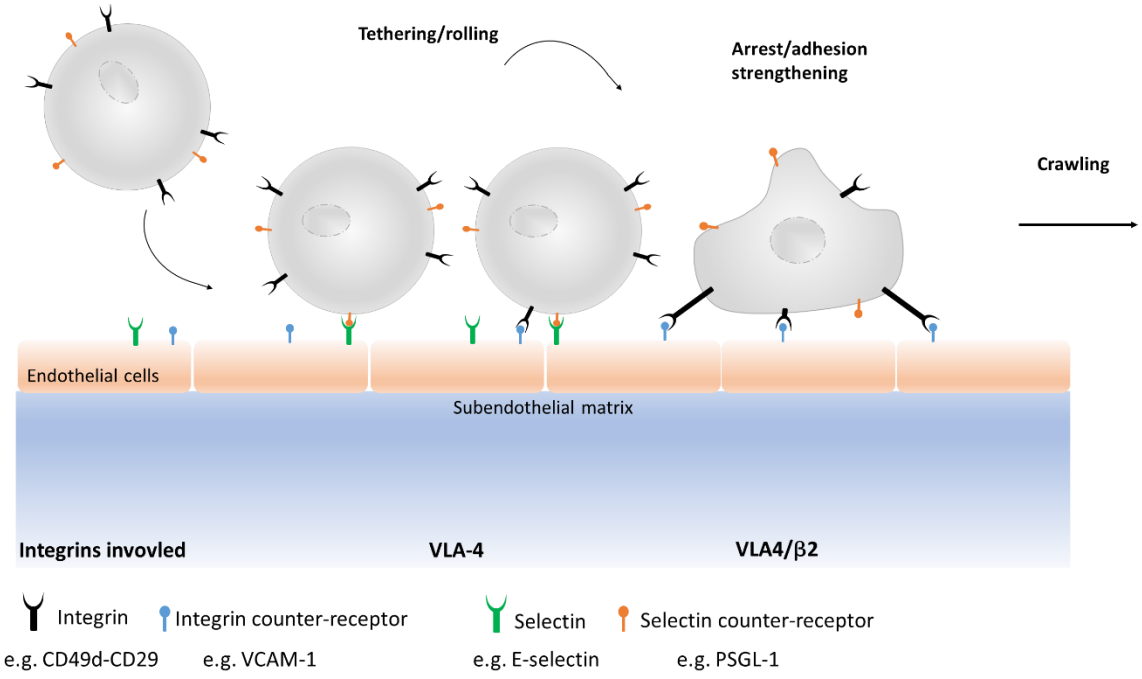

Figure 2: Integrins in monocytes recruitment , modified from (Herter and Zarbock 2013)

1.1.4 Immune checkpoints

Immune responses not only defend the body, but also have the potential to inflict massive damage to the tissue, and have to be limited upon activation. Such negative feedback can be provided by immune checkpoints. One type of immune checkpoint is represented by inhibitory receptors expressed on immune cells upon activation of the cells, and are capable of triggering immunosuppressive signaling pathways (Pardoll 2012). In the steady state, immune checkpoints are important to maintain self-tolerance, while in response to pathogenic infection, they prevent immune-mediated tissue damage. Immune checkpoint inhibitors represent a promising target in treating a variety of infectious diseases, taking into account the recent success of immune checkpoints blockade in increasing protective immune responses for cancer therapy (Pardoll 2012); (Wykes and Lewin 2018). Among the known immune checkpoints, cytotoxic T lymphocyte antigen 4 (CTLA4) and programmed cell death protein 1 (PD-1) are the most targeted in cancer therapy. CTLA4 is expressed by activated T cells together with the T cell co-stimulatory protein CD28, both molecules bind to CD80 and CD86 on DCs, but CTLA4 binds with greater affinity and avidity than CD28. While CD28 transmits a stimulatory signal, CTLA4 is able to inhibit T cell functions (Krummel and Allison 1995).

PD-1 is expressed on T cells, B cells, natural killer (NK), DCs and activated monocytes. It has two ligands, programmed cell death 1 ligand 1 (PD-L1) and PD-L2 (Freeman, Long et al. 2000), PD-1 mediated signaling in T cells upon engagement with PD-L1 expressed on DCs and tumor cells attenuates T cell receptor (TCR) signaling and inhibits T cell population expansion, cytokine production and cytolytic function (Francisco, Salinas et al. 2009).

Targeting other immune checkpoint pathways such as T cell immunoglobulin and mucin-domain containing-3 (TIM3) and T cell immunoreceptor with Ig and ITIM domains (TIGIT) is also showing promising results. TIM3 and its ligand, Galectin 9, which is present on APCs, affects Th1 cells. Galectin 9 is capable of inducing intracellular calcium flux, aggregation and death of Th1 cells *in vitro* (Zhu, Anderson et al. 2005). TIGIT affects T cells and NK cells, its ligand is CD155 on DCs. TIGIT shows immunosuppressive effects by competing with CD226 for CD155 (Dougall, Kurtulus et al. 2017).

1.1.4.1 Is NO a checkpoint inhibitor?

Taking into consideration the immunregulatory features of NO, which are frequently seen together with its protective function, and the definition of immune checkpoints as "a plethora of inhibitory pathways hardwired into the immune system that are crucial for maintaining self-tolerance and modulating the duration and amplitude of physiological immune responses in peripheral tissues in order to minimize collateral tissue damage" (Pardoll 2012), NO may serve aspects of immune checkpoint functions as well, in a broader sense. iNOS may regulate the macrophage transcriptome during *Mycobacterium tuberculosis* infection, for example, repressing NF-kB (Braverman and Stanley 2017), and inhibiting NLR family pyrin domain containing 3 (NLRP3) inflammasome–dependent processing of IL-1β (Mishra, Rathinam et al. 2013). NO effect on NF-kB was shown also *in vitro* (Matthews, Botting et al. 1996). NO interferes also with leukocytes adhesion and recruitment (Kubes, Suzuki et al. 1991); (Postat, Olekhnovitch et al. 2018).

1.2 *Leishmania*

Parasites of the *Leishmania* genus, which are the causative agent for leishmaniasis, are flagellated protozoa of the Trypanosomatidae family. Leishmaniasis are considered as the second most prevalent parasitic disease after malaria. A number of 700000 to 1 million new cases are estimated by the World Health Organization (WHO) to occur annually. Over 20 *Leishmania* species are capable of inducing disease, and over 90 sandfly species are known to transmit *Leishmania* parasites. WHO defines 3 main forms of the disease, visceral, cutaneous and mucocutaneous. The form of the disease is dependent on the species of *Leishmania* and host susceptibility (Kaye and Scott 2011).

The first historical mention of the disease dates back to first century *anno domini* (AD) on pre-Inca pottery from Peru, where representations of skin lesions and facial deformations have been found. In the tenth century, the philosopher Avicenna has documented the disease in detailed description as Balkh sore (from northern Afghanistan). Kala-azar or Dumdum fever was the name used by Indian physicians for an ancient disease defined later as visceral leishmaniasis. In 1901 William Leishman managed to identify certain organism in samples taken from the spleen of a patient died from kala-azar (thought to be trypanosomes). Later in 1903 these parasites were described as being new by Captain Donovan. Major Ross finally found the link between kala-azar and the new defined parasite and named it *Leishmania dononvani*. It took till

1921 to establish an experimental proof of the transmission to humans by sandflies (Kumar 2013).

1.2.1 Life cycle

The *Leishmania* life cycle in the mammalian host (Human) starts with a vector (sand fly) bite (*Phlebotomus* and *Lutzomyia* genera). Upon entry into the dermis, the promastigote form of the parasite, which is flagellated, elongated and extracellular, is phagocytosed, then develops into the amastgote form, which is intracellular, round to oval, aflagelated and non-motile (Kumar 2013). The amastigotes multiply within the phagocytes and are consequently released from one phagocyte to infect others. Amastigotes, following a blood meal by the sand fly, will be ingested and then re-transform into the flagellated promatigotes (Pace 2014).

The *Leishmania* parasite reproduction has for a long time been assumed to require extracellular promastigotes in the sand fly and intracellular amastigotes proliferating in the host asexually. However, now it has been suggested that sexual reproductive cycle may also take place in the sand fly vector (Shaik, Dobson et al. 2021).

Leishmania can be transmitted by sand fly bites as zoonotic (from animals to humans) or anthroponotic (from human to human) transmission (Pace 2014), nevertheless non-vector-borne transmission was reported in dogs (Karkamo, Kaistinen et al. 2014). Figure 3 illustrates the *Leishmania* life cycle.

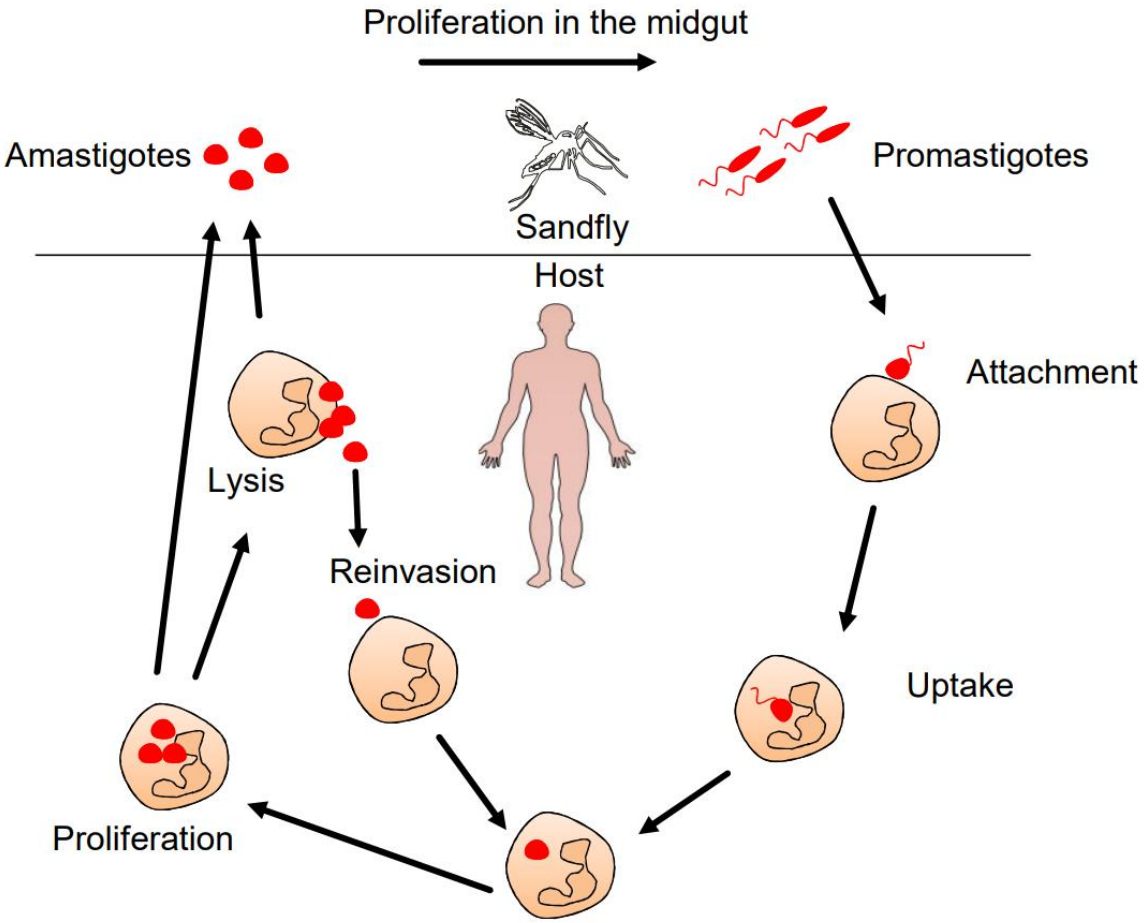

Figure 3: *Leishmania* life cycle, modefied from (Kaye and Scott 2011).

1.2.2 The immune response against *Leishmania*

The out-come of leishmaniasis is dependent on both host susceptibility and parasite species: On the one hand, *Leishmania major*, *Leishmania amazonensis*, and *Leishmania braziliensis* are causative agents of cutaneous or mucocutaneous leishmaniasis, mainly ending up with a self-healing or chronic ulcers in the skin or mucosa. On the other hand, *Leishmania donovani* and *Leishmania infantum* lead to a visceral leishmaniasis, mainly affecting the liver, spleen, and bone marrow in a systemic infection, which is often fatal if untreated (Kaye and Scott 2011).

Extensive information is available about the immune response in experimental cutaneous leishmaniasis, thanks to the mouse infection models which represent an important tool to understand the immune mechanisms that help controlling infection for cutaneous leishmaniasis.

The vector bite delivering *Leishmania* parasites into the skin dermis and damaging the tissue leads to neutrophil recruitment within a few hours (the neutrophils recruitment

peaking at 24h) followed by monocytes (Charmoy, Brunner-Agten et al. 2010). This initial myeloid cell recruitment is a hallmark of the innate immune response, which in turn initiates, and impacts on, the development of an adaptive response, mainly mediated by effector T cells infiltrating into the infected skin, and associated with massive recruitment of further monocytes (Mougneau, Bihl et al. 2011); (Hurrell, Schuster et al. 2015).

In this thesis, we utilize a C57BL/6 mouse infection model of leishmaniasis caused by *L. major* to gain a better understanding of the immune defense against intracellular (vacuolar) pathogens. In fact, this particular strain of inbred of mice has been instrumental to dissect experimentally the impact on *Leishmania* clearance by a Th1 response in comparison to a Th2 response in BALB/C mice. In particular, C57BL/6 showed resistance towards *L. major* with containment of the infection, while BALB/C showed susceptibility (Sacks and Noben-Trauth 2002). Thus, a Th1 response mediated by INF-γ in C57BL/6 mice is considered protective, while BALB/C mice induced Th2 response mediated by IL-4 are non-protective and result in a severe immunopathology. It has been reported that, in *L. major*-infected C57BL/6 mice, monocyte-derived cells on the one hand control the induction of protective Th1 responses, and on the other hand, represent the major infected cell type (De Trez, Magez et al. 2009); (León, López-Bravo et al. 2007).

Therefore, the immune response exerted in *L. major* infection in C57BL/6 mice represents a well-established model for monocyte-dominated iNOS controlled pathogens study.

1.2.2.1 Cellular components of the anti-leishmanial immune response

Neutrophils are among the first responders to *Leishmania* inoculation into the skin, and are recruited within the first hours of infection at high numbers. The role of the neutrophils in the defense against *Leishmania* is controversial. On the one hand, they have been proposed to be capable of killing the parasite (Guimarães-Costa, Nascimento et al. 2009), on the other hand, it has been shown that parasite sequestration by neutrophils might be responsible for the disease progression (Hurrell, Beaumann et al. 2017); (Peters, Egen et al. 2008). It has been shown also that at 10h post infection (p.i), the majority of *Leishmania*-infected cells were neutrophils (Romano, Carneiro et al. 2017).

After the initial recruitment of neutrophils, inflammatory monocytes are recruited to the site of infection, monocytes increase in numbers dramatically between 10h and 2d p.i.

Throughout this time-span, the major fraction of infected cells has been shown to shift from neutrophils to inflammatory monocytes, which represent permissive host cells during the acute phase of the infection (Romano, Carneiro et al. 2017). Heyde *et al.* have shown that these cells, in particular CD11c expressing Ly6C+CCR2+ monocytes, constitute also a main cell type harboring rapidly proliferating *L. major* in the ongoing infection around 3 weeks p.i (Heyde, Philipsen et al. 2018).

Recruited monocytes are also capable of differentiate and then migrate into the draining lymph nodes (LNs) and are involved in inducing and maintaining protective Th1 responses (León, López-Bravo et al. 2007). The uptake of the parasite by phagocytes is facilitated by host immunoglobulin G (IgG) and the opsonisation via complement receptors, which might guide the pathogen's uptake into different phagocyte subtypes (Liu and Uzonna 2012); (Da Silva, Hall et al. 1989). *Leishmania* parasites could be also phagocytosed by B cells, which contribute to a successful control of resistant *L. major* infection (Scott, Natovitz et al. 1986); (Woelbing, Kostka et al. 2006). B cells were also shown to shape the development of the susceptible immune response of *L. major* (Ronet, Hauyon-La Torre et al. 2010).

Apart from immune cells, it has been shown *in vivo* that *Leishmania* parasites could reside in fibroblasts in the early phase and the latent phase of the infection (Esterre, Dedet et al. 1991); (Bogdan 2000).

Alongside with the functions of innate immune cells, the resistance or susceptibility of a host against *L. major* infection is correlated with the dominance of IL-4-driven Th2 responses which promote disease, or IL-12-driven INF-γ dominated Th1 responses which promote healing (Sacks and Noben-Trauth 2002). The resistance model traditionally is assumed to result in classical activation of monocyte-derived phagocytes (Green, Crawford et al. 1990), while the susceptibility model is associated with alternative activation and induction of arginase I (Noël, Raes et al. 2004). Despite the well-established resistance or susceptibility models, recent work has shown that Th2 immunity may play a protective role during early resistance infection by reducing the size of permissive monocytes via regulation of INF-γ mediated monocytes recruitment (Carneiro, Lopes et al. 2020).

Not only Th1 and Th2 are involved in the cellular adaptive immune response against Leishmaniasis in the resistance model, but also the regulatory T cells (Treg). Treg cells which accumulate at the infection site suppress the ability of the effector T cells to eliminate the parasite (Belkaid, Piccirillo et al. 2002).

Despite the fact that *L. major* caused cutaneous *Leishmania* is usually self-healing in immune-competent indiviuals, sterile immunity with complete absence of that parasite seems not to be reached even after complete healing of the lesion. Instead, the parasite might survive for life providing concomitant immunity, which is protective against secondary challenges (Hohman and Peters 2019). This concomitant immunity might be due to a modulation of Th1 response mediated by IL-10 and/or Treg cells, also to specific phagocyte populations as a niche showing limited immune activation (Lee, Charmoy et al. 2018); (Nylén and Sacks 2007).

1.2.2.2 *Leishmania* control: iNOS, how does it do it?

The production of NO by iNOS (expressed from the *nos2* gene) is a key factor in controlling Leishmaniasis, and the importance of iNOS-produced NO is proven *in vitro* and *in vivo* (Wei, Charles et al. 1995); (Liew, Li et al. 1991); (Müller, Aeschlimann et al. 2013); (Olekhnovitch, Ryffel et al. 2014).

The induction of iNOS expression in the phagocytes can also be provoked *in vitro* and takes place within a few hours after treatment with a combination of INF-γ and lipopolysaccharides (LPS) (Pautz, Art et al. 2010). Then, iNOS catalyzes oxygenation of L-arginine to L-citrulline and NO via the intermediate N-hydroxyarginine. Figure 4 shows the reaction catalyzed by NOS.

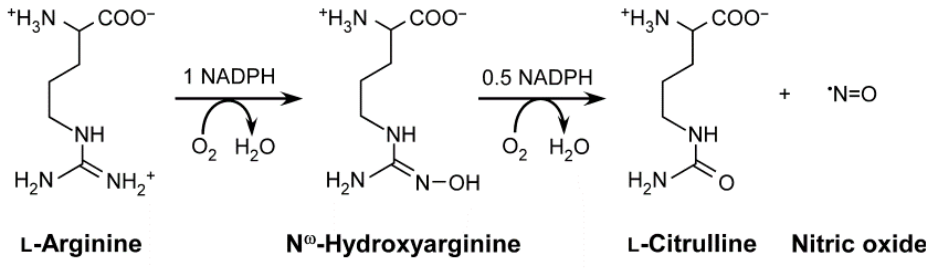

Figure 4: Reaction catalyzed by NOS, adapted from (Stuehr, Tejero et al. 2009).

It has been shown that L-N6-(1-Iminoethyl)-lysine (L-NIL) potently inhibits iNOS activity (Stenger, Thuring et al. 1995), therefore, L-NIL is widely used and accepted as NOS inhibitor *in vitro* and *in vivo* (Stenger, Donhauser et al. 1996); (Olekhnovitch, Ryffel et al. 2014).

NO is essential for the control of leishmaniasis over the course of infection, however, additional players may be involved. In the beginning of the infection, innate IFN-α/β signaling induces iNOS expression which has been shown to be crucial to avoid early

dissemination to visceral organs (Diefenbach, Schindler et al. 1998). Later, throughout the course of the infection, Th1 cells infiltrating the site of infection produce sufficient amounts of IFN-γ to induce massive induction of iNOS expression (Sacks and Noben-Trauth 2002). Müller *et al.* have shown that it is enough for effector T cells to establish stable contacts with a minority of the infected cells to trigger defense mechanisms in contacted and bystander phagocytes (Müller, Filipe-Santos et al. 2012).

Even at the latency phase, NO seems to control the persistent parasites, as iNOS inhibition at this time-point ignites rapid proliferation of the parasite and relapse of disease pathology (Stenger, Donhauser et al. 1996).

NO production by iNOS takes place in the cytoplasm, but the molecule is capable of diffusing into phagolysosome to impact the parasite directly (MacMicking 2012). NO can also diffuse out of the cell membrane which qualifies it to affect the parasite cell-extrinsically and modify the microenvironment. Indeed, it has been shown that iNOS-deficient cells are able to control *L. major* parasites when placed with iNOS-competent cells in the same environment (Olekhnovitch, Ryffel et al. 2014).

iNOS induction has been shown to block respiration in DC and macrophage cultures *in vitro* (Van den Bossche, Baardman et al. 2016). Additionally, monocyte-derived cells from *L. major* site of infection were shown to exhibit a profound block in cell respiration which is reversible by a short inhibition of iNOS (Postat, Olekhnovitch et al. 2018). NO anti-microbial activity might be exerted in part by disrupting parasite respiration, and interestingly, phagocytes in this context might be capable of partially avoiding the respiration disrupting effect by switching from oxidative phosphorylation to aerobic glycolysis (Pearce and Everts 2015).

NO has also been shown to decrease cytokine and chemokine production very broadly, affecting Th1, Th2, and immunosuppressive related cytokines (Postat, Olekhnovitch et al. 2018). Also, other publications suggest that NO production by iNOS may affect the response of Th cells at the site of infection (Bogdan 2001).

NO anti-microbial activity might also be meditated via interference with the arginase-1 activity, the competition between iNOS and arginase-1 for arginine may play a crucial role here, taking into consideration that the conversion of arginine to ornithine and urea via the arginase pathway can support the growth of parasites (see Figure 5) (Das, Lahiri et al. 2010).

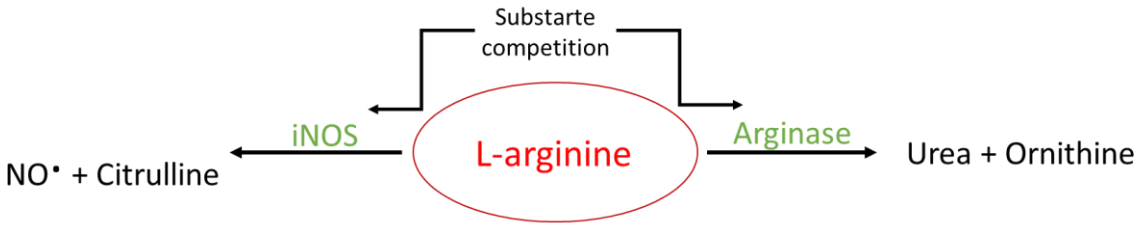

Figure 5: Competition for arginine, modefied from (Das, Lahiri et al. 2010).

Additionally, NO may induce a non-lethal parasite growth inhibition that contributes to the control of parasite numbers (Müller, Aeschlimann et al. 2013).

Besides its effect on the pathogen and cells of the host at the site of infection, NO impacts also on leukocyte adhesion to the endothelium and consequently on their ability to be recruited to the site of infection (Kubes, Suzuki et al. 1991); (Kubes, Sihota et al. 1997).

NO has also another crucial regulatory role on the inflammatory mediators, where it is thought to support a pro-inflammatory response in low concentration, and an anti-inflammatory response in high concentration (Kobayashi 2010); (Postat, Olekhnovitch et al. 2018).

The protective effects of NO are not limited to leishmaniasis. In fact, data from infections with other intercellular pathogen show a comparable involvement of iNOS in the control of infection. It has been shown that NO is capable of controlling tuberculosis infection by inhibiting NLRP3 inflammasome–dependent processing of IL-1β (Mishra, Rathinam et al. 2013). Furthermore, it was shown in the same infection model that NO blocks the recruitment of pathogen-permissive neutrophils (Mishra, Lovewell et al. 2017).

NO is not the only reactive molecule with an involvement in controlling *Leishmania*, but also the production of ROS can impact on the pathogen. ROS production may be particularly important before the development of the adaptive immune response, but it is not absolutely required, as mice deficient in generating ROS can still control the disease (Novais, Nguyen et al. 2014).

Taken together, how these various ways in which NO affects *Leishmania* physiology and the inflammatory microenvironment contributes to pathogen containment have not yet been fully elucidated.

1.2.2.3 Immune checkpoints inhibitors in the context of *Leishmania*

The need for balancing immune activation against immunopathology during *Leishmania* infection suggests there may be an important role for immune checkpoints. With their capacity of unleashing the immune response directed against the pathogen, immune checkpoint inhibitors could be a promising target for preventing and treating a range of infectious diseases. However, studies on targeting immunoinhibitory mechanisms as a therapeutic approach in the context of leishmaniasis are limited.

In C57BL/6 mice infected with an attenuated, Arginase-deficient (arg-) *L. major* strain which causes chronic infection, it has been shown that chronic disease was associated with an increase PD-1 expression on CD4+ T cells, while treatment with anti–PD-1 monoclonal antibodies (mAb) led to complete resolution of the chronic lesion (Mou, Muleme et al. 2013). Also, Joshi *et al.* have shown that PD-L1 blockade significantly reduced the splenic parasite burden in visceral leishmaniasis (Joshi, Rodriguez et al. 2009). CTLA4 is another well-characterized negative regulator of T cell activation. For this immune checkpoint, it has been shown that blockade of CTLA4 can result in enhanced host resistance to *Leishmania* (Murphy, Cotterell et al. 1998).

Although there is no data available about TIM3 or TIGIT role in leishmaniasis containment, an augmented suppression by TIM3 or TIGIT expressing Treg cells toward Th1 effector cells in the context of lymphocytic choriomeningitis virus (LCMV) infection in mice was shown (Littringer, Moresi et al. 2018), which could make them promising targets for enhancing the control of *Leishmania* infection.

As mentioned above, NO may serve aspects of immune checkpoint functions as well. However, due to its multiple roles in pathogen control, its function as an immune checkpoint is extremely difficult to dissect.

1.3. New tools to address an old disease: Intravital and mathematical tools to dissect the interaction of the immune system with *Leishmania*

1.3.1 mKikumeGr proliferating system

Information on proliferation rate of pathogens that cause long-term chronic infections are limited, however, it is of high importance to understand the balance between parasite proliferation and the immune system: First, rapidly proliferating pathogens are a source of large amounts of antigen and pathogen-associated molecular patterns (PAMPs). Second, pathogen proliferation is inversely correlated with resistance against both immune defense mechanisms and antimicrobial treatment. Thus, pathogens with very low proliferation rates can constitute a reservoir for chronic or relapsing infections, while high proliferating pathogens can be more easily cleared (Nathan 2012); (Sarathy, Dartois et al. 2013); (Orman and Brynildsen 2015). Consequently, measuring *Leishmania* proliferation under physiological conditions *in vivo* would be essential.

Several techniques that allow detecting *Leishmania* proliferation *in vivo* have been proposed in the recent years, for instance, heavy water labeling by (Kloehn, Saunders et al. 2015) or 5-Bromo-2′-deoxyuridine (BrdU) incorporation into parasite DNA (Mandell and Beverley 2017). However, these techniques allowed for neither cell-resolved analysis of pathogen proliferation, nor the application of immunofluorescence microscopy or cytometry in the cellular niche.

The usage of fluorescence protein-based *in vivo* proliferation reporter systems would fill this gap. Therefore, in this work, we determined *L. major* proliferation on a single cell level by using a novel fluorescence protein-based *in vivo* proliferation reporter system, utilizing mKikGR protein, a monomeric version of the previously reported KikGR that displays high photostability and switching rates (Müller, Aeschlimann et al. 2013); (Heyde, Philipsen et al. 2018); (Hurrell, Beaumann et al. 2017).

A photoswitch of mKikGR from green to red fluorescence is mediated by irreversible light induced β-elimination within the mKikumeGR protein. The green fluorescence which shows a fluorescence spectrum with a peak at 515 nm, changes to red fluorescence with a peaks at 591 nm, upon illumination of the protein with light of 405 nm (Habuchi, Tsutsui et al. 2008). *L. major* parasites expressing this photoconvertible protein are termed as *Lm*^{SWITCH}.

Lm^{SWITCH} showed a green fluorescence before photoconversion, which is completely converted to red upon photoconversion, thus, proliferation could be detected

quantitatively based on the dilution of the red photo-switched with the newly synthesized green mKikGR protein (Müller, Aeschlimann et al. 2013) (see figure 6).

Figure 6: Intravital two-photon measurement approach of *Lm*^{SWITCH} infected C57BL/6 mouse 48 hr after photoconversion of the same site in the dermis.

1.3.2 CFP/mNectarine system

With pathogen proliferation rates being one major factor which defines the pathogen burden at the site of infection, another important parameter is the killing of *Leishmania* by the immune system. It is not entirely clear, but important to dissect, how both parameters, pathogen proliferation and death, affect the equilibration of the immune response and *Leishmania* pathogen in the course of this long-lasting infection.

On the one hand, previous results have shown that iNOS can cause non-lethal dampening of the pathogen proliferation *in vivo*, which is partially responsible for controlling *L. major* infection (Müller, Aeschlimann et al. 2013). On the other hand, experiments from *in vitro* studies suggested that iNOS can directly kill the pathogen (Olekhnovitch, Ryffel et al. 2014).

Taking together, in order to dissect the contribution of these different mechanisms of iNOS, and considering the availability of the mKikumeGr system mentioned above, a biosensor for pathogen membrane integrity in *L. major* which is capable of quantifying direct killing activity *in vivo* has been established (Formaglio, Alabdullah et al. 2021). Briefly, as the intracellular habitat of *L. major* has a low potential of hydrogen (pH), the parasite needs to be able to uphold a high pH difference between its cytoplasma (pH 7) and the parasitophorous vacuolar space (pH 3). A probe that is sensitive to parasite intracellular pH decrease should therefore indicate if *L. major* is able to keep its cytoplasma close to neutral pH. The probe that had been established previously, and was published together with the presented thesis project (Formaglio, Alabdullah et al. 2021), consists of a cyan fluorescent protein (CFP) fused to the pH sensitive mNectarine fluorescence protein. As mNectarine fluorescence is much more sensitive to low pH than CFP, live parasites should exhibit both mNectarine and CFP

fluorescence, whereas in a dying parasite, the difference in pH should be abolished, resulting in a lower pH in the parasite cytoplasm and a decrease in mNectarine fluorescence as compared to CFP (see figure 7 (A and B)). *L. major* parasites expressing this death reporter are termed as *L. major*^{necR}.

1.3.3 ODEs models

Ordinary differential equations describe the evolution of observed variables over time, such as populations of cells, transcription factors, organ size and signaling strength. Such equations can be employed to model the transition between, and activation of, different cell populations at a site of infection, with the different functions of the model representing the dynamics of the biological system over time. Such models, once validated, can be used to make predictions for the described biological system. This can guide the development of new hypotheses regarding the dynamics and mode of action of distinct mechanisms in the biological system, which in turn can be tested experimentally (Boianelli, Nguyen et al. 2015).

In order to validate a model, “parameter estimation” or “fitting” is used, which includes a large number of simulations with different parameter values, and comparing each simulation to a real-world experimental dataset, keeping the parameter set with the lowest difference (cost) to the experimental data (Robert, Jönsson et al. 2018). Increasing the number of parameters used for a model almost always reduces the cost of a model, however increases the complexity of the model and the risk of so-called overfitting, and thus lowers the probability of generalizable predictions (Cavanaugh and Neath 2019).

In order to evaluate prediction errors, information loss and simplicity of models, estimators such as the Akaike information criterion with correction (AICc), which evaluates model quality based on both quality of fitting and the number of free parameters, can be employed (Zhao, Wirth et al. 2017).

1.4. Previous results

It has been shown in our laboratory by employing 2-photon microscopy of biosensors *for L. major* death and proliferation, that both overt pathogen killing and high pathogen proliferation take place at the peak of the immune response, while in a subsequent persistence phase, reduced pathogen proliferation in the absence of killing results in a constantly low infection burden.(see figure 7 (B and D))

The investigation of pathogen death was done with the *in vivo* reporter system introduced above, established in our Laboratory (Formaglio, Alabdullah et al. 2021). A low-dose infection of C57BL/6 mice with $5x10^3$ metacyclic *L. major*^{necR} parasites per ear were analysed by intravital 2-photon microscopy at different timepoints over the course of infection (approach and example of the obtained images are shown in figure 7A, results are shown in figure 7B). In parallel, an infection of C57BL/6 mice with $5x10^3$ metacyclic *L. major*^{SWITCH} parasites (mentioned above) was used for the Intravital 2-photon measurement of *L. major* proliferation over the course of the infection (example of the obtained images are shown in figure 7C, results are shown in figure 7D).

Additionally, the time course of low-dose *L. major* infection was defined previously with regard to pathogen burden, but also cell recruitment and iNOS expression within the recruited cells. We showed a gradual increase in parasite burden, which reached its peak at 7 weeks p.i, and eventually decreased by about 90%, but was still detectable at 19 wpi (see figure 7E). We also defined neutrophils and monocyte-derived cells populations, as reflected by the number of CD45+CD11b+ cells present at the infection site, progressively expanded until 9 wpi and contracted at later time points (see figure 7F). iNOS-expressing monocyte-derived cell population was highest between 7 and 9 wpi but remained elevated after this peak compared to before the onset of the adaptive immune response in term of absolute numbers and percentage (figure 7 G and H). In parallel, histological examination of the tissue showed substantial immune infiltration at the peak of infection, and no overt pathology was detected by 19 wpi (see figure 7I).

A

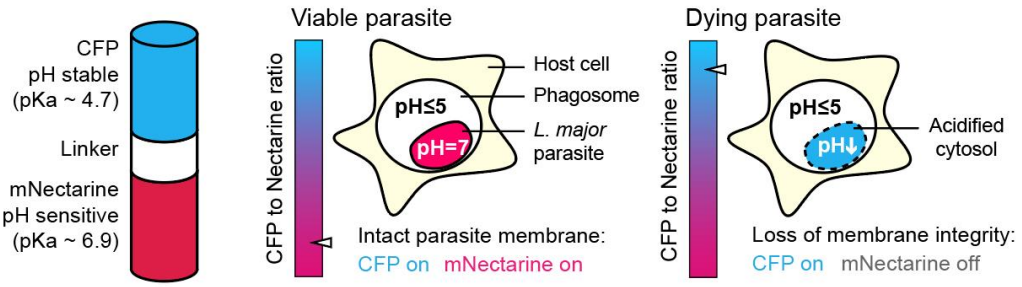
CFP
pH stable
(pKa ~ 4.7)
Linker
mNectarine
pH sensitive
(pKa ~ 6.9)
Viable parasite
CFP to Nectarine ratio
pH≤5
pH=7
Host cell
Phagosome
L. major
parasite
Intact parasite membrane:
CFP on mNectarine on
Dying parasite
CFP to Nectarine ratio
pH≤5
pH↓
Acidified
cytosol
Loss of membrane integrity:
CFP on mNectarine off

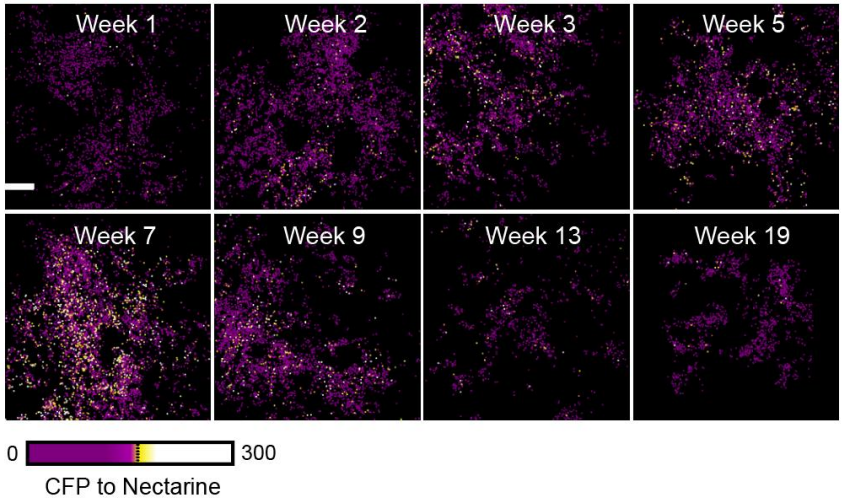
Week 1
Week 2
Week 3
Week 5
Week 7
Week 9
Week 13
Week 19
0
300
CFP to Nectarine

B

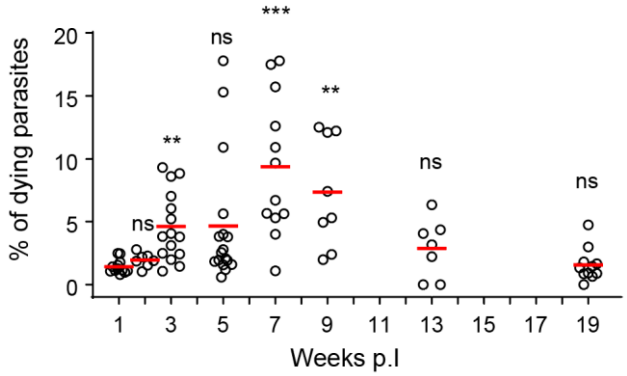
% of dying parasites
20
15
10
5
0
ns
**
ns
***
**
ns
ns
1
3
5
7
9
11
13
15
17
19
Weeks p.I

C

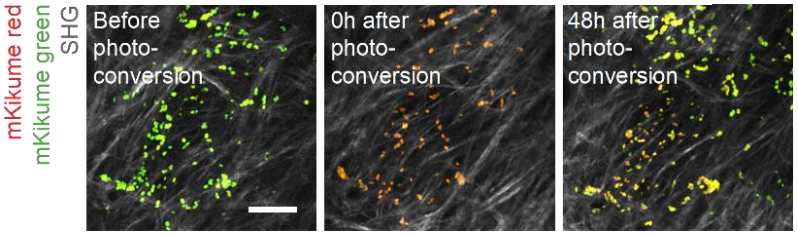
mKikume red
mKikume green
SHG
Before
photo-
conversion
0h after
photo-
conversion
48h after
photo-
conversion

D

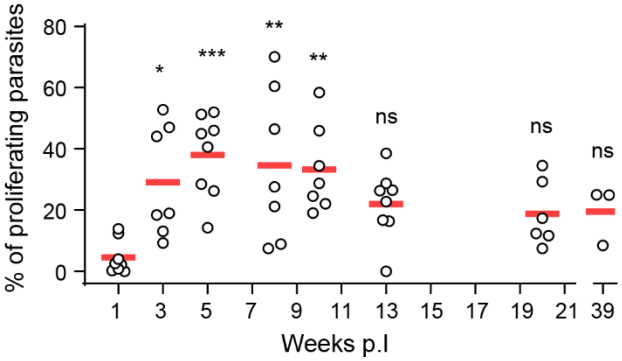
% of proliferating parasites
80
60
40
20
0
*
***
**
**
ns
ns
ns
1
3
5
7
9
11
13
15
17
19
21
39
Weeks p.I

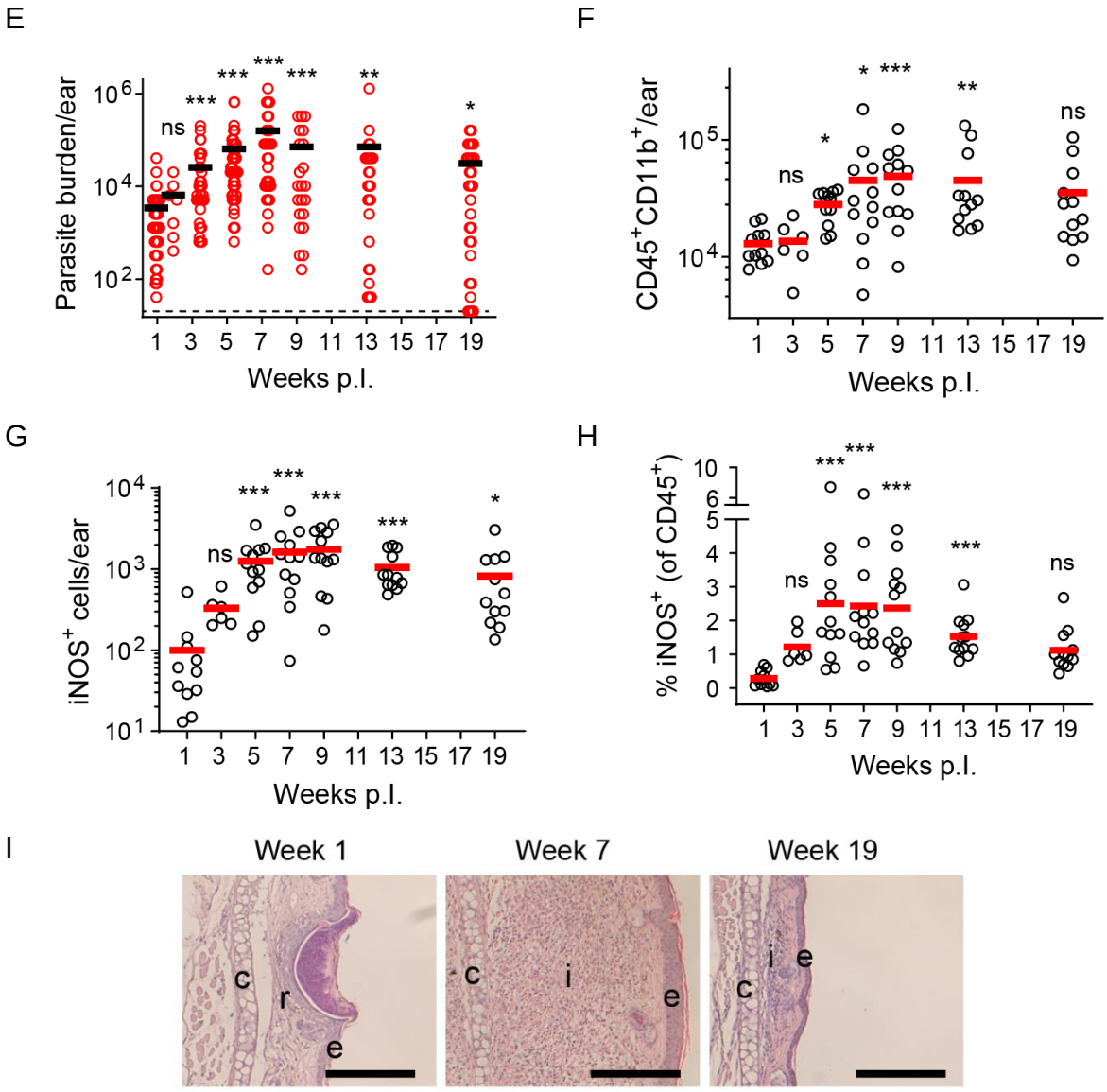

Figure 7: Previous results. A,) *L. major*^{necR} approach and death heatmaps determined by intravital two photon microscopy (IV-2PM) throughout the infection, scale bars, 100 mm. B, *L. major* death over the course of the infection. C, examples of segmented parasites before, 0 h after, and 48 h after photoconversion, Scale bar 50 mm. D, *L. major* proliferation over the course of the infection. E, Time course of low-dose *L. major* pathogen burden analyzed by limiting dilution. F, Time course of neutrophils and monocyte-derived cells populations analyzed by flow cytometry. G-H Time course of iNOS-expressing monocyte-derived cell population. I,histological examination, hematoxylin and eosin staining, c; cartilage, e; epiderm, i; infiltrate, r; regenerative tissue after injection. Each symbol represents one infected ear. Horizontal bars denote the mean. ***p < 0.001; **p < 0.01; *p < 0.05; ns, not significant, according to Kruskal-Wallis with Dunn's post-test (comparison with 1 wpi).

1.5. Aim of the study

Inhibition of proliferation and direct killing might variably contribute to pathogen containment at different time points of the infection. Also, it is unclear if parasite control is achieved cell-intrinsically or -extrinsically, as antimicrobial molecules diffuse at the site of infection and might dose-dependently either directly kill pathogens or impair their proliferation. Dissecting death and proliferation state of a pathogen is not only important to understand the pathogen-immune system balance, but also to define an optimal treatment strategy.

In this work we aim to unravel the dynamics and mode of action of parasite control, utilizing infection of C57BL/6 mice with *L. major* parasites. In this well-characterized system, we will map the course of parasite burden by classical limiting dilution analysis, moreover, recruitment, infection and activation of immune effector functions (iNOS) of leukocyte populations by flow cytometry.

These data will constitute a comprehensive resource on the changes in population sizes of pathogens and recruited host cells over course of infection. Consequently, *in silico* different hypotheses will be tested concerning the mode of parasite control by the activation/infection status of monocyte-derived cells, which constitute the main infected and main iNOS-producing phagocyte population.

In parallel, considering that the balance of delivery of regulatory and effector T cell functions to the infected tissue may impact the observed changes in pathogen physiology, we aim to map the recruitment and the expression of co-inhibitory receptors of effector T cells and regulatory T cells populations over the course of infection.

2. Results

2.1 Part I. Dissecting killing versus proliferation inhibition-based pathogen containment in a high dose infection model of *Leishmania major*

The *in vivo* biosensory systems for pathogen death and pathogen proliferation established previously in our laboratory opened the possibility to dissect direct killing of intracellular pathogen from non-lethal modes of action of iNOS, such as proliferation inhibition. One could speculate that killing and proliferation inhibition could be linked in a simple correlation to the immune activation (figure 8 A), with pathogen killing being high and pathogen proliferation being low when immune activation is high, and vice versa, also, a complex correlation is possible (figure 8 B). However, our work in low dose infection model showed that in particular, the extent to which the pathogen proliferates, and the resulting inferred proliferation inhibition by the immune system are far from being linked directly to the amplitude of the immune response. This work had shown on the one hand that overt pathogen killing occurs during the acute phase of the infection, at which pathology and immune activation are high, but not in the persistent infection phase later on. On the other hand, it could be observed that *L. major* proliferation is also low during the persistence phase of the infection, at which iNOS expression was observed to be lower than at the peak of the infection (figure 7 B and D) (Formaglio, Alabdullah et al. 2021). This work suggests a simple correlation between immune activation and killing, but not between immune activation and proliferation inhibition.

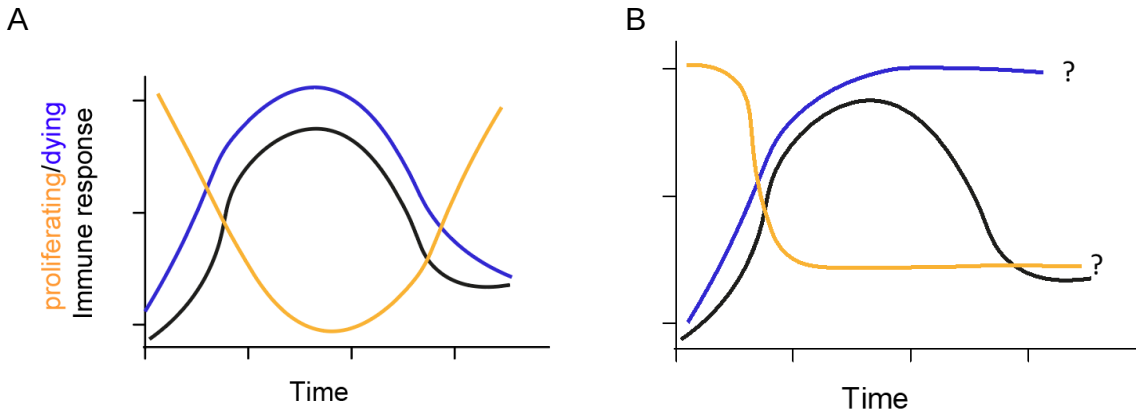

Figure 8: a scheme of possible correlations among immune response, pathogen killing and pathogen proliferation. A, a simple direct correlation. B, complex correlation.

2.1.1 ODE modelling

We and others had observed that inhibition of proliferation and direct killing might variably contribute to pathogen containment at different time points of the infection (Müller, Aeschlimann et al. 2013); (Mandell and Beverley 2017); (Olekhnovitch and Bousso 2015). Although activated phagocytes expressing iNOS are known to be critical for controlling the infection, the extent of pathogen killing versus growth inhibition has remained undetermined. Also, it is unclear if parasite control is achieved cell-intrinsically within activated phagocytes, or cell-extrinsically in a tissue-wide fashion, as antimicrobial molecules diffuse at the site of infection and might dose-dependently either directly kill pathogens or impair their proliferation (Olekhnovitch, Ryffel et al. 2014). In order to understand the dynamics and mode of action of parasite control, we set out to design mathematical models using ordinary differential equations in collaboration with Sebastian Binder and Anastasios Siokis from the laboratory of Michael Meyer-Hermann at the Helmholtz Centre for Infection Research Braunschweig. The models were set up in order to describe the temporal evolution of the pathogen burden and the activation and infection status of the monocyte-derived cells recruited to the site of infection with a high (or a low) dose of *L. major* parasites (Formaglio, Alabdullah et al. 2021).

In essence, and as described in details below, models were set up in which activated monocyte-derived cells (called monocytes for simplicity hereafter) could take their antimicrobial effect cell-intrinsically, cell-extrinsically, or both, either via direct pathogen killing, pathogen proliferation inhibition, or both. These possibilities lead to the design of the following six ordinary differential equation (ODE) models representing different hypotheses on the mode of *L. major* control :

Model 1: assumes only cell-intrinsic pathogen killing by activated monocytes.

Model 2: assumes only cell-intrinsic pathogen proliferation inhibition by activated monocytes.

Model 3: assumes both intrinsic pathogen killing and intrinsic pathogen proliferation inhibition by activated monocytes.

Model 4: assumes intrinsic and extrinsic pathogen killing, dependently of monocyte activation, but in all monocytes.

Model 5: assumes intrinsic and extrinsic pathogen proliferation inhibition, dependently of monocyte activation, but in all monocytes..

Model 6: assumes intrinsic and extrinsic pathogen killing and pathogen proliferation inhibition, dependently of monocyte activation, but in all monocytes.

In all models, with *L. major* being obligate intracellular, the presence of recruited cells adds to pathogen proliferation.

2.1.2 Monocyte sub-population ODEs

In order to shape these models into equations, ODEs describing the dynamics of the four different activated and/or infected sub-populations of monocyte-derived cells at the infection site were set up. The equations included non-activated monocyte-derived cells (M) which are recruited to the site of infection and can become activated as a result of pathogen burden and thus express iNOS (M_a), become infected (M_i), or both via sequential activation or infection in either order (M_{ai}) (Figure 9).

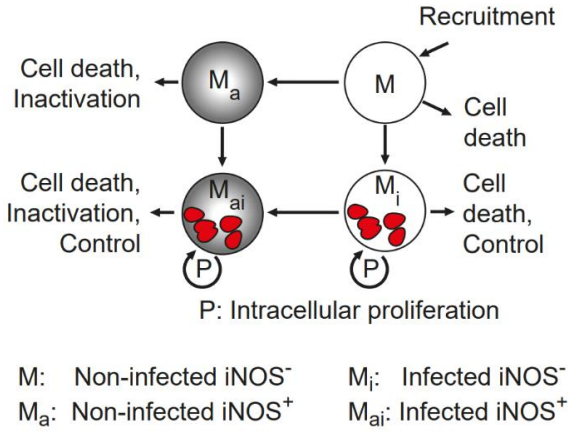

Figure 9: ordinary differential equation model of monocyte-derived cells according to their activation (iNOS expression) and infection state. Arrows: possible state transitions. M, non-activated, non-infected cells; Ma, activated (iNOS expressing); Mi, infected; Mai, activated and infected; P, parasite intracellular proliferation. Gray shading: activation (iNOS expression), red: parasites.

Explanation of the parameters and variables used in the following ODEs is shown in table 1 :

Table 1	
k_{Mrec}	Basal recruitment of Monocytes
a, S_{M}	Scaling factors for parasite-burden monocyte recruitment
k_{i}	Rate of infection
k_{a}	Rate of activation

k_{ai}	Rate of activation of infected monocytes
k_{ia}	Rate of infection of activated monocytes
k_{r}	Rate of parasite killing
k_{p}	Rate of parasite proliferation
C_{P}	Carrying capacity (parasites in the lesion)
k_{D}	Delay rate for the interval between infection and inflammatory cell recruitment and activation
$\beta \leq 1$	Reduced parasite proliferation because of cell-intrinsic growth inhibition in the respective models
C_{iP}	Rescaling pathogen proliferation for growth inhibition by activated monocytes
C_{im}	Rescaling the delay function for monocyte activation
$d_{\mathrm{M(i,a,ai)}}$	Death rate of monocytes (non-activated, infected, activated, or both)
d_{P}	Parasite death rate
$M(t)$	Non-infected non-activated monocytes population over time
$Mi(t)$	Infected monocytes population over time
$Ma(t)$	Activated monocytes population over time
$Mia(t)$	Infected Activated monocytes population over time
$P(t)$	Parasite burden over time
$D(t)$	Sigmoid delay resulting from time interval between pathogen burden increase and immune activation

Here, equations 1-4, explained in respective figures (figure 10-13), are describing the dynamics of the monocyte-derived cell populations dependently of the parasite tissue burden, as well as a delay function in equation 5, which describes the delay between detection of the pathogen and the resulting cell recruitment in the course of an inflammatory response.

$$\frac{dM(t)}{dt} = k_{\mathrm{Mrec}} + \frac{aP(t)}{S_{\mathrm{M}}+P(t)} - k_{\mathrm{i}}P(t)M(t) - k_{\mathrm{a}}\frac{D(t)}{C_{\mathrm{im}}+M_{\mathrm{a}}(t)+M_{\mathrm{ai}}(t)}M(t) - d_{\mathrm{M}}M(t) \quad (1)$$

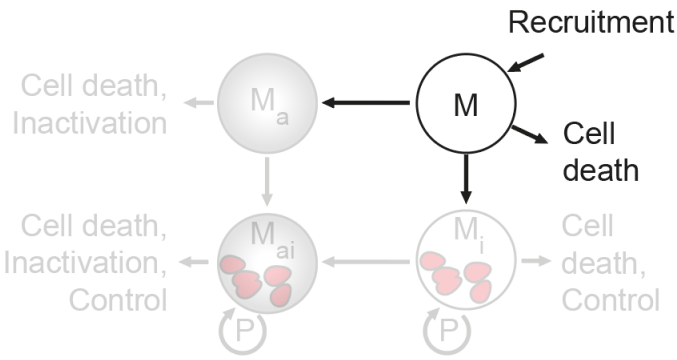

Figure 10: non-activated, non-infected sub-population. Upon infection, basal recruitment at the site of infection, k_{Mrec}, as well as recruitment of monocytes due to the parasite burden, $\frac{aP(t)}{S_{\mathrm{M}}+P(t)}$, are considered. Newly recruited monocyte-derived phagocytes either phagocytose or are actively invaded by pathogen dependently of the parasite burden P at time t of the infection, resulting in their infection $k_{\mathrm{i}}P(t)M(t)$. Furthermore, monocyte-derived phagocytes residing at the site of infection interact with newly recruited Th1 cells, resulting in their activation $k_{\mathrm{a}}\frac{D(t)}{C_{\mathrm{im}}+M_{\mathrm{a}}(t)+M_{\mathrm{ai}}(t)}M(t)$. Natural death of monocyte is taken into consideration as well $d_{\mathrm{M}}M(t)$.

$$\frac{dM_{\mathrm{i}}(t)}{dt} = k_{\mathrm{i}}P(t)M(t) - k_{\mathrm{ai}}\frac{D(t)}{C_{\mathrm{im}}+M_{\mathrm{a}}(t)+M_{\mathrm{ai}}(t)}M_{\mathrm{i}}(t) - d_{\mathrm{M_i}}M_{\mathrm{i}}(t) \quad (2)$$

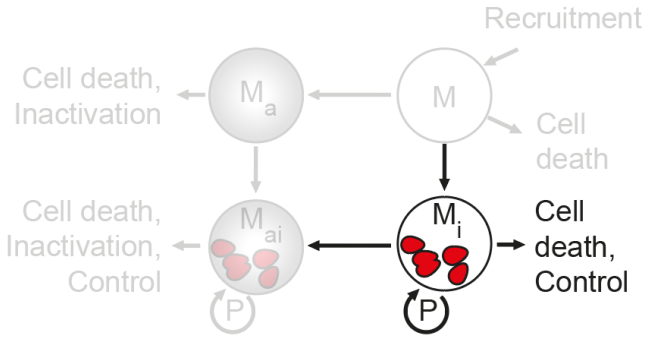

Figure 11: infected sub-population. The main source of infected monocytes M_{i} is monocyte-derived phagocytes M that either phagocytose or are actively invaded by pathogen, resulting in their infection $k_{\mathrm{i}}P(t)M(t)$. As newly recruited monocytes, also infected monocytes can get activated at a specific rate $k_{\mathrm{ai}}\frac{D(t)}{C_{\mathrm{im}}+M_{\mathrm{a}}(t)+M_{\mathrm{ai}}(t)}M_{\mathrm{i}}(t)$. Natural death of monocyte is taken into consideration through $d_{\mathrm{M_i}}M_{\mathrm{i}}(t)$.

$$\frac{dM_a(t)}{dt} = k_a \frac{D(t)}{C_{im}+M_a(t)+M_{ai}(t)} M(t) - k_{ia}P(t)M_a(t) - d_{M_a}M_a(t) \quad (3)$$

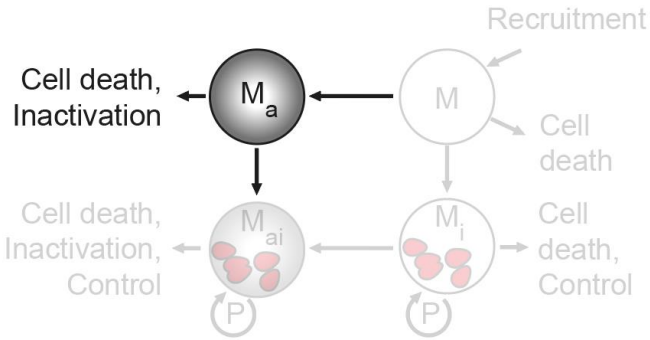

Figure 12: activated sub-population. Non-infected (M) monocyte-derived phagocytes get activated $k_a \frac{D(t)}{C_{im}+M_a(t)+M_{ai}(t)} M(t)$. Natural death of monocyte is taken into consideration $d_{M_a}M_a(t)$.

$$\frac{dM_{ai}(t)}{dt} = k_{ai} \frac{D(t)}{C_{im}+M_a(t)+M_{ai}(t)} M_i(t) + k_{ia}P(t)M_a(t) - d_{M_{ai}}M_{ai}(t) \quad (4)$$

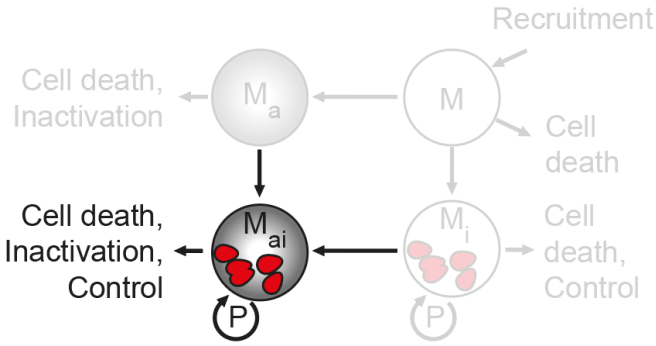

Figure 13: activated infected sub-population. Two sources contribute mainly to the infected and activated monocyte population M_{ai} population: Infected monocytes (M_i) can get activated $k_{ai} \frac{D(t)}{C_{im}+M_a(t)+M_{ai}(t)} M_i(t)$, and non-infected activated monocytes (M_a) get infected $k_{ia}P(t)M_a(t)$. Natural death of M_a is taken into consideration through $d_{M_{ai}}M_{ai}(t)$.

$$\frac{dD(t)}{dt} = k_D P(t)[1 - D(t)]D(t) \quad (5)$$

Since the scope of the model was to understand the effect of monocyte-derived phagocytes, the population of Th1 cells and their interactions with monocytes was not explicitly modeled. Instead, the time interval between infection and activation of a Th1 response was modeled with a sigmoid delay function, D(t), with rate k_D and dependent on the parasite burden.

2.1.3 Models ODEs

In order to understand the mode of *L. major* NO-mediated control, and to dissect direct killing and proliferation inhibition, as well as cell-intrinsic and extrinsic control, six hypotheses were formulated and tested.

Figure 14 shows a graphical illustration of the models.

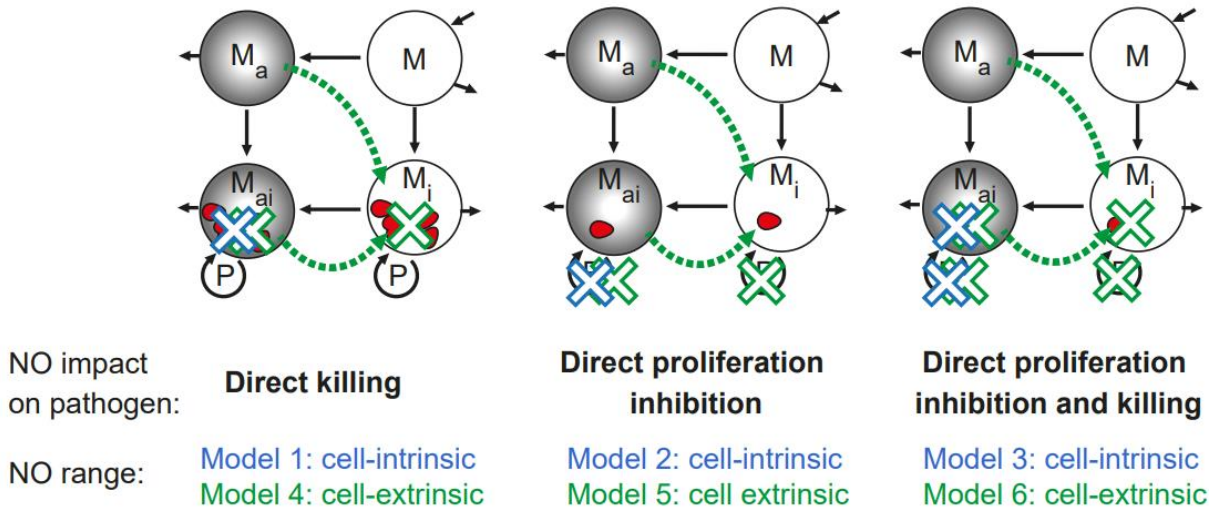

Figure 14: *L. major* containment in the different models. Blue: cell-intrinsic killing and proliferation inhibition by activated, infected cells (models 1–3). Green: cell-extrinsic killing and proliferation inhibition within all infected cells exerted by all activated cells (models 4–6).

The corresponding equations 6a-f are explained in respective figures below (figure 15-20).

$$\frac{dP(t)}{dt} = k_{\mathrm{P}}\left(1 - \frac{P(t)}{C_{\mathrm{P}}}\right)P(t)[M_{\mathrm{i}}(t) + M_{\mathrm{ai}}(t)] - k_{\mathrm{r}}P(t)M_{\mathrm{ai}}(t) - d_{\mathrm{P}}P(t) \quad (6a)$$

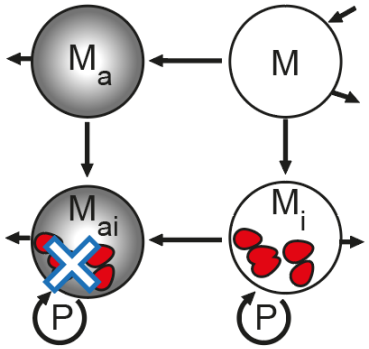

Figure 15: model 1, parasites proliferate in both infected acivated and non-activated monocyte-derived phagocytes, with the same rate $k_{\mathrm{P}}\left(1 - \frac{P(t)}{C_{\mathrm{P}}}\right)P(t)[M_{\mathrm{i}}(t) + M_{\mathrm{ai}}(t)]$. Parasites are also actively killed only by infected activated monocytes $k_{\mathrm{r}}P(t)M_{\mathrm{ai}}(t)$, and undergo death at a given rate through $d_{\mathrm{P}}P(t)$.

$$\frac{dP(t)}{dt} = k_{\mathrm{P}}\left(1 - \frac{P(t)}{C_{\mathrm{P}}}\right)P(t)[M_{\mathrm{i}}(t) + \beta M_{\mathrm{ai}}(t)] - d_{\mathrm{P}}P(t) \quad (6b)$$

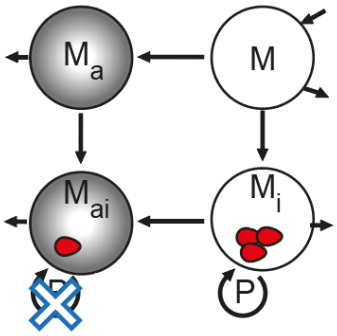

Figure 16: model 2, impaired parasite proliferation in infected activated monocytes modeled through a factor $\beta \leq 1$ through $k_{\mathrm{P}}\left(1 - \frac{P(t)}{C_{\mathrm{P}}}\right)P(t)[M_{\mathrm{i}}(t) + \beta M_{\mathrm{ai}}(t)]$. Parasites undergo also natural death through $d_{\mathrm{P}}P(t)$.

$$\frac{dP(t)}{dt} = k_{\mathrm{P}}\left(1 - \frac{P(t)}{C_{\mathrm{P}}}\right)P(t)[M_{\mathrm{i}}(t) + \beta M_{\mathrm{ai}}(t)] - k_{\mathrm{r}}P(t)M_{\mathrm{ai}}(t) - d_{\mathrm{P}}P(t) \quad (6c)$$

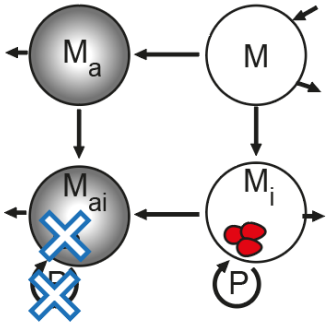

Figure 17: model 3, a combination of the previous two models, shown in figures 15 and 16.

$$\frac{dP(t)}{dt} = k_{\mathrm{P}}\left(1 - \frac{P(t)}{C_{\mathrm{P}}}\right)P(t)[M_{\mathrm{i}}(t) + M_{\mathrm{ai}}(t)] - k_{\mathrm{r}}P(t)[M_{\mathrm{ai}}(t) + M_{\mathrm{a}}(t)] - d_{\mathrm{P}}P(t) \quad (6d)$$

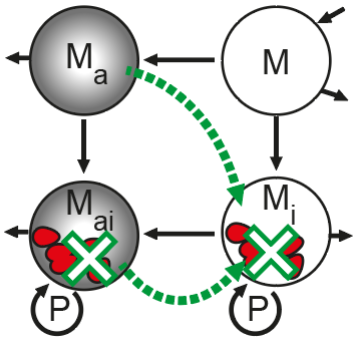

Figure 18: model 4, Parasites proliferate at the same rate in both infected non-activated and activated monocyte-derived phagocytes $k_{\mathrm{P}}\left(1 - \frac{P(t)}{C_{\mathrm{P}}}\right)P(t)[M_{\mathrm{i}}(t) + M_{\mathrm{ai}}(t)]$, parasites are not only killed by infected activated but also by non-infected activated monocyte-derived phagocytes through the term $k_{\mathrm{r}}P(t)[M_{\mathrm{ai}}(t) + M_{\mathrm{a}}(t)]$. Parasites undergo natural death through $d_{\mathrm{P}}P(t)$.

$$\frac{dP(t)}{dt} = k_{\mathrm{P}}\left(1 - \frac{P(t)}{C_{\mathrm{P}}}\right)P(t)\frac{M_{\mathrm{i}}(t)+M_{\mathrm{ia}}(t)}{C_{\mathrm{iP}}+M_{\mathrm{ai}}(t)+M_{\mathrm{a}}(t)} - d_{\mathrm{P}}P(t) \quad (6e)$$

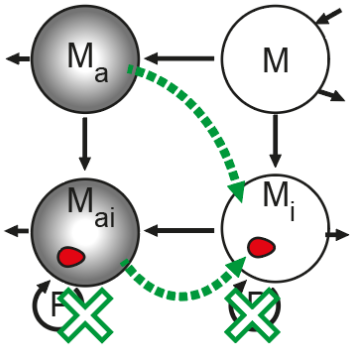

Figure 19: model 5, Impaired parasite proliferation by the presence of infected and non-infected activated monocyte-derived phagocytes through the term $k_{\mathrm{P}}\left(1 - \frac{P(t)}{C_{\mathrm{P}}}\right)P(t)\frac{M_{\mathrm{i}}(t)+M_{\mathrm{ia}}(t)}{C_{\mathrm{iP}}+M_{\mathrm{ai}}(t)+M_{\mathrm{a}}(t)}$. Parasites undergo also natural death through $d_{\mathrm{P}}P(t)$.

$$\frac{dP(t)}{dt} = k_{\mathrm{P}}\left(1 - \frac{P(t)}{C_{\mathrm{P}}}\right)P(t)\frac{M_{\mathrm{i}}(t)+M_{\mathrm{ai}}(t)}{C_{\mathrm{iP}}+M_{\mathrm{ai}}(t)+M_{\mathrm{a}}(t)} - k_{\mathrm{r}}P(t)[M_{\mathrm{ai}}(t) + M_{\mathrm{a}}(t)] - d_{\mathrm{P}}P(t) \quad (6f)$$

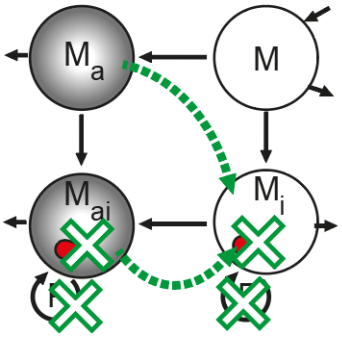

Figure 20: model 6, a combination of the previous two models, shown in figures 18 and 19.

The equations in (6a), (6b) and (6c) represent the cell-intrinsic properties. Model 1 in (6a) considers cell-intrinsic pathogen killing only, so the pathogen multiplication is taking place in the infected populations $P(t)[M_{\mathrm{i}}(t) + M_{\mathrm{ai}}(t)]$, while activated population monocyte-derived cells are killing the pathogen $-k_{\mathrm{r}}P(t)M_{\mathrm{ai}}(t)$. Model 2 in (6b) considers only cell-intrinsic pathogen proliferation inhibition, represented by the value of β in $\beta M_{\mathrm{ai}}(t)$. A mix of the two modes of action i.e. cell-intrinsic pathogen killing and pathogen proliferation inhibition is represented in model 3 (6c).

In (6d), (6e) and (6f) equations show the cell-intrinsic and -extrinsic properties. Model 4 assumes cell-intrinsic and -extrinsic pathogen killing, therefore, in contrast to model 1, killing is also dependent on $M_{\mathrm{a}}(t)$, not only $M_{\mathrm{ai}}(t)$. Model 5 represents pathogen proliferation inhibition, here, through $\frac{M_{\mathrm{i}}(t)+M_{\mathrm{ia}}(t)}{C_{\mathrm{iP}}+M_{\mathrm{ai}}(t)+M_{\mathrm{a}}(t)}$ the effect of activated monocyte populations on the infected populations is shown. In model 6 (6f), both pathogen killing and proliferation inhibition is assumed.

The estimation of the parameters of the models by numerical optimization required experimental data. In particular, the temporal evolution of pathogen burden and proportion of activated and infected sub-populations were required. Consequently, we performed infection experiments as shown in 2.1.4

2.1.4 Obtaining experimental data

Low dose infection data (mentioned above 1.4 provided by Pauline Formaglio, current affiliation: Institut Pasteur Paris) and high dose infection data (generated in the course of this work) were used to fit the models with experimental infection data (Formaglio, Alabdullah et al. 2021). For this, C57BL/6 mice were infected in the ear dermis with 2 x 10^6 *L. major* dsRed stationary phase in the high dose model, whereas an infection of C57BL/6 mice with 5x10^3 metacyclic *L. major* parasites was used in the low dose model. For the high dose model, animals were killed after 1, 3, 5, 7, 11 and 15 weeks post infection (figure 21A), and ears were used for limiting dilution assays in order to assess the pathogen burden within the infected ears. In parallel, ear-extracted cell suspensions were analyzed via flow cytometry (gating strategy figure 21B) to define the activation and infection status of the monocyte-derived cells in the infection site at different time points.

A

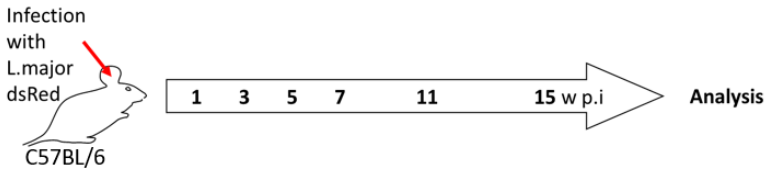

B

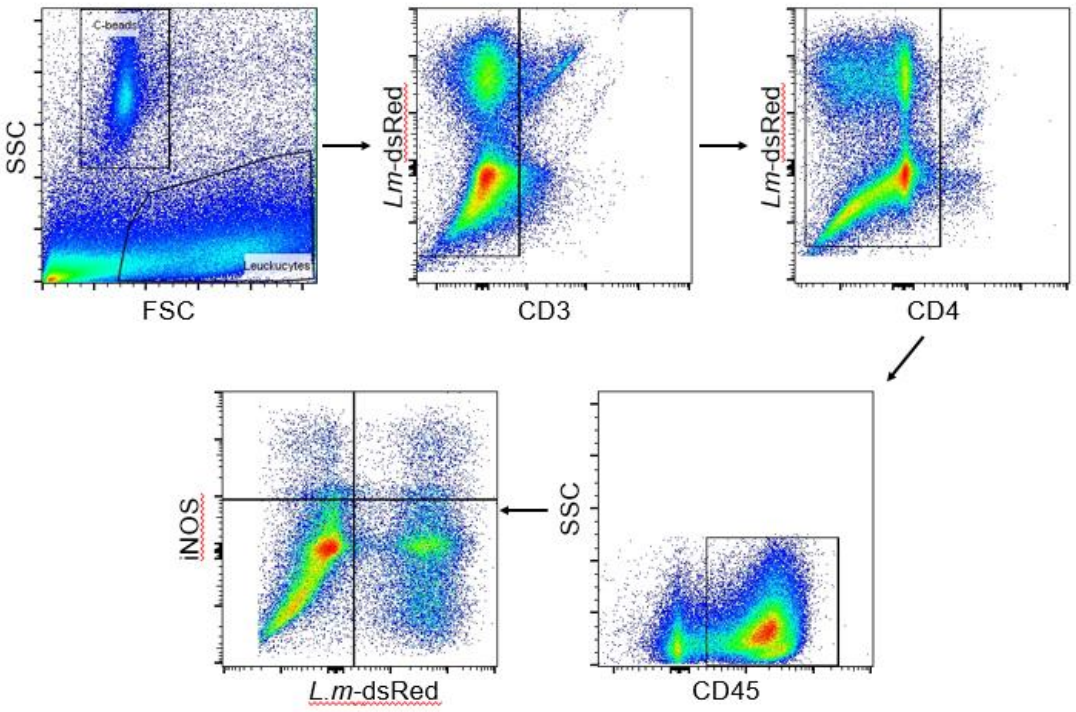

C

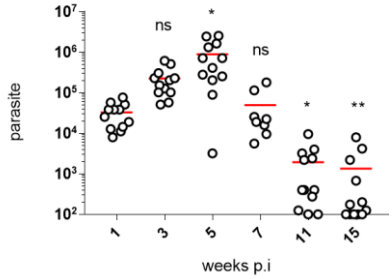

D

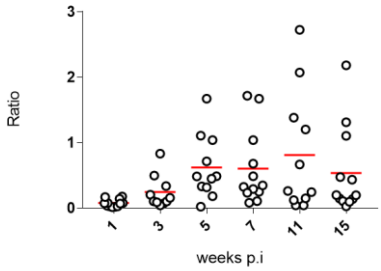

E

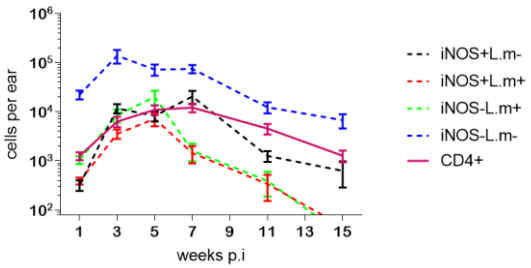

Figure 21: *L. major* high dose infection. A, experimental setup. B, gating strategy. C, pathogen burden time course. D, isolation bias time course. E, activated/infected as well CD4+ sub-populations over the course of infection. **p < 0.01; *p < 0.05; ns, not significant, according to Kruskal-Wallis with Dunn's post-test (comparison with 1 wpi data). Each symbol represents one infected ear. Horizontal bars denote the mean. Mean with SEM representation is shown in E, sample size is 10 to 12 ears per

population per time point. Data cumulated from five independent experiments.

While in the low dose model (see figure 7E- H) a peak in pathogen burden and immune activation was observed at week 7 to 9 p.i., in the high dose infection model, the infection reached its peak in term of pathogen burden and immune activation around week 5 p.i and then dropped slowly toward week 15 p.i to very low pathogen numbers (figure 21C and E). Our finding is in line with previous reports which showed that a higher pathogen load (resulting from parasite inoculation with sand fly salivary protein) is capable to speed up the kinetics of the course of infection (Belkaid, Kamhawi et al. 1998); (Guimaraes-Costa, Shannon et al. 2021).

Microorganisms are known to cause tissue damage, directly by the microorganism itself and indirectly as a result of the immune response (Nash, Dalziel et al. 2015). We have also shown that *L. major* is capable of changing the infection site architecture differently over the course of infection (see figure 7I), which might, especially in high dose infections with rapid changes, impact on the isolation efficiency of immune cells used for analysis. Consequently, in order to check the reliability of the cells extraction processes over the course of infection, we sought to compare the pathogen numbers in the ears samples (measured using limiting dilution assay (LDA)) with pathogen numbers inferred by flow cytometry measurements. In order to do so, we assumed that the maximal possible pathogen number within a single infected monocyte-derived cell to be 50. This assumption is based on previously published data of confocal imaging of the site of infection, in which it could be concluded that the parasite diameter is around 3 µm while a phagocyte is in the range of 20 µm (Heyde, Philipsen et al. 2018). We assumed also that at the peak of the infection (5 weeks p.i) the infected monocytes-derived cells would be almost filled with pathogens. If we defined the dsRed mean fluorescence intensity (MFI) of the single infected Monocytes-derived cell at this time-point (using counting beads in the samples), we would be able to define single pathogen fluorescence intensity. After that, the total number of pathogens in an infected ear was calculated back, by dividing the dsRed MFI value of each ear sample on the single pathogen FI. The isolation bias (IB) is *L. major* pathogen numbers measured via flow cytometry divided on *L. major* pathogen numbers measured via dilution assay, figure 21D shows the change of this IB over the course of infection. Interestingly, we found that IB is higher at 5, 7 and 11 wpi, in comparison to the early

and late stage of infection, suggesting that the cell extraction processes is more efficient around the peak of infection/immune response.

2.1.5 Fitting the ODE models to experimental data

According to the gating strategy shown in figure 21B, we had defined the four sub-populations of monocyte-derived cells at the site of infection. The absolute numbers of cells in each sub-population were defined using counting-beads, and the numbers were corrected using the average isolation bias value identified for each different time point (figure 21E). Then, the models parameters were estimated by numerical optimization based on these experimental data of *L. major* burden, infection and activation in collaboration with Sebastian Binder and Anastasios Siokis from the laboratory of Michael Meyer-Hermann at the Helmholtz Centre for Infection Research Braunschweig. The initial population of non-infected non-activated M(0), and *L. major* burden P(0), were estimated because their amount is not known at the time of infection. The remaining populations $M_i(0)$, $M_{ia}(0)$ and $M_a(0)$ were assumed zero initially. All other parameter values (mentioned above in table 1) for the six models were optimized.

Selection of the best model was done upon the calculation of the corrected Akaike information criterion (AICc) which evaluates model quality based on both quality of fitting and the number of free parameters (Zhao, Wirth et al. 2017). AICc was calculated by the following formula:

$AICc = 2P + RSS^2 + N\,log(2\pi) + 2\frac{P(P+1)}{N-P-1}$, where P is the number of fitted parameters and N the number of data points. RSS the normalized residual sum of squares was calculated by the following formula, $RSS = \frac{\sum_i (y_i - f(x_i))^2}{max(y_i)}$, where y_i is the experimental mean value for each data point, and $f(x_i)$ is the ODE solution.

Individual models fitting results are shown in figures 22-27.

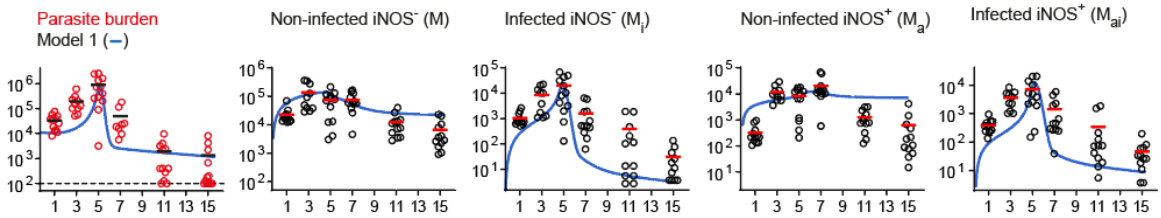

Figure 22: model 1 fitting, 20 parameters; RSS (cost) 1,38; AICc 159,18. Model one is capable of predicting raise, peak and drop of the parasite burden, M, Mi and Mai. Although the model well represented raise and peak of Ma population, it predicts a longer

lasting activation. However, Model 1 cannot be rejected according to cost or $e^{2*\Delta(\mathrm{AICc})}$ value.

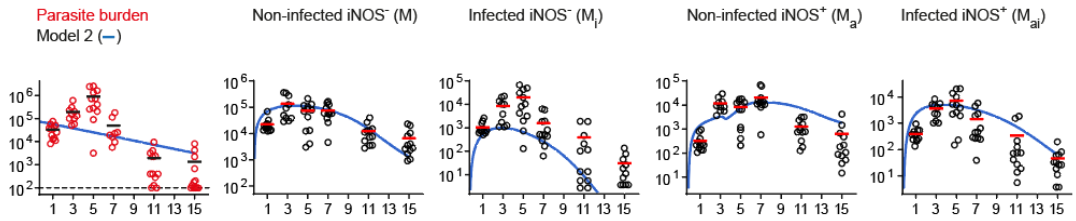

Figure 23: model 2 fitting, 20 parameters; RSS (cost) 2,76; AICc 164,92. Although model 2 can represent M, Ma and Mai population progression over the course of infection, it predicts lower and faster progression of M_i, and it is not able to show the kinetics of parasite burden. Model 2 is rejected due to the $e^{2*\Delta(\mathrm{AICc})}$ value.

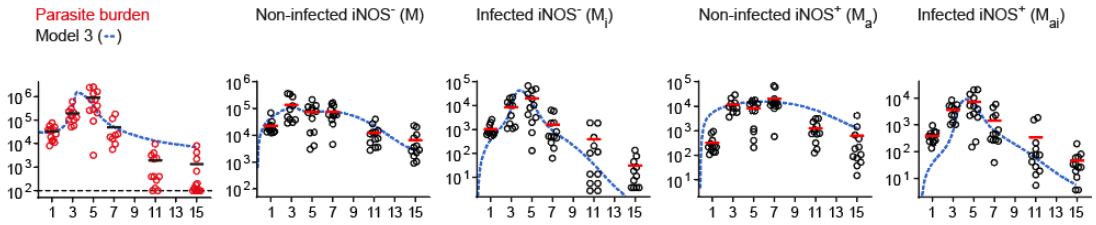

Figure 24: model 3 fitting, 21 parameters; RSS (cost) 0,97; AICc 182,38. Model 3 predicts very low numbers of infected cells in the late phase in term of M_i. Model 3 is rejected due to the $e^{2*\Delta(\mathrm{AICc})}$ value.

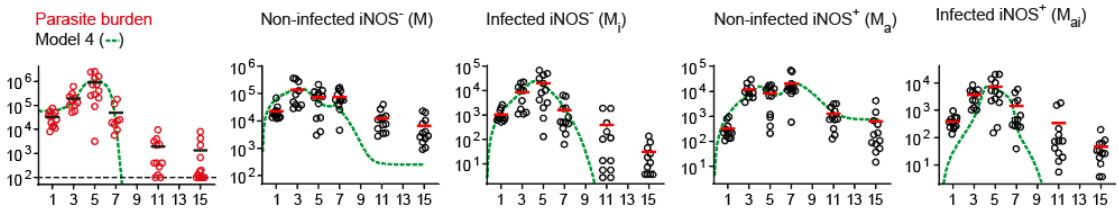

Figure 25: model 4 fitting, 20 parameters; RSS (cost) 0,5; AICc 157,53. Model 4 predict the progression of the studied populations very accurately for the first half of the infection. Therefore, despite it predicts sterile immunity in the late phase of the infection, it shows the best overall fitting and cannot be rejected according to the $e^{2*\Delta(\mathrm{AICc})}$ value.

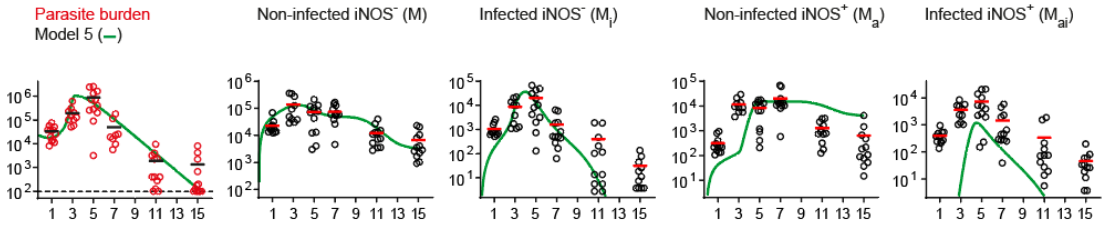

Figure 26: model 5 fitting, 20 parameters; RSS (cost) 2,06; AICc 161,53. Model 5 perdicts high values for the M_a population at the late phase, delayed increase especially of the M_a and M_{ai} populations and strongly blunted M_{ai} presence. Model 5 is rejected due to cost and $e^{2*\Delta(\mathrm{AICc})}$ value.

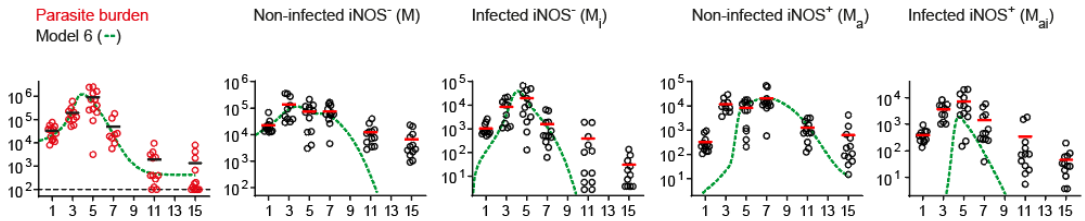

Figure 27: model 6 fitting, 21 parameters; RSS (cost) 1,73; AICc 184,46. Model 6 has 21 parameters, also it shows, as model 5, delayed increase of the M_a and M_{ai} populations and blunted M_{ai} presence. Model 6 is rejected due to the $e^{2*\Delta(\mathrm{AICc})}$ value.

The fitting suggested that cell-intrinsic models relied on a long-lasting presence of non-infected, activated monocytes (M_a) that was higher than in the experimental data, as only activated cells can control the parasite if infected. In contrast, cell-extrinsic models showed a faster decrease and lower amplitude of infected activated monocytes (M_{ai}) than observed experimentally, which could be explained by the fact that in such models, the infection could be controlled theoretically exclusively by non-infected activated cells (M_a).

As the course of pathogen burden and the immune reaction have been shown to evolve at different speeds depending on the initial infection dose, fitting was also performed with a low dose infection in a parallel work in our group (pathogen burden data replotted from figure 7E), similar results were obtained (figure 28) (Formaglio, Alabdullah et al. 2021).

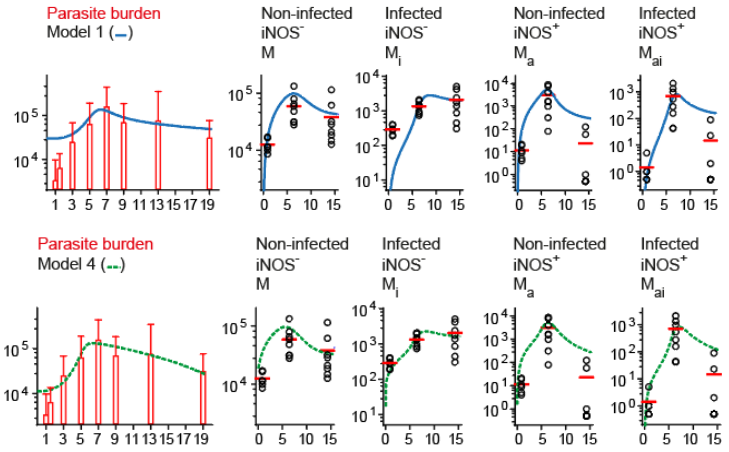

Figure 28: Low dose infection models fitting. Model 1: parameters 20; RSS (cost) 0,77; AICc 209,06. Model 4: parameters 20; RSS (cost) 1,7; AICc 208,95. Note that the prominent difference in the early occurrence of infected, non-activated M_i in model 1 versus model 4, is also observed in the high dose model.

Overall, models 1 and 4 explained best the events progress over the course of infection both regarding the quality of the model (represented by AICc value) and the low cost of fitting (figure 29). This suggested that killing of the pathogen alone, but not proliferation inhibition, could be sufficient to explain a dominant direct effect of iNOS on the pathogen control, with pathogen proliferation being mainly dependent on the availability of recruited monocyte-derived phagocytes.

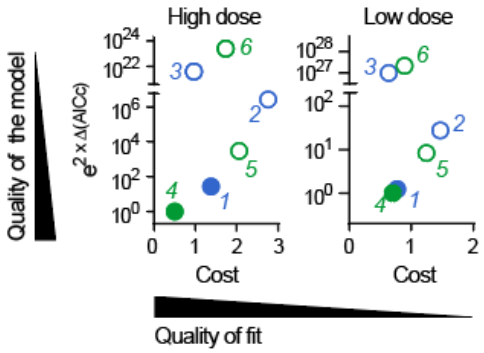

Figure 29: Costs of fitting plotted against quality of the model determined as a function of the AICc (corrected Akaike information criterion). Low-cost, high-quality models appear in the lower left corner of the graphs. The AICc of the model with the lowest AICc (model 4) was set to 0. The models that cannot be excluded by $e^{(2 \times \Delta AICc)}$ are represented by filled circles; all other models are represented by empty circles.

We also examined the models fitting with data from viability and proliferation reporter systems (obtained in the low dose infection by Pauline Formaglio). Simulation of parasite death and parasite proliferation in the mathematical models involving only pathogen killing recapitulated the evolution of dying and proliferating parasite fractions measured over the course of infection better than models involving direct proliferation inhibition (figure 30), performed by Anastasios Siokis (Helmholtz Centre for Infection Research Braunschweig).

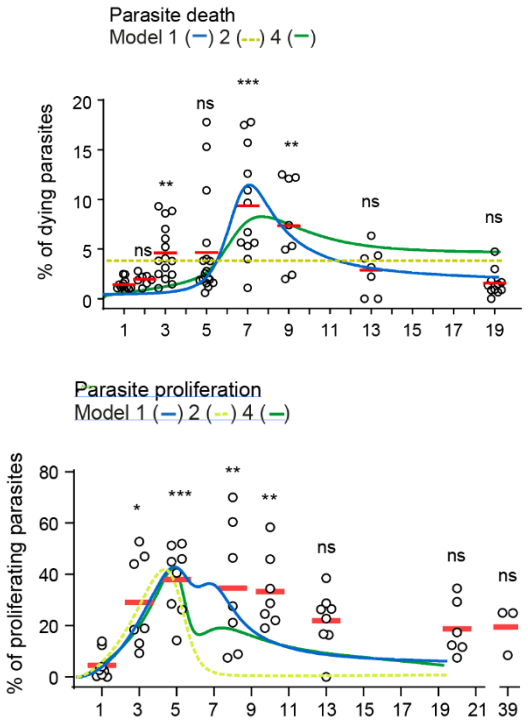

Figure 30: death and proliferation reporters models fitting. Data from Figure 7 (B and D) were fitted into models 1, 2 and 4.

2.2. Part II. iNOS inhibition increases pathogen growth due to higher monocyte recruitment

Our results from model selection showed that the direct effect on the pathogen exerted by iNOS is mainly killing. In contrast to this finding, earlier work had established a connection between pathogen proliferation and NO presence in the site of infection (Müller, Aeschlimann et al. 2013). Also, Heyde *et al*. have shown the importance of monocytes (namely $CD11c^{+}Ly6C^{+}CCR2^{+}$) on the parasite's ability to undergo cycles of replication and as a niche of intracellular proliferation (Heyde, Philipsen et al. 2018). Alongside with previous results from the *in vivo* reporters (figure 7D) suggesting low pathogen proliferation in the persistent phase. We hypothesized that the proliferation rate of the pathogen could be linked to the presence of infectable monocytes rather than to direct NO effects on *L. major*. In line with this, we speculated that pathogen proliferation inhibition via NO might be mediated by a blockade of immune cell recruitment into the site of infection, which has been shown to be an important immunomodulatory mechanism (Kubes, Suzuki et al. 1991); (Kubes, Sihota et al. 1997); (Postat, Olekhnovitch et al. 2018).

To date, iNOS inhibition experimentation did not dissect the different NO effects. Therefore, while blocking of iNOS was shown to have effects on pathogen over the course of the infection and pathology, these readouts were the combined result of changes in pathogen killing, pathogen proliferation and monocyte recruitment. In this work, we have dissected killing and proliferation inhibition contribution by experimental optimizing of ODE models, but it has not been shown experimentally whether iNOS-mediated proliferation inhibition is due to the altered availability of infectable monocytes.

In order to test if pathogen proliferation inhibition is mediated by blockade of immune-cells recruitment, we blocked leukocyte extravasation using anti-CD18/CD49d antibodies while at the same time inhibiting iNOS using the inhibitor L-NIL. This allowed us to check which aspect of iNOS inhibition is reversible by the absence of recruitment of the permissive cellular compartment. In this context, leukocytes recruitment, pathogen proliferation, ear thickness and pathogen burden were measured.

2.2.1 Recruitment

In order to verify that our experimental system is capable of blocking monocyte recruitment caused by iNOS inhibition, we set out to detect newly recruited monocytes in the site of infection by using a photoconvertible fluorescent protein-expressing

mouse model (Heyde, Philipsen et al. 2018). For this, Tg(CAG-KikGR)33Hadj/J mice which constitutively express a green-to-red photoconvertible fluorescence protein were infected with *L. major* WT (non-fluorescent) parasites (high-dose). At day 19 p.i the site of infection was photoconverted, and 2 days later (3 weeks p.i) the ears were harvested and processed for flow cytometry measurement. In this system, newly recruited monocytes present in the lesion for less than two days would appear green, whereas cells present in the lesion at the time of photoconversion were red fluorescent. Figure 31A is showing the experimental setup and figure 31B the gating strategy.

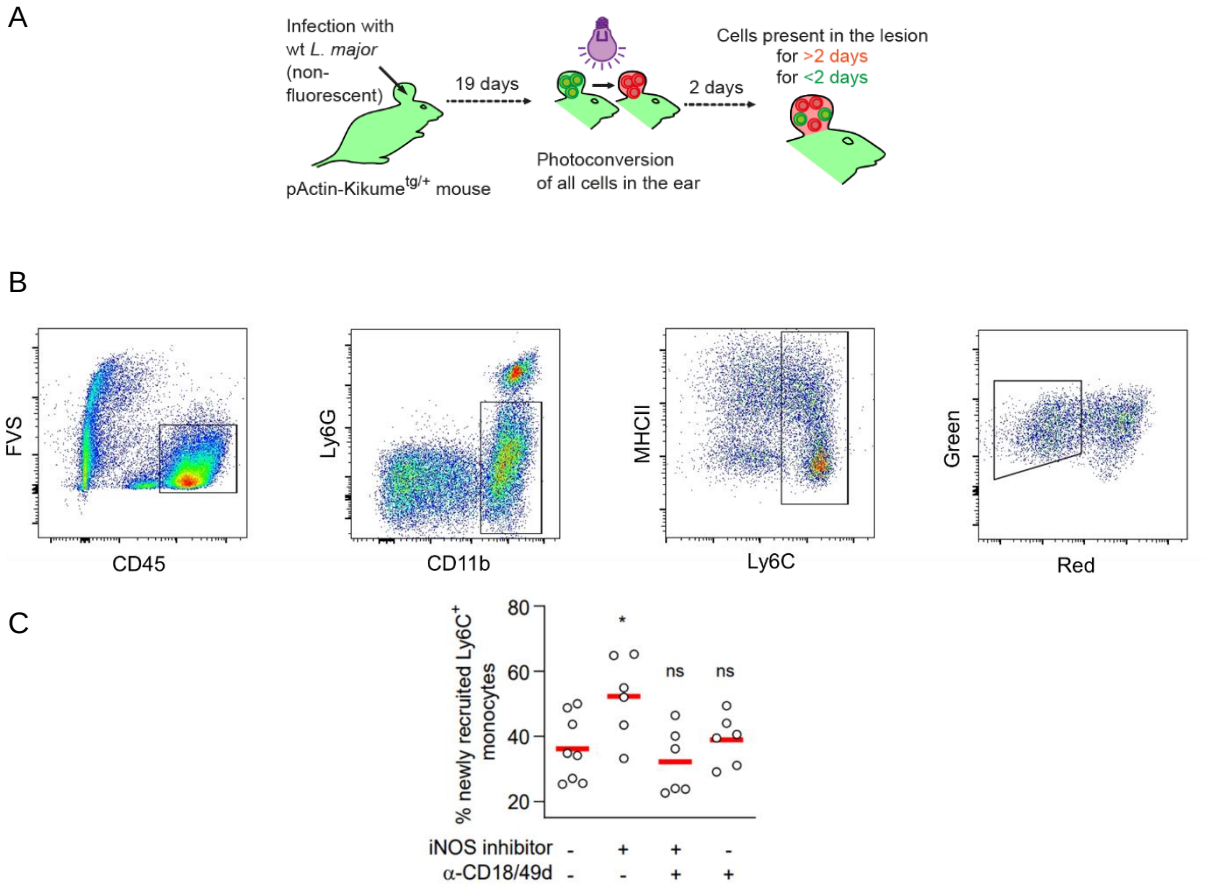

Figure 31: monocytes recruitment in KikGr mice. A, experimental setup (FVS, fixable viability stain). B, gating strategy. C, Fraction of Ly6C+ cells recruited within the last two days before analysis. Each dot represents an individual ear, data pooled from two independent experiments. ns, not significant; *p < 0.05, according to Kruskal-Wallis with Dunn's post-test (comparison with control (no treatment)).

As shown in figure 31C, an increase in the proportion of newly recruited monocyte-derived Ly6C+ phagocytes in iNOS-inhibited mice was detected, whereas anti-

CD18/CD49d injection blunted the recruitment even if iNOS was inhibited. Of importance, anti-CD49/CD18 alone does not change the percentage of newly recruited cells, probably because of the present effect of iNOS which already strongly block this recruitment.

2.2.2 Ear thickness and pathogen burden

As we had confirmed in our experimental model that iNOS inhibition is indeed accompanied by increased monocyte-derived cell recruitment, which is reversible by the injection of anti-CD18/CD49d, we sought to investigate a possible recruitment related change in ear thickness, pathogen burden or infection rate. Consequently, we run parallel experiments using the experimental settings shown in figure 32A in order to measure the ears thickness (figure 32D), the pathogen burden using LDAs (figure 32E), and to define different cell populations via flow cytometry (gating strategy shown in figure 32B). We were able to show a significant effect of iNOS inhibition on ear thickness, which was reversible by the additional injection of anti-CD18/CD49d. Importantly, we were also able to show a higher percentage of infected cells in the recruitment blockade conditions, which might be caused by the absence of “dilution” of infected monocytes of the newly recruited cells (figure 32C).

Although we were able to show a reversible effect of iNOS inhibition in term of ear thickness, the pathogen load showed no significant differences among the studied groups, only a trend of higher burden under the activation inhibition conditions was observed. When we simulated the activation inhibition and/or recruitment blockade in the two favorable mathematical models (models 1 and 4), we observed the same out-come regarding pathogen burden, i.e. an increase by inhibition of activation, but no difference upon blocking of recruitment (figure 32F and G). This suggested that the effect of activation inhibition on the pathogen numbers might be faster than the recruitment inhibition effect. The recruitment inhibition effect on pathogen numbers is expected to require longer to occur due to many recently recruited phagocytes left at the site of infection, whereas, iNOS dependent pathogen killing is taking place directly considering the short half-life of seconds of NO (Thomas, Liu et al. 2001).

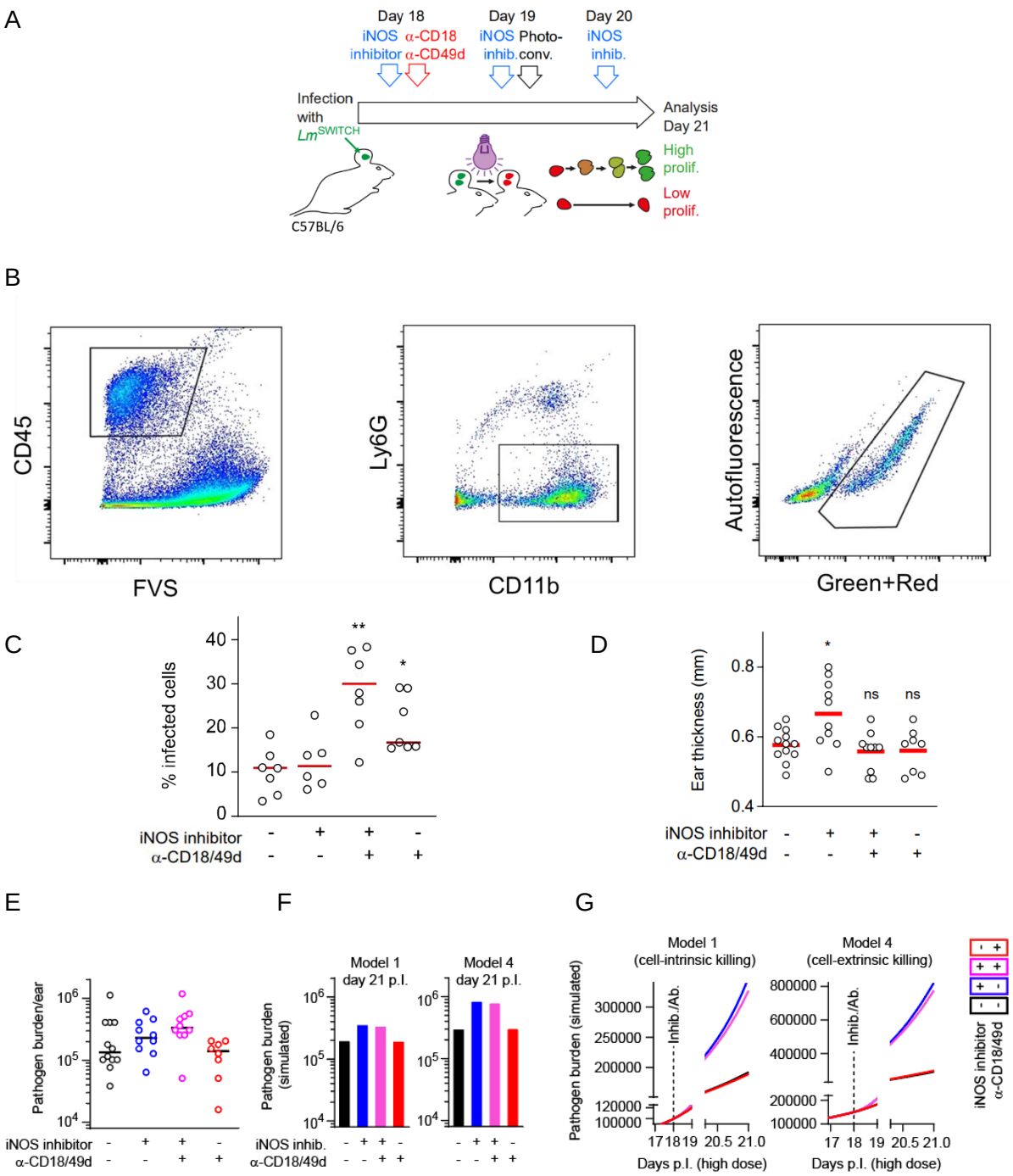

Figure 32: Recruitment related changes. A, experimental setup. B, gating strategy used to obtain data in C. C, Fraction of infected cells, data are pooled from 2 independent experiments. D, Ear thickness at day 21. E, pathogen burden determined experimentally using limiting dilution analysis. Data in D and E are pooled from 4 independent experiments. F, Simulated pathogen burden in the ODE model of cell-intrinsic killing (left panel) or cell-extrinsic killing (right panel). Simulated *L. major* numbers shown at day 21 p.i. for untreated (black bars), activation-inhibited (blue

bars), recruitment-inhibited (red bars) or a combined inhibition (pink bars) conditions, with treatment initiated at day 18 p.i. G, Simulation of pathogen burden in the ODE model of cell-intrinsic (left) or cell-extrinsic (right) killing of L. major in untreated (black curves), activation-inhibited (blue curves), recruitment-inhibited (red curves) or combined inhibition (pink curves) for three days, starting from day 18 p.i. Each circle represents one infected ear. Horizontal bars denote the median. ns, not significant; *p < 0.05; **p < 0.01, according to Kruskal-Wallis with Dunn's post-test (comparison with control (no treatment)).

2.2.3 Pathogen proliferation

In order to determine the impact of recruitment inhibition on pathogen proliferation, we measured *L. major* proliferation rate using our well-established *in vivo* reporter, under the same conditions by intravital 2-photon microscopy. For this, C57BL/6 mice were infected with *Lm*^{SWITCH} (high dose), L-NIL (iNOS inhibition) was administered intraperitoneally (IP) for three days (at day 18,19 and 20 p.i), whereas cells recruitment inhibition (anti-CD18/CD49d) was administered IP on day 18, according to the experimental scheme shown in figure 32A.

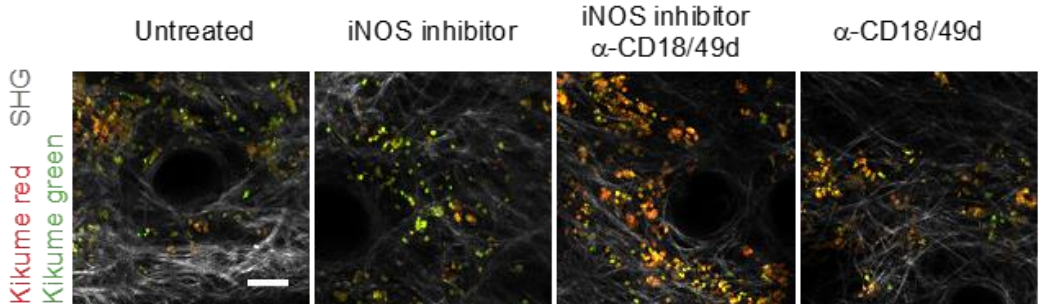

Figure 33: Parasite proliferation IV-2PM data. Scale bar, 20 mm. Segmented red and green channels and collagen (second harmonic) SH signals (gray) are shown from one z plane of a three-dimensional image.

On day 21 p.i we acquired large field IV-2PM images before, 0h after, and 48h after photoconversion (figure 33). The obtained images were then rough segmented according to a summed up channel of mKikume red and green using the Imaris software. Afterwards, we exported and converted the positions and fluorescence properties of the segmented cells (including autofluorescent objects) to cytometry files

using the DiscIt software (Moreau, Lemaître et al. 2012). Next, we filtered out autofluorescent objects (such as hair follicles and keratinocytes) by excluding objects with a low mKikume green 520/540 nm ratio (Müller, Aeschlimann et al. 2013), also objects exhibiting high fluorescence above 625 nm as compared to mKikume red emission (560-620nm) were excluded from the analysis (figure 34).

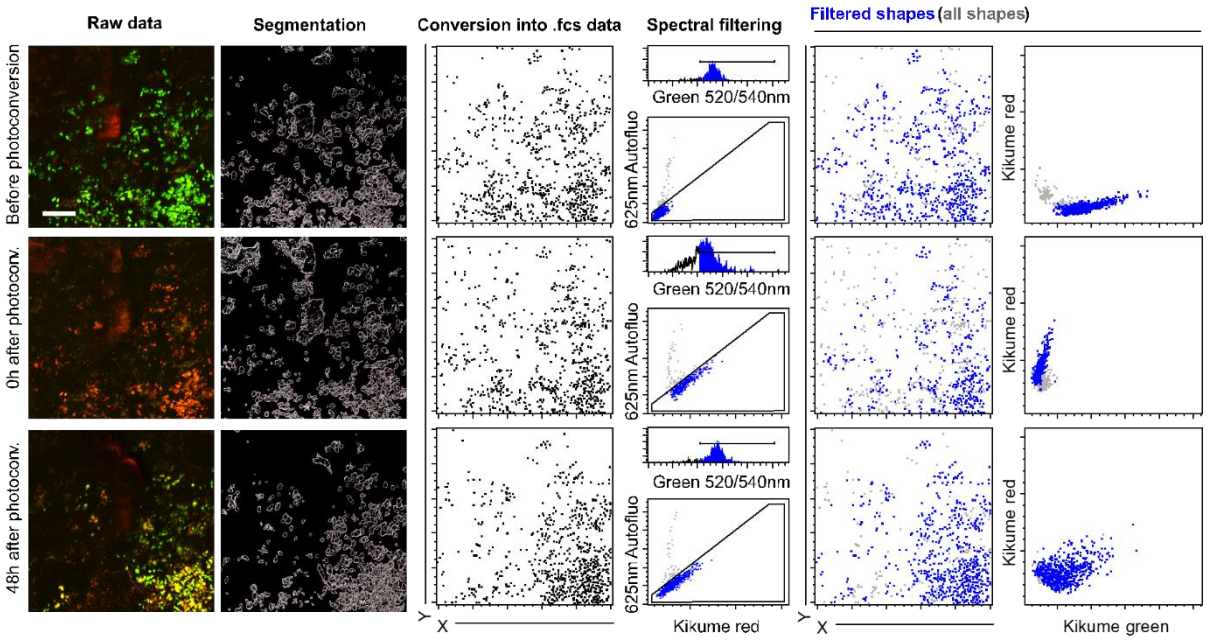

Figure 34: Fluorescence data extraction and filtering strategy. An example of data from the same site of imaging before (top), 0 h after photoconversion (middle) and 48h after photoconversion (bottom) is shown. Segmented shapes from the Imaris software are shown, which were converted into flow cytometry data. Spectral filtering was done sequentially, first selecting objects with a high ratio of 520/540 nm emission, and then selecting objects with a high Kikume Red (560-625 nm) to far red autofluorescence (>625 nm) ratio. Positively selected populations are shown in blue. Scale bar, 50 µm.

In order to compensate for tissue depth and photoconversion differences between the different imaged sites, the resulting filtered datasets were normalized in order to ensure comparability. The normalization was done using following strategy (figure 35) to align the fluorescence values before and 0h after photoconversion: The median green and red fluorescence values below the 10^{th} and over the 90^{th} percentile of the preconversion controls and the 0h after photoconversion controls were determined

(white-filled circles) and the linear regression (hairline) between the respective median coordinates was determined (figure 35A). Preconversion controls, 0h after photoconversion controls, and 48h after photoconversion values were then drift transformed in a way the linear regression curves ran through the 0/0 (dashed crosshair) coordinate (figure 35B). Subsequently, Cartesian coordinates were turned into angular coordinates, and were normalized in a way that the slope angle of the linear regression of the control before photoconversion (green) became 0, and the slope angle of the 0h after photoconversion (red) control was 90° (figure 35C). Then, the datasets were normalized between 0 and the 90th percentile of the control values (figure 35D).

Figure 36 shows a summary of the obtained results.

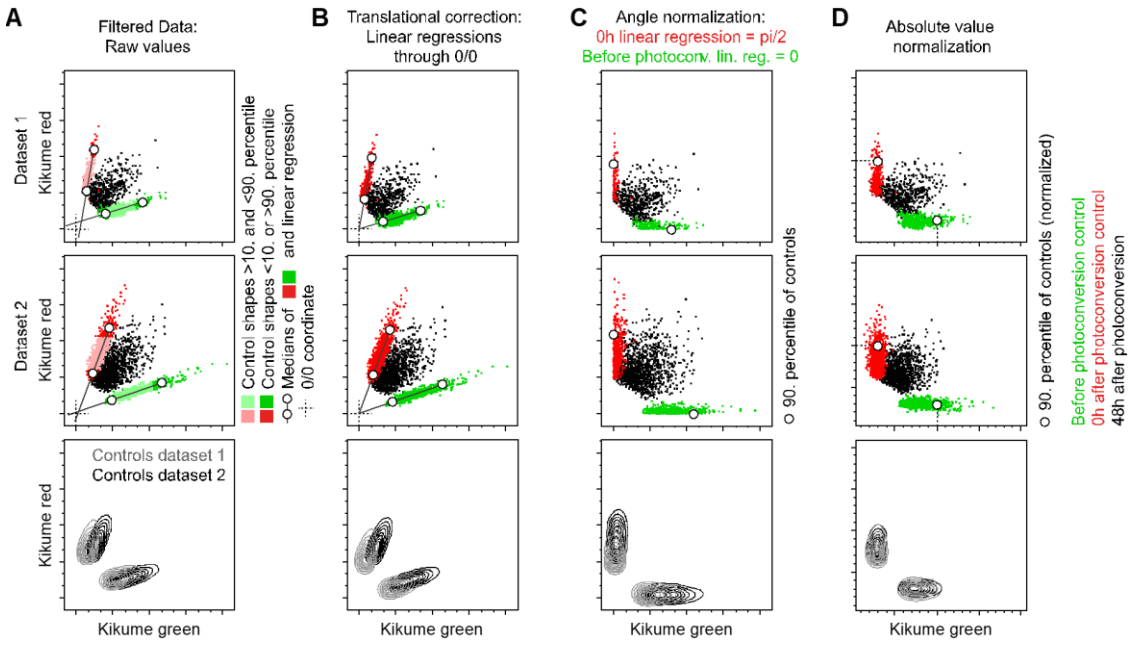

Figure 35: Quantification of pathogen proliferation. A. Determination of slopes of the preconversion (green) and 0 h after photoconversion (red) control populations by determining the median (circles) red and green values of the 10th and 90th percentile in the control populations (percentiles determined according to the Kikume green in the preconversion control, according to Kikume red in the 0h after photoconversion control). The data of two independent examples (top and middle panel) are shown, as well as the overlay of the contour plots of the preconversion and 0h after photoconversion control (bottom panel). B. Lateral correction: linear regression curves run through 0/0 (dotted lines). C. Angle normalization: linear regression curves of

preconversion and 0h after photoconversion controls run at a slope angle of 0 and pi/2, respectively, through the 0/0 coordinate. Circles denote the 90th percentile red fluorescence of the 0h after photoconversion and 90th percentile green fluorescence of the preconversion control. D. Normalization of the data to the 90th percentile of the control fluorescences.

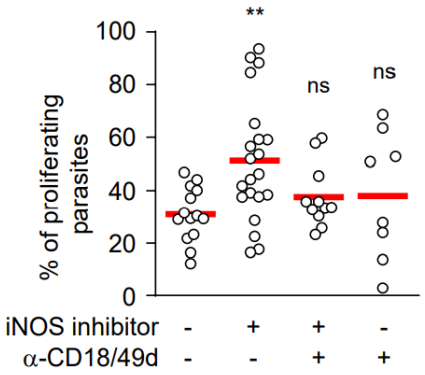

Figure 36: Effect of blocking monocyte recruitment. Fraction of proliferating parasites. Each symbol represents one imaged area. Data from at least 8 imaged areas acquired in three independent experiments.

Strikingly, we observed that iNOS inhibition resulted in an increase in pathogen proliferation rate, which could be reversed by injection of anti-CD18/CD49d, indicating that iNOS-dependent inhibition of recruitment of monocyte-derived cells is contributing to the increase in pathogen proliferation.

2.3. Part III. Dissecting different iNOS-dependent functions and their impact on pathogen proliferation

It has been shown that NO is capable of suppressing the respiratory capacity of monocytes: WT macrophages engage glycolysis but stop relying on oxidative phosphorylation upon activation, while iNOS deficient macrophages use both respiration and glycolysis upon activation (Postat, Olekhnovitch et al. 2018). NO anti-microbial activity might therefore be exerted in part by disrupting parasite respiration, activated phagocytes in this context might be capable of partially avoiding the respiration disrupting effect (Pearce and Everts 2015). Also, it has been shown that NO is capable of restricting monocyte-derived cell activity as measured by TNF-α, CCL2, and CCL3 independently of pathogen burden (Postat, Olekhnovitch et al. 2018). Consequently, we wanted to test if metabolic reprogramming, and the resulting change in the cytokine micro-milieu could be contributing to the increased pathogen proliferation caused by iNOS inhibition.

2.3.1 Metabolic reprogramming

Mitochondrial respiration, which involves cellular consumption of oxygen, and glycolysis, which involves efflux of protons, are the two major pathways for mammalian cells to produce energy (Kelly and O'Neill 2015). By detecting extracellular changes in these analytes, conclusions can be drawn regarding the rates of cellular respiration and glycolysis. As shown previously (Postat, Olekhnovitch et al. 2018), iNOS inhibition augmented oxidative phosphorylation, while cells from infected control animals mainly engaged glycolysis.

In order to test if the metabolic reprogramming of host cells during iNOS inhibition impacts on the pathogen proliferation dependently of the blockade of cell recruitment, phagocytes isolated from *Lm*^{SWITCH} (high dose) infected control mice, L-NIL treated (iNOS inhibition) and L-NIL+anti-CD18/CD49d treated mice (iNOS inhibition and blocked recruitment) were subjected to metabolic flux analysis. The experiment was done in collaboration with Yan Fu, Ina Sauerland and Anna Krone.

While we could observe an increase in oxygen consumption indicating an augmented oxidative phosphorylation upon iNOS inhibition, the additional blockade of recruitment did not alter the effect of iNOS inhibition on cellular metabolism (figure 37). Therefore, we concluded that the decreased pathogen proliferation upon a blocked recruitment of monocytes was independent of the metabolic reprograming of the host cells.

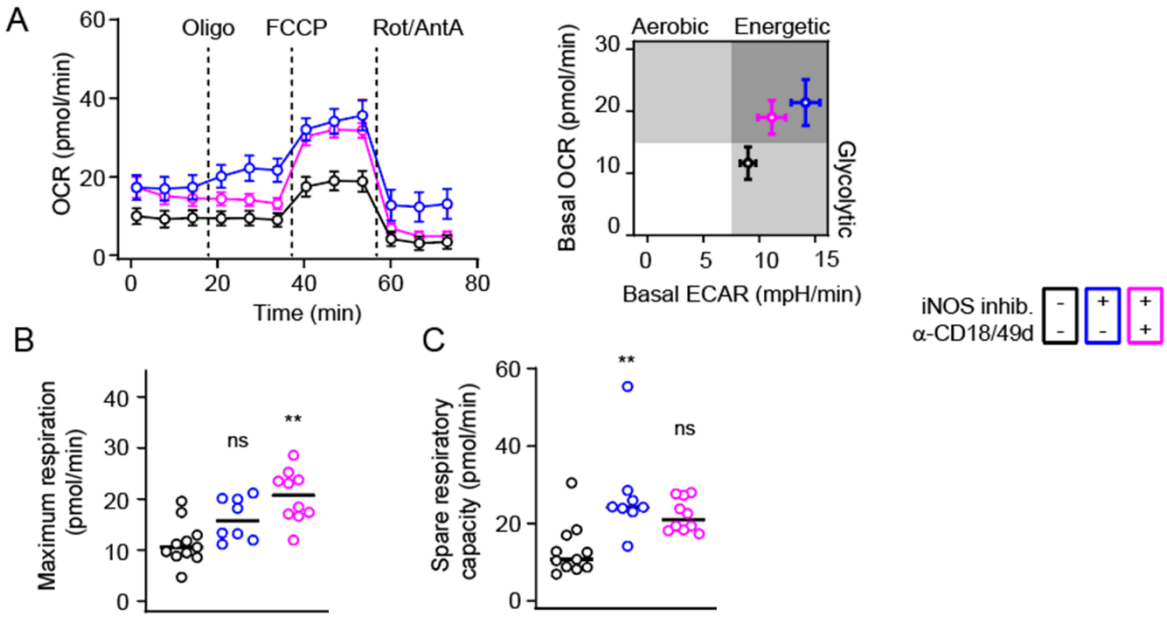

Figure 37: Metabolic flux analysis of monocyte-derived cells isolated from the infected ear tissue at 3 weeks p.i. A, left: oxygen consumption rate (OCR) in cells from control (black), L-NIL-treated (blue) and L-NIL and anti-CD18/CD49d-treated (magenta). Right: basal OCR and extracellular acidification rate (ECAR). Circles show the mean ± SEM of at least 5 replicates, consisting of pools of isolated monocytes normalized to 10^5 viable cells, collected in three independent experiments from 16 infected ears per group. B, Maximum respiration. C, spare respiratory capacity. Each circle shows one replicate of 10^5 pooled viable cells, collected in three independent experiments from 16 infected ears per group in total. Horizontal bars denote the median. ns, not significant; **p < 0.01, according to Kruskal-Wallis with Dunn's post-test (comparison with control (no treatment) condition).

2.3.2 Cytokines micro-milieu

It has been found previously that through metabolic reprogramming, NO produced at the site of infection dampens the production of cytokines and chemokines by monocyte-derived cells (Postat, Olekhnovitch et al. 2018). Consequently, as our data indicated that iNOS-dependent inhibition of recruitment of monocyte-derived cells is contributing to the increase in pathogen proliferation, we wanted to check if the cytokine micro-milieu could be responsible for the increased pathogen proliferation observed under iNOS inhibition.

IL1β is a central mediator of pro-inflammatory responses (Dinarello 2011), and NO was shown also to affect the production of IL1β (Mishra, Rathinam et al. 2013). Thus, in order to check IL1β levels under activation/recruitment inhibition, we measured the expression of the IL1β gene by quantitative PCR (in collaboration with Ina Sauerland), and the production of IL1β in the cells via flow cytometry (figure 38A). Again, in both experiments, inhibition of iNOS resulted in increased gene expression and production of IL1β. Experimental conditions with additionally impaired phagocyte recruitment showed the same level of IL1β as activation inhibition (figure 38B). Thus, the changes in parasite proliferation occurred independently of the expression of IL1β.

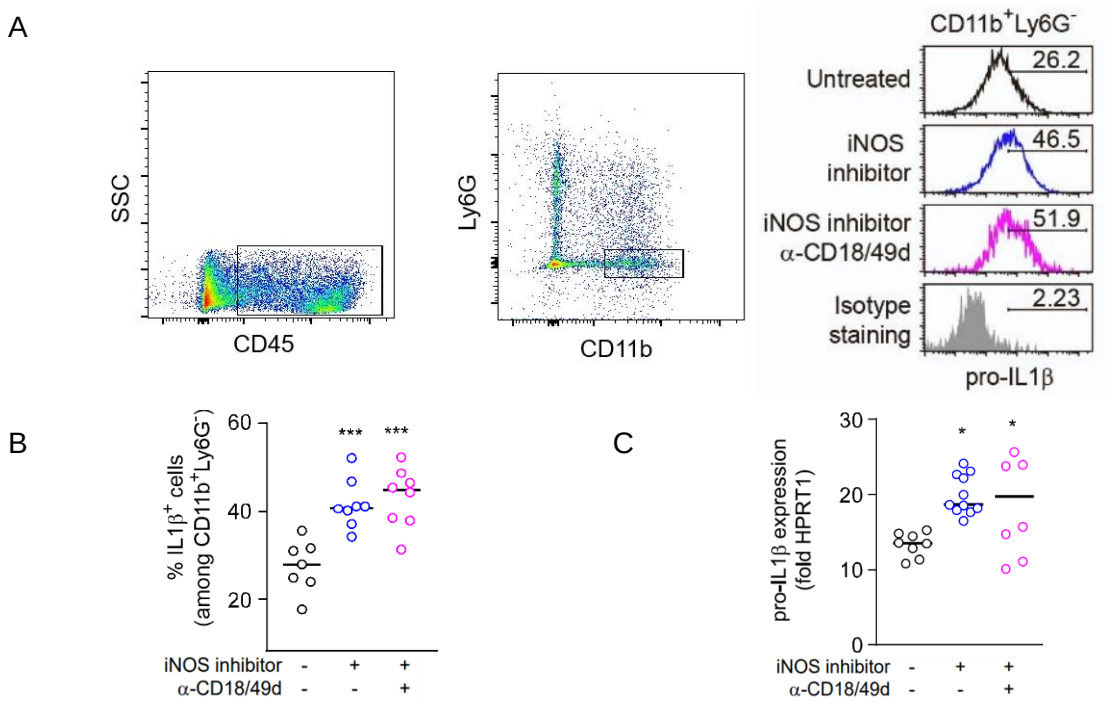

Figure 38: IL1β levels under activation/recruitment inhibition. A, Flow cytometry analysis of pro-IL1β in CD11b+Ly6G-phagocytes isolated from the site of infection of control (black), L-NIL treated (iNOS inhibition, blue) and L-NIL/anti-CD18/49d treated (pink) infected mice. B-C, Flow cytometry (B) and quantitative PCR (C) of pro-IL-1β expression by monocytes as described in Figure 37. Each circle represents one infected ear. Horizontal bars represent the mean in B and denote the median in C. *, $p < 0.05$; ***, $p<0.001$, according to one-way ANOVA with Dunnett's post test in B and Kruskal-Wallis with Dunn's post-test in D (comparison with control (no treatment)).

2.3.3 Monocytes, but not neutrophils increase *L. major* burden at the site of infection

Our work has shown the importance of monocyte-derived cells at the site of infection as permissive host cells (see 2.2.3). Also, data on pathogen proliferation over the course of the infection suggests that towards later time points of the infection, *L. major* exhibits a slower proliferation rate (see 1.4). Considering that our experiments on activation and recruitment inhibition took place around the peak of infection, we wanted to investigate the effect of permissive host cells presence at later time points in the persistent phase (experimental setup is shown in figure 39A). In order to do so, C57BL/6 mice were infected with *Lm*^{SWITCH} (high dose) parasites, at week 10 p.i, monocytes were isolated from donor CD45.1 bone marrow cells, activated over-night with LPS and IFNγ or kept untreated, and injected into the ear dermis at the site of infection. Three days later (i.e.70 days p.i) analysis via flow cytometry (analysis is shown in figure 39B) or LDA was performed.

In newly recruited CD45+ monocytes at the site of infection (3 days after injection), we found that inactivated cells were present at the site of infection, and detected also activated cells, however at a lower level (figure 39D).

Of importance, the injection of inactivated monocytes into the site of infection showed significant higher burden and percentage of infected cells, while activated monocytes injected ears showed a trend towards the same direction, however, it was not significant (figure 39C).

To make sure the change in the infection percentage is not due to a change in overall newly recruited cells, we measured the absolute numbers of all monocytes or neutrophils at the site of infection, which consisted mainly of CD45.2 host monocytes. Neither monocytes nor neutrophils showed a difference in absolute numbers upon monocytes deposition (figure 39E).

Additionally, correlation analysis of donor cell numbers versus pathogen burden suggested that the number of injected monocytes correlates with an increase in the pathogen numbers (figure 39F).

A

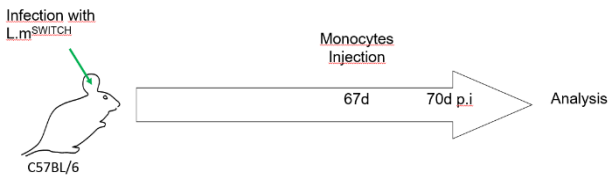

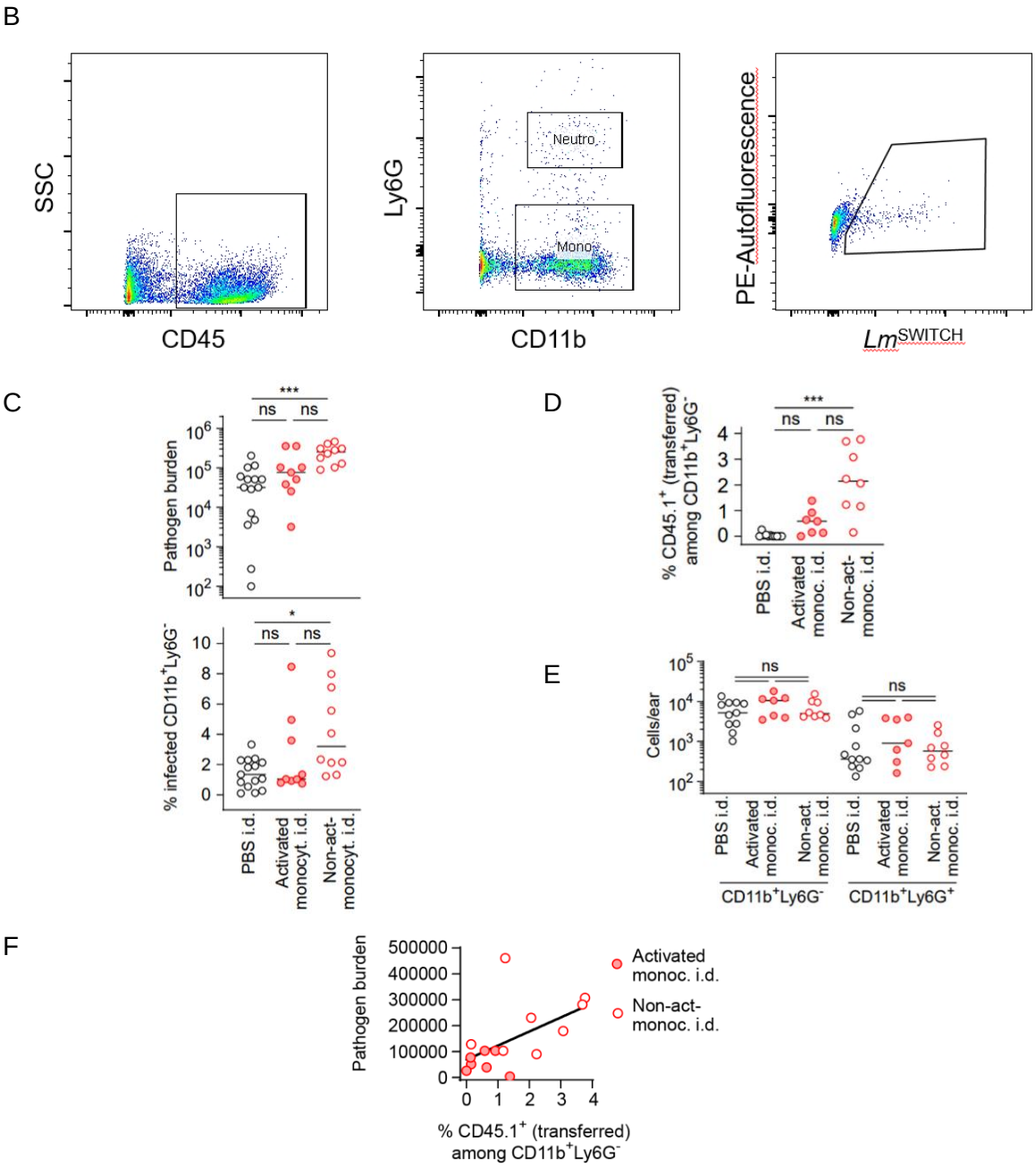

Figure 39: Effect of monocyte administration at later time points. A, experimental setup. B, flow cytometry analysis strategy. C, analysis of pathogen burden (top panel) and infection rate in Ly6G-CD11b+ monocyte-derived cells by flow cytometry (bottom panel). D, fraction of injected CD45.1+ donor cells among all Ly6G-CD11b+ monocyte-derived cells at the site of infection. E, total number of Ly6G-CD11b+ monocyte-derived cells (left) and Ly6G+CD11b+ neutrophils (right) isolated from the site of infection. F, correlation between the pathogen burden and fraction of monocytes detected 3 days after intradermal deposition into the site of injection (Spearman r = 0.585; p = 0.024). Each circle represents one infected ear at

10 wpi (high-dose infection) injected with PBS (black circles) or with activated (filled red circles) or non-activated (empty red circles) bone marrow monocytes into the infection site three days before analysis. Horizontal bars denote the median. ns, not significant; *p < 0.05; ***p < 0.001, according to Kruskal-Wallis with Dunn's post-test.

In the context of the infection with *Mycobacterium tuberculosis*, which also survives and proliferate in inflammatory phagocytes, Mishra *et al.* have shown that NO contribute to the infection containment by repressing neutrophil recruitment. Consequently, we wanted to investigate if an increased neutrophil recruitment could as well affect the pathogen burden or the infection percentage in later stages of *L. major* infection. In order to do so, we induced irritant contact dermatitis at 10 weeks p.i of *Lm*^{SWITCH} (high dose) (experimental setup is shown in figure 40A) using 2,4-dinitrofluorobenezene (DNFB), which, upon primary application, has been reported to induce a neutrophil-dominated innate immune response (Bonneville, Chavagnac et al. 2007). For this, a single dose of DNFB was applied epicutaneously to the infection site, or a vehicle as a control, 3 days later we measured the results via LDA and flow cytometry.

As expected, neutrophil numbers were significantly higher after DNFB application in comparison to the control, while CD11b+Ly6G- population remained unchanged (figure 40B). Interestingly, the pathogen burden and the infection percentage were not affected by sensitization treatment (figure 40C and D).

In conclusion, monocyte deposition, but not neutrophil recruitment, can increase pathogen numbers or infection percentage in the persistent phase of the infection.

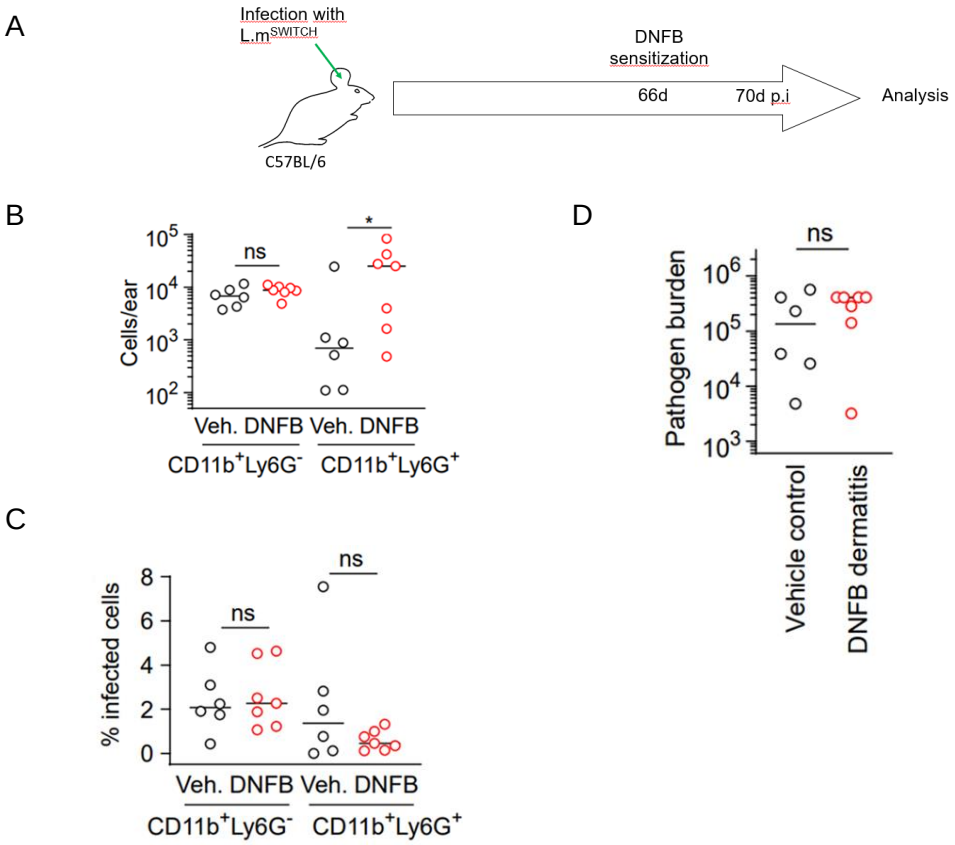

Figure 40: Effect of neutrophil recruitment at late time point of infection. A, experimental setup. B, cell numbers determined for Ly6G-CD11b+ monocyte-derived cells (left) and Ly6G+CD11b+ neutrophils (right) isolated from the site of infection. C, fraction of infected cells for the populations shown in B. D, pathogen burden determined by limiting dilution. Black circles represent vehicle-treated infection sites, and red circles represent DNFB-treated infection sites. Each circle represents one infected ear. Data collected in at least two independent experiments. Horizontal bars denote the median. ns, not significant; *p < 0.05; ***p < 0.001, according to Kruskal-Wallis with Dunn's post-test in B and C, or Mann-Whitney test in D.

2.4 Part IV: Long term effects of iNOS and recruitment during the acute phase of the infection: Implications from modelling

In this work, we found out that the pathogen load showed no short term changes under recruitment inhibition condition, whereas inhibition of iNOS is capable of increasing the pathogen burden. We speculated that the recruitment inhibition effect on pathogen numbers may require longer to occur due to many recently recruited phagocytes left at the site of infection even after inhibition of phagocyte recruitment, while iNOS dependent pathogen killing is taking place directly considering the short half-life of seconds of NO (Thomas, Liu et al. 2001). In order to address a possible long-term effect of the recruitment inhibition, C57BL/6 mice were infected with *Lm*^{SWITCH} (high dose), L-NIL (iNOS inhibition) was administered IP for three days (at day 18,19 and 20), whereas cells recruitment inhibition (anti-CD18/CD49d) was administered IP on day 18. In contrast to the experimental setup we used in figure 32A, the infection was analyzed 3 weeks later after the activation/recruitment inhibition, i.e. on day 42 p.i. (figure 41A shows the experimental setup).

Right after the inhibition at three weeks p.i, we had observed a high percentage of infected cells in all conditions involving recruitment inhibition, which might be due to the fact that the monocytes at the site of infection are constantly replenished by non-infected cells under control conditions (figure 32C). In contrast, a significantly lower percentage of infected cells was detected 3 weeks after inhibition as compared to controls (figure 41C). While the pathogen burden within short term of the treatment showed no significant differences but a trend of higher pathogen burden in the activation inhibition conditions (figure 32E), in the long term, not only a trend towards lower infection in the activation inhibition conditions but also in inhibited phagocyte recruitment was observed (figure 41B). Interestingly, a parallel simulation (performed in the models 1 and 4) of the effect of a three days inhibition of iNOS and/or phagocyte recruitment on the long term predicted the same trends for infected cells and pathogen burden (figure 41D and E). Therefore, we concluded that while the inhibition of monocyte recruitment revealed less dramatic effects on the pathogen burden than iNOS inhibition in a short time frame, the changes in pathogen density, reflected by the higher percentage of infected cells, influenced the course of the infection in the long-term perspective.

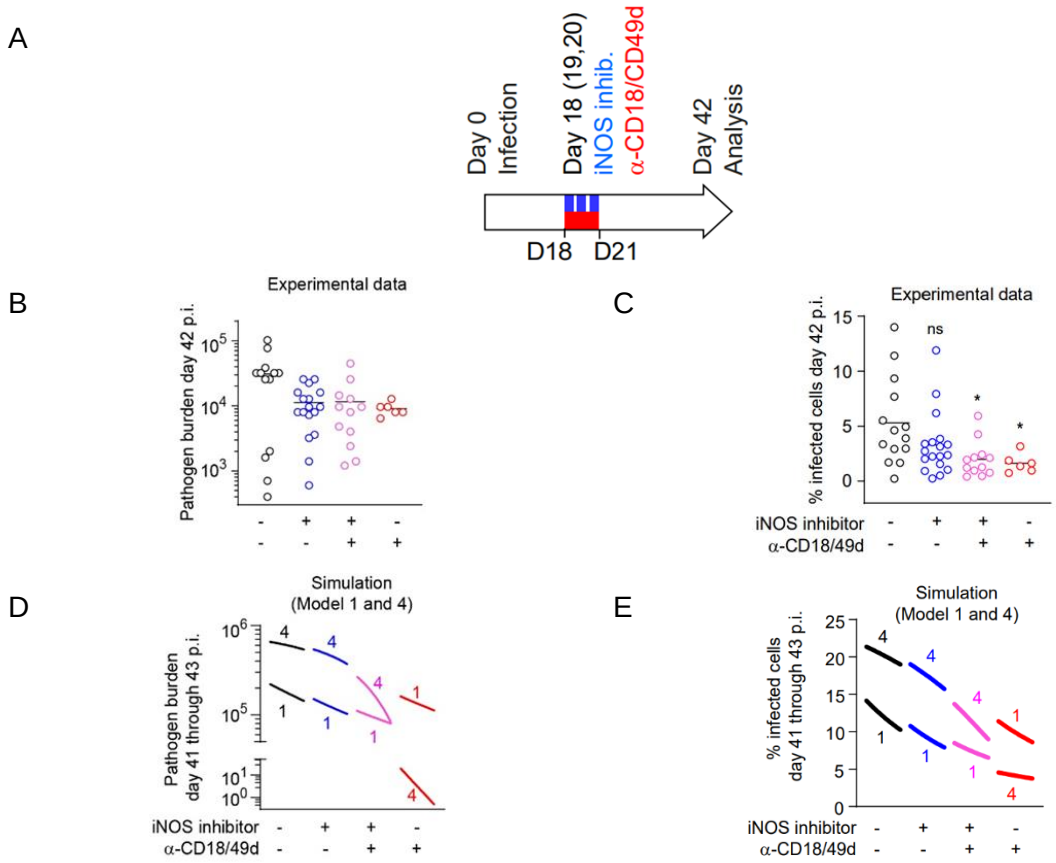

Figure 41: Activation and recruitment inhibition effects on the long term. A, experimental setup for transient iNOS inhibition (blue) and anti-CD18/CD49d-mediated recruitment blocking (red). B, pathogen burden determined by limiting dilution analysis at day 42 p.i, after treatment from day 18 p.i on with three doses of L-NIL (blue), one dose of anti-CD18/CD49d (red), both (pink), or not treated (black). C, fraction of infected Ly6G-CD11b+ monocyte-derived cells determined by flow cytometry at day 42 p.i, treated according to A. D and E, simulated pathogen burden and infection rates (fraction of Mi + Mai among all monocytes) respectively for models 1 and 4 modeled according to A, curves show the time course from day 41 to day 43, numbers indicate the model (1 or 4) for each curve. Each circle represents one infected ear. Horizontal bars denote the median. ns, not significant; *p < 0.05, according to Kruskal-Wallis with Dunn's post-test (comparison with control (no treatment)).

2.5 Part V: Mapping Teff/Treg balance and immune checkpoint expression to the course of *L. major* infection

In the self-limiting form of the disease in C57BL/6 mice, the protective immune responses against *L. major* is expected to be mediated by a Th1 response via the production of IFN-γ. However, recent work has shown that Th2 immunity may play a protective role during early resistance infection (Carneiro, Lopes et al. 2020). On the other hand, Th17 effects have been shown to promote the disease in the susceptible more than the resistant model (Lopez Kostka, Dinges et al. 2009). Furthermore, the involvement of regulatory T cells in the cellular adaptive immune response against Leishmaniasis in the resistance model is well established (Belkaid, Piccirillo et al. 2002). The interactions of effector and regulatory T cells (Teff and Treg) among each other, and with the pathogen, might affect the progress of leishmaniasis. How these interactions in the infected tissue influence the course of the disease, and what immunomodulatory mechanisms are in place at the infection site, has remained unclear. Thus, we sought to map the proportions of different populations of CD4+ T cells, for which we could already from previous experiment in this work observe a strong increase in the beginning, and slow decrease upon pathogen control (figure 42). Furthermore, we set out to quantify the expression of co-inhibitory receptors.

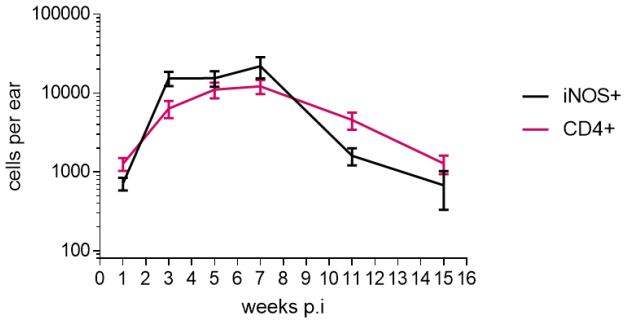

Figure 42: CD4+ and the activation of phagocytes over the course of infection. Replotted from Figure 21 E, the black line represent a sum of iNOS+L.m- and iNOS+L.m+ sub-populations. Mean with SEM representation is shown.

In order to do so, we infected C57BL/6 mice with *L. major* WT (high dose). Then, the infected ears were harvested and processed at 1, 3, 5, 7, and 11 weeks p.i to measure T cell subsets ratio and co-inhibitory receptors expression via flow cytometry (analysis is shown in figure 43A).

Of importance, the relative fraction of regulatory FoxP3+ among all CD4+ T cells at the site of infection showed no change over the course of infection (figure 43B). Analysis of the expression of the co-inhibitory receptors PD-1, TIM3 and TIGIT (figure 43C) revealed that in the CD4+FoxP3+ population, PD-1+ fraction was not changed, while both TIM3+ and TIGIT+ fractions went steadily up and showed an elevation towards later phases of the infection. On the other hand, in the effector T cells CD4+FoxP3- population, the three co-inhibitory receptors levels lined up with the progress of the immune response, and all co-inhibitory receptors peaked for effector cells around week 5-7 p.i, and decreased by week 11 p.i. Altogether, the co-inhibitory receptors expression on effector T cells is proportional to the inflammatory pathology and immune activation, but on the regulatory T cells, their induction seemed to lag behind the immune activation, suggesting different roles at different phases of the infection.

A

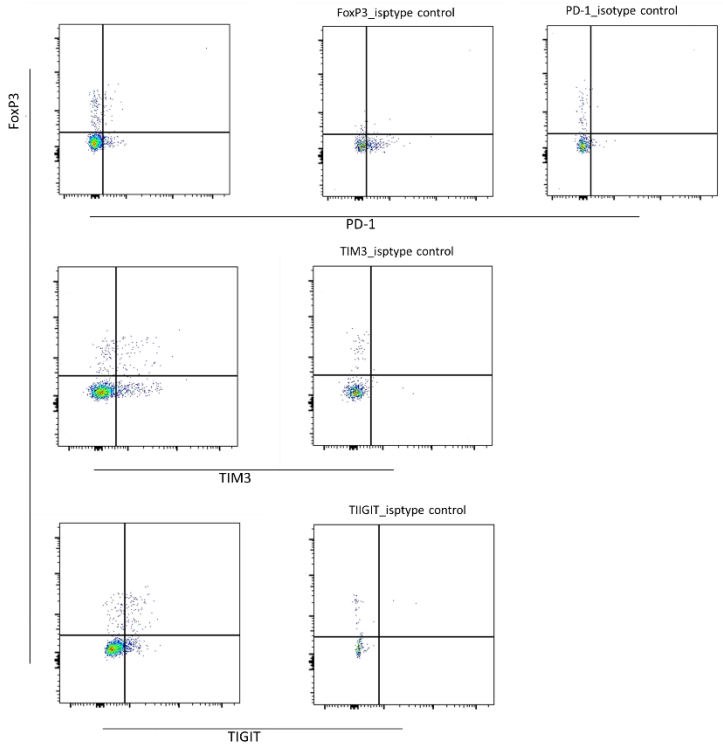

B

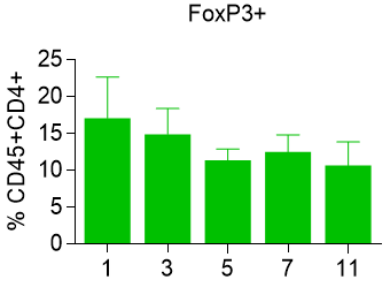

C

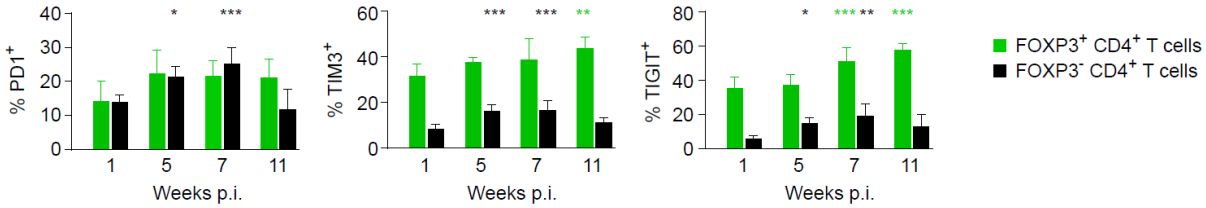

Figure 43: T cell subsets ratio and co-inhibitory receptors expression in infected ears. A, flow cytometry analysis (ears samples). B, CD4+FoxP3+ population progression in the infected ears. C, co-inhibitory receptors progression in CD4+FoxP3+ (green bars) or CD4+FoxP3- (black bars) populations in the infected ears. Data collected in at least two independent experiments. Significance determined against week 1 p.i condition of each cell type, color-coded. *p < 0.05; **p < 0.01;***p < 0.001, according to Kruskal-Wallis with Dunn's post-test.

NO not only changes the cytokine milieu and activation status of myeloid cells, but is also capable of regulating and modulating T cell activation (Bingisser, Tilbrook et al. 1998); (Harari and Liao 2004). As co-inhibitory receptor expression might change with differential activation, we wanted to test a possible effect of iNOS inhibition on TIGIT, PD-1, CTLA4 and TIM3 expression in regulatory and effector T cells at the site of *L. major* infection. We measured the expression at two time points selected before and after the peak of the infection, i.e. 3 and 7 weeks p.i. However, apart from a minimal effect of iNOS inhibition on TIM3+ fraction of CD4+FoxP3+ population, we found no major impact of NO on co-inhibitory receptors expression (figure 44). Thus, despite its dramatic effect on monocyte recruitment and pathogen proliferation viability (Postat, Olekhnovitch et al. 2018); (Müller, Aeschlimann et al. 2013); (Olekhnovitch, Ryffel et al. 2014), iNOS inhibition at the site of *L. major* infection does not seem to have a major impact on coinhibitory receptor expression by effector or regulatory T cells.

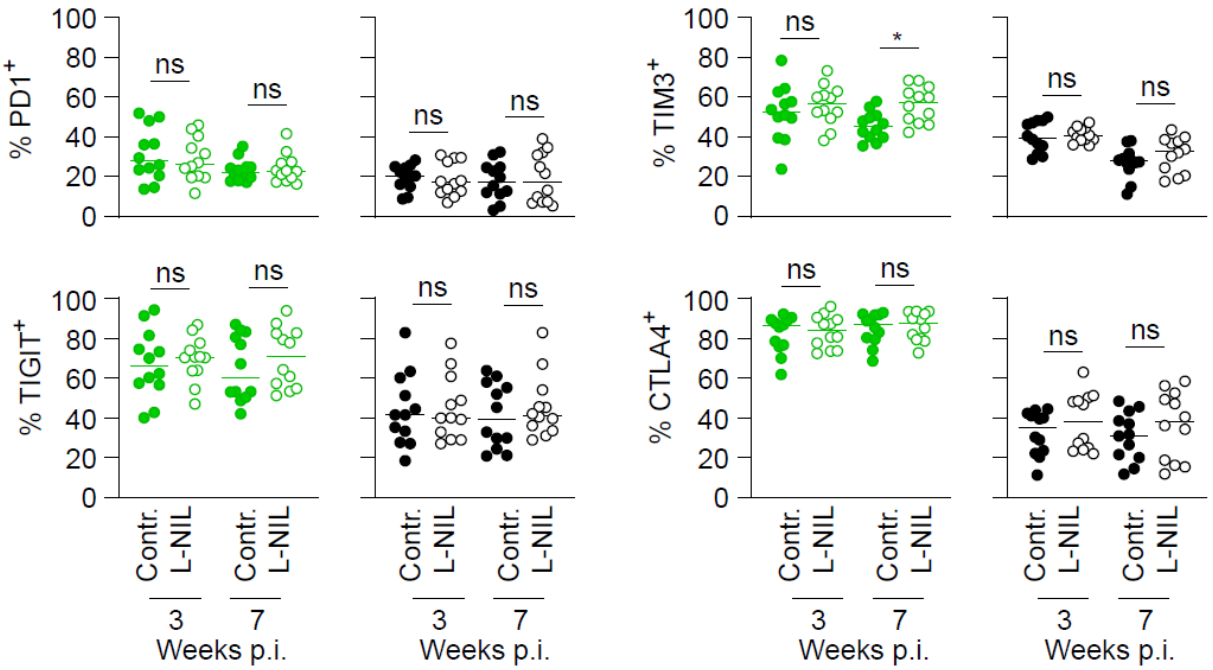

Figure 44: Activation inhibition effect on co-inhibitory receptors expression in infected ears. L-NIL injection (3 days before analysis) effect is shown in CD4+FoxP3+ (green circles) and CD4+FoxP3- (black circles) on control (filled circles) and L-NIL treated (empty circles) at 3 and 7 weeks p.i. Data collected in at least two independent experiments. Horizontal bars denote the median. ns, not significant; *p < 0.05, according to Kruskal-Wallis with Dunn's post-test.

In parallel to the analysis of the site of infection, we investigated the same parameters in the cervical lymph nodes draining the site of infection (dLN), and inguinal lymph nodes as non-draining controls from the same animals (ndLN). In line with our findings in infection site in the ear, CD4+FoxP3+ population of the draining lymph nodes showed no change over the course of infection, and was also comparable to the ndLNs levels (figure 45A).

Out of the studied co-inhibitory receptors, only PD-1 showed significantly higher expression in CD4+FoxP3- population in the draining than in the non-draining lymph nodes, whereas TIM3, TIGIT or CTLA4 showed no difference between draining and non-draining lymph nodes, neither in FoxP3+ nor in FoxP3- T cell populations (figure 45B).

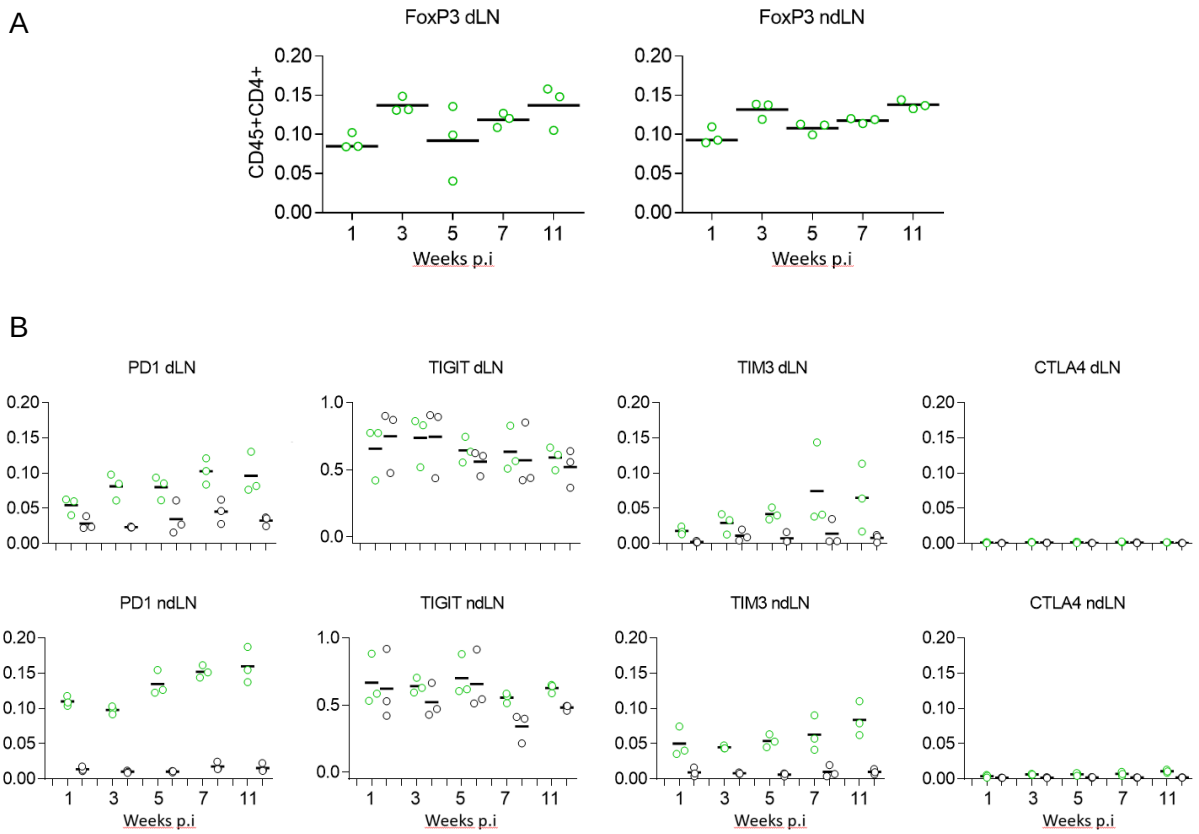

Figure 45: T cell subsets ratio and co-inhibitory receptors expression in the lymph nodes. A, CD4+FoxP3+ population progression in the draining and non-draining lymph nodes. B, co-inhibitory receptors progression in CD4+FoxP3+ (green circles) or CD4+FoxP3- (black circles) populations in the draining and non-draining lymph nodes. Horizontal bars denote the mean in A and the median in B. 2way ANOVA, Bonferroni´s multiple comparisons test was used to compare drainage and time course.

In order to assess a possible impact of iNOS on PD-1 expression by T cells in the lymph nodes, we tested whether iNOS inhibition affects the expression of PD-1 at 3 and 7 weeks p.i in draining and non-draining lymph nodes (figure 46). We however found no effect of iNOS on PD-1 expression in the secondary lymphoid organs draining the site of infection, or non-draining lymph node controls.

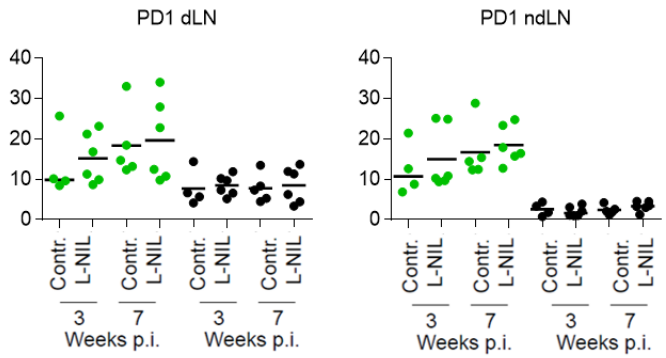

Figure 46: Activation inhibition effect on PD-1 expression In draining and non-draining lymph nodes in CD4+FoxP3+ (green circles) or CD4+FoxP3- (black circles) populations. Horizontal bars denote the mean. Kruskal-Wallis with Dunn's post-test was used.

3. Discussion

Because of its versatile functions and diverse roles in the host, the different possible modes of action of NO for pathogen containment have remained hard to dissect *in vivo*. We showed, by fitting ODE models to experimental data, and experimental validation using *in vivo* reporter systems for pathogen viability and proliferation, that killing of the pathogen, but not proliferation inhibition, is the dominant mechanism of iNOS with regard to a direct impact on the pathogen during acute infection. However, we showed also that antibody-mediated blockade of monocyte recruitment abolished the effect of iNOS inhibition on pathogen proliferation, whereas *in situ* monocyte deposition, but not neutrophil recruitment, increased pathogen burden at late stage.

3.1 Balance between the pathogen and the immune response

Many pathogens have evolved to maintain a low-level persistent infection, which might be utilized by the pathogen itself to prolong their survival, or by the immune system to avoid recurrent infections through concomitant immunity (Mandell and Beverley 2017) (Monack, Mueller et al. 2004) (Belkaid, Piccirillo et al. 2002) (Belkaid, Hoffmann et al. 2001). Additionally, inflammatory monocytes as a niche for proliferation might be a product of coevolution of the pathogen with Th1 responses, which fight pathogens, still pathogens are able to survive exactly in cells recruited in the course of such responses. In this context, Heyde et al. reported that a monocyte-derived cell subset, which is known for its role in inducing adaptive immune responses against *Leishmania*, represents a reservoir for efficient intracellular multiplication and spread to new host cell (Heyde, Philipsen et al. 2018). Also, Romano et al. have shown that infected monocyte populations, which represent the initial mononuclear host cell for parasite replication in a primary infection, managed at a distal site of secondary infection in mice with persistent primary infection to rapidly produce iNOS, which was critical for parasite killing (Romano, Carneiro et al. 2017). The importance of inflammatory monocytes as a niche for proliferation is not limited to *L. major* cutaneous infection, but applies also to visceral leishmaniasis caused by *Leishmania donovani* (Terrazas, Varikuti et al. 2017). Whereas the significance of a tightly controlled size of permissive host cell controlled by a balanced Th1/Th2 immunity during early *Leishmania* infection was shown recently (Carneiro, Lopes et al. 2020).

3.2 What is the role of NO in pathogen control?

NO, which is produced by the inducible NO synthase iNOS, whose expression is activated in monocyte-derived phagocytes upon IFN-γ and TNF-α stimulation in the

context of PAMPs. NO has a well-established antimicrobial effects mediated by multiple mechanisms. NO is capable of killing *L. major in vitro* (Olekhnovitch, Ryffel et al. 2014), while *in vivo*, viable parasites can be observed in iNOS-expressing cells (Mandell and Beverley 2017). NO is also capable of reduce the pathogen proliferation (Olekhnovitch, Ryffel et al. 2014) (Müller, Aeschlimann et al. 2013). Of note, there is evidence that the parasite also inhibits iNOS itself (Balestieri, Queiroz et al. 2002), consequently, iNOS production and NO production might not forcibly overlap completely. However, in our model, we see a clear impact of iNOS induction on pathogen survival (Figure 7B and G).

The discrepancy of the findings of potent killing of *Leishmania* parasite by activated cells *in vitro* versus sublethal restriction of parasite proliferation *in vivo* represented a gap in our understanding of the mode of action of NO. How it exerts its protective effect is hard to investigate, as with its pleiotropic effects not only on the pathogen itself, but also on the immune response in the complex microenvironment described above, its different functions are difficult to dissect *in vivo*.

Here in this work we tried to define the exact modes of action of NO over the course of infection by not only dissecting its different impact on the pathogen using *in vivo* reporter systems and mathematical modeling, but also by selectively manipulating individual aspects of NO function, such as the inhibition of monocyte recruitment, or metabolic reprogramming of host phagocytes. Thus we were able to show that three previously independent observations of NO function in the infected tissue might be related to one and the same mode of action: 1) NO-mediated sublethal growth inhibition (Müller, Aeschlimann et al. 2013), 2) the collective production of NO by numerous iNOS-expressing phagocytes, generating an antimicrobial microenvironment that provides tissue-wide rather than cell-intrinsic control of *Leishmania* infection (Olekhnovitch, Ryffel et al. 2014) and 3) NO impact on myeloid cells recruitment at the site of *L. major* infection (Postat, Olekhnovitch et al. 2018). Our data suggest that NO effects on growth inhibition and tissue wide pathogen control might be the result of an inhibited monocyte recruitment.

3.3 Dissecting death and proliferation, why is it important?

Although used extensively for imaging, fluorescently labeled microorganisms have so far been used merely as “markers” for infected cells. Pathogen physiology has remained an important gap in the knowledge on host-pathogen interactions during infection, especially for imaging of host-pathogen interactions *in vivo*. In this work we

make use of two different reporter strains of *L. major* in order to dissect death and proliferation as NO-mechanism.

The importance of defining death and proliferation contribution in NO-mediated containment of *Leishmania* is in line with the finding that pathogen viability itself can be detected by the immune system, and notably, in the absence of the activity of virulence factors. Rapidly proliferating pathogens would represent source of large amounts of not only antigen and pathogen-associated molecular patterns (PAMPs) but also of so-called vita-PAMPs. vita-PAMPs molecules, that occur only in live microbes, shape the reactivity of immune cells against the encountered pathogen and might be critical for the efficient induction and execution of immune responses (Mourao-Sa, Roy et al. 2013). Although vita-PAMPs have not been studied in *Leishmania*, it might be possible that the immune system also in these organisms have evolved ways of telling apart live from dead or even high from low proliferating pathogens. Besides the detection of specifically live, or even proliferating pathogens, quantitative differences in pathogen killing and associated pathogen lysis and release of pathogen products can influence the activation of inflammatory signaling through differential release of pathogen-associated molecular pattern molecules (Shimada, Park et al. 2010) (Peng, Broz et al. 2011).

On the other hand, pathogen proliferation has been shown to be inversely correlated with resistance against both immune defense mechanisms and antimicrobial treatment, in other words, pathogens with low proliferation rates have the potential of representing a reservoir for chronic or relapsing infections (Nathan 2012) (Sarathy, Dartois et al. 2013).

Experimental work in our laboratory that has provided the basis of this thesis showed that killing and proliferation inhibition are far from being linked directly to the amplitude of the immune effector response. Instead, the time course of pathogen killing and proliferation inhibition revealed that on the one hand, overt pathogen killing occurs during the acute phase of the infection, at which pathology and immune activation are high, but not in the persistent infection phase later on. On the other hand, it could be observed that *L. major* proliferation is also low during the persistence phase of the infection, and is highest at the peak of the infection when iNOS expression is also high, arguing against a direct growth inhibition exerted proportionally to the extent of iNOS activation (Formaglio, Alabdullah et al. 2021).

iNOS inhibition results in expansion of pathogen numbers even after overt pathology has subsided (Stenger, Donhauser et al. 1996), suggesting that NO also might be

responsible for the low pathogen proliferation we have reported at late time points of infection. However, taking into consideration that pathogen killing coincided with heightened pathology and immune activation (Formaglio, Alabdullah et al. 2021), leaves us with the question: How does the high NO concentration at the infection peak permit high pathogen proliferation?

Our work here shows that very different mechanisms mediate pathogen proliferation inhibition and direct killing. The finding of Mandell and Beverley that *Leishmania* persists not in immunoprivileged cell types but instead within phagocytes that express iNOS supports this assumption (Mandell and Beverley 2017). Also, the amount of NO produced during the persistence phase might not be high enough to exert direct pathogen killing, as it was shown that parasite killing requires a minimum concentration of NO, nevertheless, the NO concentration might still however be high enough to inhibit monocyte recruitment (Olekhnovitch, Ryffel et al. 2014).

3.4 Mathematical models

In order to dissect direct killing and proliferation inhibition, ODE models were designed in collaboration with the group of Michael Meyer-Hermann (HZI Braunschweig). Initially, the models were based on the assumption of direct proliferation inhibition as a mechanism of NO mediated pathogen containment (Müller, Aeschlimann et al. 2013). However, it was revealed after fitting the models with experimental data and consequent experiments in this work that the main contribution to pathogen proliferation rate came from the availability of host cells, which is inherent to models which include pathogens that proliferate intracellularly (see ODE models chapter). Of note, the absence of an extracellular proliferation component in the modeling is based on experimental findings that we (Heyde, Philipsen et al. 2018) and others (Mandell and Beverley 2017) have reported, showing all parasites at the site of infection reside within cells. From a mathematical point of view, adding an extracellular proliferation component would make the models much more complex and undesirable according to AIC model selection. In line with this, the transition from infected to uninfected through intracellular killing of the parasite, and activated to unactivated as a result of iNOS downregulation after pathogen control are not taken into account. We therefore would expect that these transitions between different states of the monocytes are compensated by the death rates of the individual cell populations, as well as the recruitment rates. In consequence, these parameters are not representing actual

recruitment and death rates, but convolved values that implicitly include state transitions of the monocytes.

Our finding from the mathematical models, which was confirmed experimentally, that the link between recruitment of phagocytes to an infection site and pathogen control is complex is well in line with different modeling approaches in other infection models. Indeed, Segovia-Juarez et al. performed an agent-based modeling of Mycobacterium tuberculosis granuloma formation in the lung. As one of the findings of this work, prevention of macrophage overcrowding within the granuloma seems to be a key element for containing the infection (Segovia-Juarez, Ganguli et al. 2004).

Of importance, the peak in pathogen proliferation in our work coincided with high immune cell recruitment but preceded the peak of pathogen killing by 1–2 weeks (both in modelling and in reporter systems). The time points 5 and 7 weeks p.i. (at which the difference between iNOS expression and killing is observed) are likely to represent two very interesting phases for the course of infection: At week 5 p.i., although iNOS expression is high, the phagocyte population is constantly replenished by newly recruited cells. In contrast, at week 7 p.i, phagocyte recruitment and pathogen burden have reached their maximum. Considering that efficient iNOS induction allowing pathogen killing might take several days (Olekhnovitch, Ryffel et al. 2014), the newly recruited monocytes may contribute to the observed delay in proportional parasite death by temporarily diluting the effective fraction of NO producing cells, and by increasing the proportion of proliferating pathogen.

3.5 Monocytes as a niche for proliferation

Monocytes exert diverse roles mediating immune response against *Leishmania*. On the one hand, they represent the main iNOS-producing cells (De Trez, Magez et al. 2009) and consequently the main pathogen killers (Goncalves, Zhang et al. 2011), additionally, Romano et al. have shown that inflammatory monocytes are even more efficient in parasite killing in a secondary infection (Romano, Carneiro et al. 2017). Furthermore, monocytes plays an important role in antigen presentation in the infection site and in lymph nodes (León, López-Bravo et al. 2007), and it was shown that *L. major* may utilize monocytes as “Trojan horses” to migrate to secondary lymphoid organs and peripheral sites (Hurdayal, Nieuwenhuizen et al. 2019).

On the other hand, Heyde et al. have reported that newly recruited inflammatory phagocytes represent a niche for rapidly proliferating *L. major* in cutaneous *Leishmania* (Heyde, Philipsen et al. 2018). Also Terrazas et al. reported an importance of

inflammatory monocytes in promoting parasite survival in visceral leishmaniasis (Terrazas, Varikuti et al. 2017).

Thus, monocytes may represent a double-edged sword in terms of enabling pathogen elimination and at the same time providing a permissive niche for pathogen proliferation. Here in this work, in line with the dual role of monocytes, we show that the NO-mediated feedback, which restricts recruitment of the cellular compartment permissive for *L. major*, is not only preventing an over-shooting immune response but also mediating the dampening effect on pathogen proliferation observed previously (Müller, Aeschlimann et al. 2013). The finding of this work, i.e. that anti-inflammatory mechanisms can contribute to fighting the pathogen, is well in line with previous findings showing that *L. major*-infected mice deficient in the immune checkpoint PdI1, despite having larger inflammatory lesions, seem not to control *L. major* more efficiently than wild type control animals (de Freitas, Gálvez et al. 2020).

In this work, we show that *in situ* deposition of monocytes is capable of reactivating an infection at the late stage, at which pathology has already subsided. We show also that non-activated monocytes increased pathogen numbers more than activated ones. This, most probably, is not related to the ability of the activated monocytes to kill the pathogen, considering the fraction of activated cells was not enough to produce iNOS mediated control of the pathogen, as earlier work on collective NO production kinetics in parasite killing shows that a 5% frequency of iNOS-competent phagocytes is not sufficient to permit parasite killing (Olekhnovitch, Ryffel et al. 2014). Instead, the activated fraction cells might be more vulnerable to cell death which may make them less efficient as a proliferation niche, or they could already die in the process of deposition, making the effective number of deposited monocytes smaller. Compensating such possible apoptosis-related death difference between activated and non-activated fractions faced a technical obstacle, as the number of cells to be prepared for injection would increase by factor ten in order to keep the same number of cells as for the non-activated monocytes.

Our finding regarding the reactivation of the infection through monocyte deposition is interesting also in accordance with clinical data showing that skin inflammation can induce *Leishmania* lesion in persistent phase (Kerr, Dawe et al. 2009) (Rab, Hassan et al. 1992), showing that certain inflammatory responses could promote pathogen relapses observed in patients.

3.6 NO modulation of the inflammatory microenvironment

It has been shown before that NO-dependent cell recruitment reduction is mediated by downregulating cytokines and chemokines production, mostly via dampening of mitochondrial respiration within monocyte-derived cells (Postat, Olekhnovitch et al. 2018). Of note, some pathogens are capable of utilizing inflammatory conditions in their favor. For instance, an inflammation can shift the balance between the protective microbiota and the pathogen *Salmonella enterica* serovar Typhimurium in favor of the pathogen (Stecher, Robbiani et al. 2007). Also, Mishra et al. show that the role of NO in inhibiting *Mycobacterium tuberculosis* growth is mediated by repression of the neutrophil recruitment signaling cascade (Mishra, Lovewell et al. 2017). Therefore, as inflammatory conditions may promote pathogen survival, the induction of a modified cytokine milieu might, also in the absence of monocyte recruitment, promote pathogen proliferation. However, we show in this work that the effect on pathogen proliferation is mainly dependent on the presence of monocyte-derived cells, neither on the metabolic alteration of the inflammatory cells at the site of infection, nor an increase in inflammatory cytokine production *per se*.

Our data shows that transient inhibition of iNOS (i.e, 3 days at day 18-21 p.i), but not recruitment blockade, resulted in an immediate change in the pathogen burden. The delay of an effect for recruitment on the pathogen burden is most probably due to different kinetics of the shortage of newly recruited cells in comparison to inhibition of pathogen killing. Indeed, the expected half-life of NO in the tissue is in the range of seconds (Thomas, Liu et al. 2001), thus, iNOS inhibition is expected to take effect immediately. In contrast, the turnover time of cells newly recruited to the site of infection is several days (Heyde, Philipsen et al. 2018).

Interestingly, while inhibition of cell recruitment did not change pathogen burden immediately, the fraction of infected cells dramatically increased, clearly indicating a shortage of infectable monocytes. Furthermore, on a long term perspective (42 dpi), the short term inhibition of either iNOS or cell recruitment at day 18-21 resulted in a lower pathogen burden. The change in the pathogen burden might be related to an accelerated course of the infection, which has been shown earlier to be correlated with higher infection dose (Belkaid, Mendez et al. 2000). In particular, the immediate increase in pathogen burden due to a transient iNOS inhibition might mimick such a higher infection dose. Antibody-mediated blocking of immune cell recruitment also dampened pathogen burden over the long term perspective. We can only speculate whether also recruitment inhibition accelerates the kinetics of pathogen control, leading

to lower pathogen burden in the long term perspective. If so, the high proportion of infected cells, which results from the lack of newly recruited monocytes, might, despite the unchanged overall pathogen burden, be interpreted as an increased pathogen density by the immune system, resulting in a more vigorous response and faster containment.

3.7 Balancing T cell responses with *Leishmania* infection, a temporal map

Modulating the length and magnitude of effector immune responses and minimizing collateral tissue damage is indispensable for a successful pathogen containment. Immune checkpoints are crucial to control such a balance. Previous findings in line with our work suggest that the correlation between immune activation and pathogen control is not strictly inverse correlated, with more immune activation not forcibly resulting in better pathogen control (Mishra, Lovewell et al. 2017) (Stecher, Robbiani et al. 2007). We, in this work, and others (de Freitas, Gálvez et al. 2020) have shown that immunomodulatory feedback mechanisms are linked with pathogen control via complex interactions, and are not only restricting the inflammation, but also have an impact of the pathogen niche and, consequently, proliferation. Therefore, studying the course of regulatory T cell infiltration and the induction of immune checkpoint mechanisms over time during *Leishmania* infection is important to understand the dynamics of pathogen control and the course of the disease.

We were able to show differential expression of inhibitory checkpoints among T cell populations at the site of infection. TIM3 and TIGIT levels tend to scale up toward the persistent phase in regulatory T cells population. Whereas PD-1, TIM3 and TIGIT levels on effector T cells line up with the progress of the immune response. We show also that the percentage of regulatory T cell out of total T cells is not changing over the course of infection, still, a differential impact of regulatory T cells might be exerted by other means.

To date, an extensive number of studies investigating the effect of inhibitory checkpoints on T cells are available (Harding, McArthur et al. 1992) (Kamphorst, Wieland et al. 2017) (Zhu, Anderson et al. 2005). Nevertheless, most of these studies focus specifically on antitumor immunity or autoimmunity (Zhang, Chikuma et al. 2016) (Gao, Zhu et al. 2012) (Syed Khaja, Toor et al. 2017).

PD-1 blockade was shown to downregulate FoxP3 expression in regulatory T cells, and increase the ratio of effector T cells to regulatory T cells. Additionally, TIGIT and TIM3 co-expressing regulatory T cells were shown to be superior in suppressing tumor

microenvironment, moreover, antibody-mediated blockade of both TIGIT and TIM3 can inhibit the suppressive activity (Sasidharan Nair and Elkord 2018). Furthermore, an augmented suppression by TIM3 or TIGIT expressing regulatory T cells cells toward effector T cells in the context of LCMV infection in mice was also shown (Littringer, Moresi et al. 2018).

With the finding that some of these coinhibitory receptors are differentially regulated throughout the infection with *L. major*, our results shed a light on the potential kinetics of inhibitory checkpoint expression on effector and regulatory T cells populations during the control of *Leishmania* infection.

4. Materials and methods

4.1. Methods

4.1.1. Pathogen

L. major LRC-L137 V121 wild-type, dsRed or mKikume expressing *L. major*^{SWITCH} parasites (Müller, Filipe-Santos et al. 2012); (Müller, Aeschlimann et al. 2013) were grown in M119 medium (Sigma-Aldrich) supplemented with 10% heat-inactivated fetal calf serum (Biowest), 0.1 mM adenine, 1 mg/ml biotin, 5 mg/ml hemin, and 2 mg/ml biopterin (all from Sigma-Aldrich) at 26 C° for a maximum of 6 passages.

4.1.2. Mice

C57BL/6J (WT) and mKikumeGR expressing (Tg(CAG-KikGR)33Hadj/J) mice were bred in the Central Animal Laboratory (ZTL) of the Medical Faculty of Otto-von-Guericke-University Magdeburg, or purchased from Charles River (Sulzfeld, Germany). All mice were housed under SPF conditions, sex- and age-matched animals between 7 and 14 weeks were used for infections. All animal experiments were reviewed and approved by the Ethics Committee of the Office for Veterinary Affairs of the State of Saxony-Anhalt, Germany (permit license numbers IMKI/G/03-1253/14, IMKI/G/01-1314/15 and IMKI/G/01-1575/19) in accordance with legislation of both the European Union (Council Directive 499 2010/63/EU) and the Federal Republic of Germany (according to § 8, Section 1 TierSchG, and TierSchVersV).

4.1.3. Infection experiments

Stationary phase parasite cultures were centrifuged (1000 g, 10 min, RT) and resuspended in PBS. $2x10^6$ (for flow cytometry experiments) or $5x10^5$ (for intravital 2-photon experiments) parasites were subsequently injected into the ear dermis. Mice were lightly anesthetized for infection with a mixture of ketamine (Ketamin-ratiopharm, 70 mg/kg body weight) and xylazine (Rompun 2%, Bayer, 7 mg/kg body weight) and inoculated into each ear pinna with 10 µL of parasite suspension using a microsyringe (NanoFil, World Precision Instruments) mounted with a 35G-beveled needle.

4.1.4. Limiting dilution assays

Infected mice ears were separated in two sheets (ventral and dorsal) and enzymatically digested in RPMI 1640 medium (Pan Biotech) containing 1 mg/ml collagenase-Liberase (Roch / Sigma-Aldrich) and 50 ng/ml DNase (Thermo Fisher) for 60 min at 600 rpm and 37°C, the suspensions were passed through a 70 µm cell strainer. Cells were centrifuged at 4°C with 300 g for 10 min. Cells suspensions were then used for

Limiting dilution and flow cytometry assays. 10% of cell suspension were centrifuged (3500 g, 5 min, RT) and resuspended in *Leishmania* culture medium. Quadruplicate samples of each homogenate were serially diluted in 1:2 steps 16 times in *Leishmania* culture medium in parafilm-sealed 96-well plates. After 14 days at 26°C, the highest dilution which exhibited parasite growth was identified for each replicate and the initial parasite number was defined as the median value of the replicates.

4.1.5. Flow cytometry

The samples were Fc-blocked using anti-CD16/32 antibody before antibody staining. External surface staining using CD45-PerCP-Cy5.5, CD45-APC-Cy7, CD45-BUV496, CD3e-BV421,CD3e-PerCP-Cy5.5, Ly6C-PE-Cy7, Ly6G-APC, Ly6G-APC-Cy7, MHCII-BV510, CD11b-BUV395, CD45.1-BV510, CD45.2-APC-Cy7, TIM3-BV605, PD-1-BV785, CTLA4-PE, TIGIT-BV421 or CD4 - AF488 in PBS for 30m at RT was performed.

If a subsequent iNOS intra-cellular staining was needed, the cells were fixed in PFA 4% for 1h at 4 °C, permeabilized for 15 min at RT with 1x Perm/Wash buffer (BD Biosciences) and then intra-cellularly stained using iNOS-APC (in addition to the Fc-block) in 1x Perm/Wash buffer (BD Biosciences) for 30m at RT.

For cytokines intracellular staining, after the Fc-block, extra-cellular staining and paraformaldehyde (PFA)-fixation steps, extracted cells were plated in 48-well plates in 1 mL complete RPMI supplemented with BD GolgiPlug (diluted at 1:1000) for 4 h at 37Cº. cells were then permeabilized using 1x Perm/Wash buffer (BD Biosciences) 15 min at RT. Cells were then submitted to the cytokines intracellular staining (pro-IL1-b-APC) 45 min at 4Cº.

For FoxP3 intracellular staining, eBioscience™ Foxp3/Transcription Factor Staining Buffer Set was used according to the manufacturer instructions using FoxP3-AF488 antibodies.

For calculation of absolute cell numbers, 30000 CountBright Absolute Counting beads (Thermo Fisher) were added to the samples before measurement. Analysis was performed with a Fortessa (BD Biosciences) or Attune NxT (Thermo Fisher). Data were analyzed by using the FlowJo 10.6.2 software (FlowJo, LLC).

4.1.6. Monocyte injection and DNFB sensitization experiments

Monocytes were isolated from bone marrow via negative magnetic selection using the Monocyte Isolation Kit (BM) (Miltenyi Biotec). The cells were incubated for 24h in RPMI

(10% FCS, 5% P/S) in a 24 well plate (10^6 cells/ml/well). In order to activate the monocytes, LPS (1µg/ml) and INF-γ (10 ng/ml) were added to the designated wells. After 24h incubation, cells were centrifuged (450 g, 8 min, 4°C) and resuspended in PBS. The content of each 2 wells were suspended in 10 µl PBS and injected into the ear dermis 3 days prior to analysis by flow cytometry and limiting dilution analysis of pathogen burden.

To induce irritant contact dermatitis, a single dose of 20 µl of 0.5% 2,4-dinitrofluorobenezene (DNFB, Sigma-Aldrich) in acetone/olive oil (4:1) was applied onto the infected ear. Vehicle controls were treated with the solvent only.

4.1.7. Intravital 2-photon imaging

Mice were injected with 100 mg/kg Ketamine and 10 mg/kg Xylazine i.p before every imaging session, and were supplemented additionally with 3 mg/kg Acepromazin i.p after the onset of anesthesia for mKikume imaging only in the final imaging session. The ventral side of the ear was prepared for intravital microscopy as described (Müller, Aeschlimann et al. 2013). In brief, the animals were placed on a heating stage adjusted to 37 °C, their ear was fixed to a metal platform using double-sided tape and was covered with Vidisic carbomer gel (Bausch+Lomb). A coverslip sealed to a surrounding parafilm blanket was placed onto the gel and fixed above the ear. 2-photon imaging was performed with a W Plan-Apochromat 20x/1,0 DIC VIS-IR objective using a Zeiss LSM 700 upright microscope with the ZEN software environment (Version 2.1, Zeiss), equipped with a Mai Tai DeepSee Ti:Sa laser (Spectra-Physics) tuned to 920 or 980 nm to image mKikume expressing *Lm*^{SWITCH}, with the emitted signal being split by 465 nm, 520 nm, 555 nm, and 620 nm long pass dichroic mirrors and filtered with 509/22 nm (green Kikume, 520 nm part), 543/20 nm (green mKikume, 540 nm part), 589/54 nm (red mKikume, mNectarine), 660/80 nm (far red autofluorescence) and SHG unfiltered below 465 nm.

4.1.8. Photoconversion

Mice anaesthetized with 100 mg/kg ketamine and 10 mg/kg xylazine i.p. were photoconverted on the ear (ventral side) with violet light at 405 nm wavelength using an assembly of 2 × 2 LED diodes (Strato, half-viewing angle: 15°; Radiant Power: 10 mW), illumination time was set to 2 minutes at a distance of 2 cm. Before and after photoconversion of the parasites, a three-dimensional image of the site of infection spanning at least 500 µm x 500 µm x 30 µm was acquired by using intravital 2-photon

microscopy. The readout image of the same site was localized 48 h later using triangulation as described previously (Müller, Aeschlimann et al. 2013).
To analyse the dynamics of host cell recruitment at the site of infection (Heyde, Philipsen et al. 2018), mKikume-expressing, *L. major* wild type-infected mice were photoconverted 2 days before analysis (i.e. day 19 p.i.) by flow cytometry. For flow cytometry of mKikume-expressing mouse cells, non-photoconverted mKikume was acquired using 488 nm excitation and 530/30 nm emission, photoconverted mKikume was detected using 561 nm excitation and 610/10 nm emission.

4.1.9. Image processing and quantification for proliferation measurement

Large field intravital images acquired before, 0 h after and 48 h after photoconversion were rough segmented according to a summed up channel of Kikume red and green using the Imaris Software (Versions 9.3.1. through 9.5.1., Bitplane, Perkin Elmer). The positions and fluorescence properties of the segmented cells (including autofluorescent objects) were exported and converted to cytometry files using the DiscIt software (Moreau, Lemaître et al. 2012)). Autofluorescent objects, such as hair follicles and keratinocytes, were filtered out by excluding objects with a low Kikume green 520/540 nm ratio, as described previously (Muller et al., 2013). Furthermore, objects exhibiting high fluorescence above 625 nm as compared to Kikume red emission (560-620nm) were also excluded from the analysis. The resulting filtered datasets were used for data normalization in order to ensure comparability between individual mice.

In order to normalize the Kikume red and green values from different mice, the following strategy aligning the fluorescence values before and 0h after photoconversion was established: The median green and red fluorescence of the green values below the 10th and over the 90th percentile of the preconversion controls, and analogously of the red values of the 0h after photoconversion controls were determined and the linear regression between the respective median coordinates was determined. All fluorescence values (including 48h after photoconversion measurements) were then drift transformed in a way the linear regression curves ran through the 0/0 coordinate. Cartesian coordinates were then turned into angular coordinates were normalized with the following formula so that the slope angle of the linear regression of the control before photoconversion becomes 0, and the slope angle of the 0 h after photoconversion control equals 90° : $\alpha' = \frac{\pi}{2} * \frac{\alpha-\theta}{\theta'-\theta}$ where α' is

the normalized angular coordinate, α is the initial angular coordinate, θ is the initial slope angle of the linear regression calculated for the before photoconversion dataset and $\theta'$is the initial slope angle of the linear regression calculated for the 0 h after photoconversion dataset . Finally, the datasets were normalized between 0 and the 90th percentile of the control values. Illustration in figure 35.

4.1.10. Metabolic assays

Single cell suspensions were prepared from infected ears at 3 weeks p.I. as described above. For MACS purification of inflammatory monocyte-derived cells, CD11c MicroBeads (Miltenyi Biotec) were employed according to the manufacturer's instructions, as it was previously shown that inflammatory monocyte-derived cells express this marker (Heyde, Philipsen et al. 2018); (Postat, Olekhnovitch et al. 2018). The isolated cells were counted and pooled from several infected ears to reach constant cell number within each experiment of 6 – 8 x10^4 cells per well, which were plated in XFe96 cell culture plates coated with Cell-Tak (Fisher Scientific). Seahorse XF DMEM medium was supplemented with 10 mM glucose, 2 mM glutamine and 1mM pyruvate with an adjusted pH of 7.4. Metabolic analysis was performed by analyzing each sample using an XFe96 Extracellular Flux Analyzer (Seahorse Bioscience). According to the manufacturer's instructions, baseline ectracellular acificication rate (ECAR) and oxygen consumption rate (OCR) was measured in untreated cells, and OCR was additionally determined in response to 1 µM Oligomycin, 1.5 µM Fluorocarbonyl cyanide phenylhydrazone (FCCP) and 0.5 µM Rotenone plus Antimycin A (MitoStress Test Kit, Agilent).

4.1.11 Quantitative PCR analysis

1000 cells/sample were taken from MACS-purified inflammatory monocyte-derived cells (CD11c MicroBeads, see 4.1.10) lysed in 10ml lysis buffer (RNeasy Plus lysis buffer, QIAGEN) containing 5% SUPERase-In RNase-Inhibitor 20U/ml (Invitrogen). RNA from lysed cells was purified using Agencourt® RNAClean XP beads (Beckman Coulter) according to manufacturer's instruction. Reverse transcription and cDNA clean-up was performed using the Smart-seq2 protocol as previously described (Picelli, Faridani et al. 2014). Primers for pro-IL1β (5´-TACCTGTGTCTTTCCCGTGG-3´ and 5´-AGCAGGTTATCATCATCATCCCA_3´) and HPRT1 as a housekeeping gene (5´-CAGGCCAGACTTTGTTGGAT-3´ and 5´-GGCTTTGTATTTGGCTTTTCC-3´) were used for quantitative PCR analysis in a SYBR Green PCR Master Mix (Applied

Biosystems). To run the quantitative PCR, 40 cycles of 95°C (15 s), and 60°C (60 s) followed by a dissociation protocol 95°C (15 s), 60°C (20 s), and 95°C (15 s) were performed on a ABI Prism® 7000 Sequence detection system (Applied Biosystems). For each samples, technical duplicates were performed. Samples which exhibited a too low cDNA concentration for the housekeeping gene (ct > 26) were excluded from the analysis

4.1.12. Statistical analysis

Statistical analysis was performed using the Prism software (Version 8.0, GraphPad). To compare multiple samples or pairwise analysis within datasets with more than two experimental groups, one-way analysis of variance (ANOVA) were done for datasets that had passed a Shapiro-Wilk normal distribution test, Kruskal-Wallis tests were performed for datasets with non-normal distribution. Appropriate multiple comparison post-tests (Dunnet's for multiple comparisons with the control group in ANOVA, Dunn's test for Kruskal-Wallis analyses) were employed as indicated in the respective figure legends. Bonferroni´s multiple comparisons test was used in two-way ANOVA to test an impact of time and drainage from the infection site in the analysis of T cells in lymph nodes. Tests used are indicated in the respective figure legends.

4.2. Materials

4.2.1. Kits

Assay	Source	Identifier
Monocyte Isolation Kit (BM)	Miltenyi Biotec	Cat#30-100-629
CD11c MicroBeads	Miltenyi Biotec	Cat#130-108-338 and 130-125-835
MitoStress Test Kit	Agilent	Cat#103707-100
CountBright Absolute Counting beads	Thermo Fisher	Cat#C36950
Foxp3/Transcription Factor Staining Buffer Set	invitrogen	Cat#00-5523-00
Agencourt® RNAClean XP beads	Beckman Coulter	Cat#A63987

4.2.2. Antibodies

Antibody	Source	Identifier
anti-CD18	BD Biosciences	Cat#555280
anti-CD49d	BioXcell	Cat#BE0071-1MG
Anti-CD16/32	BioLegend	Cat#101302
APC-anti-iNOS	eBioscience	Cat#17-5920-82
APC-anti-pro-IL1β	eBioscience	Cat#17-7114-80
MHCII (I-A/I-E)-Brilliant Violet 510	BioLegend	Cat#107635
CD45-APC/Cy7	BioLegend	Cat#103115
CD45-PerCP/Cy5.5	BioLegend	Cat#103131
CD45-Brilliant UV496	BD Biosciences	Cat#749889
CD45.1- Brilliant Violet 510	BioLegend	Cat#110741
CD45.2- APC/Cy7	BioLegend	Cat#109823
CD3e- PerCP/Cy5.5	BioLegend	Cat#100327
CD3e-Brilliant Violet 421	BioLegend	Cat#100341
CD11b-Brilliant UV395	BD Biosciences	Cat#563553
CD4-AF488	BioLegend	Cat#100532
Ly6C-PE/Cy7	BioLegend	Cat#128017
Ly6G-APC/Cy7	BioLegend	Cat#127623
Ly6G-APC	BioLegend	Cat#127613
TIM3- Brilliant Violet 605	BioLegend	Cat#119721
PD-1- Brilliant Violet 785	BioLegend	Cat#135225
CTLA4-PE	BioLegend	Cat#106305
TIGIT- Brilliant Violet 421	BioLegend	Cat#142111
FoxP3-AF488	BioLegend	Cat#320011

4.2.3. Biochemical and Chemical Regents

Reagent	Source	Identifier
M199 medium	Sigma-Aldrich	Cat#FG0615
FCS	Biowest	Cat#S1400
Adenine	Sigma-Aldrich	Cat#A8626, CAS Number 73-24-5

Biotin	Sigma-Aldrich	Cat#B4501, CAS Number 58-85-5
Hemin	Sigma-Aldrich	Cat#H9039, CAS Number 16009-13-5
Biopterin	Sigma-Aldrich	Cat#B2517, CAS Number 22150-76-1
Ketamine	Ratiopharm	ATC Code N01AX03
Rompun	Bayer	ATC Code N05CM92
Acepromazin	CEVA GmbH	ATC Code QN05AA04
L-NIL	Sigma-Aldrich	Cat#I8021, CAS Number 159190-45-1
DNFB	Sigma Aldrich	Cat#D1529, CAS Number 70-34-8
Olive oil	Sigma-Aldrich	Cat#O1514, CAS Number 8001-25-0
Penicillin/ Streptomycin	Gibco/ThermoFisher	Cat#15140122
Liberase TL	Roche/Sigma-Aldrich	Cat#5401020001
DNase I	ThermoFisher/Invitrogen	Cat#18047-019
Paraformaldehyde	Sigma-Aldrich	Cat#158127, CAS Number 30525-89-4
Perm/Wash buffer	BD Biosciences	Cat#554723
RPMI 1640	Pan Biotech	Cat#P04-18500
GolgiPlug	BD Biosciences	Cat#555029
LPS	Sigma-Aldrich	Cat#L8274, EC Number 297-473-0
IFN-γ	R&D Systems	Cat#485-MI
Seahorse XF DMEM medium	Agilent	Cat#103575-100
RNeasy Plus Micro Kit	Qiagen	Cat#74034
SUPERase-In RNase-Inhibitor	ThermoFisher/Invitrogen	Cat#AM2694
SYBR Green PCR Master Mix	ThermoFisher/Applied Biosystems	Cat#4309155
FVS 780	BD Biosciences	Cat#565388
FVS 450	BD Biosciences	Cat#562247

4.2.4. Software

Software	Source	Version
BD FACSDiva	BD Biosiences	8.0.2
NxT Software	Thermo Fisher	4.2
FlowJo	LLC, BD Biosiences	10.6.2
ZEN	Zeiss	2.1
Imaris	Bitplane, Perkin Elmer	9.3.1. through 9.5.1

5. References

Albina, J. E., J. A. Abate and W. L. Henry, Jr. (1991). "Nitric oxide production is required for murine resident peritoneal macrophages to suppress mitogen-stimulated T cell proliferation. Role of IFN-gamma in the induction of the nitric oxide-synthesizing pathway." J Immunol **147**(1): 144-148.

Balestieri, F. M., A. R. Queiroz, C. Scavone, V. M. Costa, M. Barral-Netto and A. Abrahamsohn Ide (2002). "Leishmania (L.) amazonensis-induced inhibition of nitric oxide synthesis in host macrophages." Microbes Infect **4**(1): 23-29.

Bamias, G., J. Rivera-Nieves and M. B. Grisham (2018). Chapter 65 - Recruitment of Inflammatory and Immune Cells in the Gut. Physiology of the Gastrointestinal Tract (Sixth Edition). H. M. Said, Academic Press**:** 1579-1614.

Belkaid, Y., K. F. Hoffmann, S. Mendez, S. Kamhawi, M. C. Udey, T. A. Wynn and D. L. Sacks (2001). "The role of interleukin (IL)-10 in the persistence of Leishmania major in the skin after healing and the therapeutic potential of anti-IL-10 receptor antibody for sterile cure." J Exp Med **194**(10): 1497-1506.

Belkaid, Y., S. Kamhawi, G. Modi, J. Valenzuela, N. Noben-Trauth, E. Rowton, J. Ribeiro and D. L. Sacks (1998). "Development of a natural model of cutaneous leishmaniasis: powerful effects of vector saliva and saliva preexposure on the long-term outcome of Leishmania major infection in the mouse ear dermis." J Exp Med **188**(10): 1941-1953.

Belkaid, Y., S. Mendez, R. Lira, N. Kadambi, G. Milon and D. Sacks (2000). "A natural model of Leishmania major infection reveals a prolonged "silent" phase of parasite amplification in the skin before the onset of lesion formation and immunity." J Immunol **165**(2): 969-977.

Belkaid, Y., C. A. Piccirillo, S. Mendez, E. M. Shevach and D. L. Sacks (2002). "CD4+CD25+ regulatory T cells control Leishmania major persistence and immunity." Nature **420**(6915): 502-507.

Bingisser, R. M., P. A. Tilbrook, P. G. Holt and U. R. Kees (1998). "Macrophage-derived nitric oxide regulates T cell activation via reversible disruption of the Jak3/STAT5 signaling pathway." J Immunol **160**(12): 5729-5734.

Bogdan, C. (1997). "Of microbes, macrophages and nitric oxide." Behring Inst Mitt(99): 58-72.

Bogdan, C. (2000). The Function of Nitric Oxide in the Immune System. Handbook of Experimental Pharmacology. **143**.

Bogdan, C. (2001). "Nitric oxide and the immune response." Nat Immunol **2**(10): 907-916.

Bogdan, C. (2001). "Nitric oxide and the regulation of gene expression." Trends Cell Biol **11**(2): 66-75.

Boianelli, A., V. K. Nguyen, T. Ebensen, K. Schulze, E. Wilk, N. Sharma, S. Stegemann-Koniszewski, D. Bruder, F. R. Toapanta, C. A. Guzmán, M. Meyer-Hermann and E. A.

Hernandez-Vargas (2015). "Modeling Influenza Virus Infection: A Roadmap for Influenza Research." Viruses **7**(10): 5274-5304.

Bonneville, M., C. Chavagnac, M. Vocanson, A. Rozieres, J. Benetiere, I. Pernet, A. Denis, J. F. Nicolas and A. Hennino (2007). "Skin contact irritation conditions the development and severity of allergic contact dermatitis." J Invest Dermatol **127**(6): 1430-1435.

Boyle, K. B., D. Gyori, A. Sindrilaru, K. Scharffetter-Kochanek, P. R. Taylor, A. Mócsai, L. R. Stephens and P. T. Hawkins (2011). "Class IA phosphoinositide 3-kinase β and δ regulate neutrophil oxidase activation in response to Aspergillus fumigatus hyphae." J Immunol **186**(5): 2978-2989.

Braverman, J. and S. A. Stanley (2017). "Nitric Oxide Modulates Macrophage Responses to Mycobacterium tuberculosis Infection through Activation of HIF-1α and Repression of NF-κB." J Immunol **199**(5): 1805-1816.

Carneiro, M. B., M. E. Lopes, L. S. Hohman, A. Romano, B. A. David, R. Kratofil, P. Kubes, M. L. Workentine, A. C. Campos, L. Q. Vieira and N. C. Peters (2020). "Th1-Th2 Cross-Regulation Controls Early Leishmania Infection in the Skin by Modulating the Size of the Permissive Monocytic Host Cell Reservoir." Cell Host Microbe **27**(5): 752-768.e757.

Cavanaugh, J. E. and A. A. Neath (2019). "The Akaike information criterion: Background, derivation, properties, application, interpretation, and refinements." WIREs Computational Statistics **11**(3): e1460.

Charmoy, M., S. Brunner-Agten, D. Aebischer, F. Auderset, P. Launois, G. Milon, A. E. Proudfoot and F. Tacchini-Cottier (2010). "Neutrophil-derived CCL3 is essential for the rapid recruitment of dendritic cells to the site of Leishmania major inoculation in resistant mice." PLoS Pathog **6**(2): e1000755.

Da Silva, R. P., B. F. Hall, K. A. Joiner and D. L. Sacks (1989). "CR1, the C3b receptor, mediates binding of infective Leishmania major metacyclic promastigotes to human macrophages." J Immunol **143**(2): 617-622.

Das, P., A. Lahiri, A. Lahiri and D. Chakravortty (2010). "Modulation of the arginase pathway in the context of microbial pathogenesis: a metabolic enzyme moonlighting as an immune modulator." PLoS Pathog **6**(6): e1000899.

de Freitas, E. S. R., R. I. Gálvez, V. R. A. Pereira, M. E. F. de Brito, S. L. Choy, H. Lotter, L. Bosurgi and T. Jacobs (2020). "Programmed Cell Death Ligand (PD-L)-1 Contributes to the Regulation of CD4(+) T Effector and Regulatory T Cells in Cutaneous Leishmaniasis." Front Immunol **11**: 574491.

De Trez, C., S. Magez, S. Akira, B. Ryffel, Y. Carlier and E. Muraille (2009). "iNOS-producing inflammatory dendritic cells constitute the major infected cell type during the chronic Leishmania major infection phase of C57BL/6 resistant mice." PLoS Pathog **5**(6): e1000494.

Diefenbach, A., H. Schindler, N. Donhauser, E. Lorenz, T. Laskay, J. MacMicking, M. Röllinghoff, I. Gresser and C. Bogdan (1998). "Type 1 interferon (IFNalpha/beta) and type 2 nitric oxide synthase regulate the innate immune response to a protozoan parasite." Immunity **8**(1): 77-87.

Dillman, J. F., V. L. Dawson and T. M. Dawson (2001). "Overview of the pathway and functions of nitric oxide." Curr Protoc Toxicol **Chapter 10**: Unit 10.11.

Dinarello, C. A. (2011). "Interleukin-1 in the pathogenesis and treatment of inflammatory diseases." Blood **117**(14): 3720-3732.

Dougall, W. C., S. Kurtulus, M. J. Smyth and A. C. Anderson (2017). "TIGIT and CD96: new checkpoint receptor targets for cancer immunotherapy." Immunol Rev **276**(1): 112-120.

Esterre, P., J. P. Dedet, S. Guerret, M. Chevallier, C. Frenay and J. A. Grimaud (1991). "Matrix remodelling and fibroblast phenotype in early lesions of human cutaneous leishmaniasis." Pathol Res Pract **187**(8): 924-930.

Everts, B., E. Amiel, G. J. van der Windt, T. C. Freitas, R. Chott, K. E. Yarasheski, E. L. Pearce and E. J. Pearce (2012). "Commitment to glycolysis sustains survival of NO-producing inflammatory dendritic cells." Blood **120**(7): 1422-1431.

Fang, F. C. (1997). "Perspectives series: host/pathogen interactions. Mechanisms of nitric oxide-related antimicrobial activity." J Clin Invest **99**(12): 2818-2825.

Formaglio, P., M. Alabdullah, A. Siokis, J. Handschuh, I. Sauerland, Y. Fu, A. Krone, P. Gintschel, J. Stettin, S. Heyde, J. Mohr, L. Philipsen, A. Schröder, P. A. Robert, G. Zhao, S. Khailaie, A. Dudeck, J. Bertrand, G. F. Späth, S. Kahlfuß, P. Bousso, B. Schraven, J. Huehn, S. Binder, M. Meyer-Hermann and A. J. Müller (2021). "Nitric oxide controls proliferation of Leishmania major by inhibiting the recruitment of permissive host cells." Immunity **54**(12): 2724-2739.e2710.

Förstermann, U., E. I. Closs, J. S. Pollock, M. Nakane, P. Schwarz, I. Gath and H. Kleinert (1994). "Nitric oxide synthase isozymes. Characterization, purification, molecular cloning, and functions." Hypertension **23**(6 Pt 2): 1121-1131.

Förstermann, U. and W. C. Sessa (2012). "Nitric oxide synthases: regulation and function." Eur Heart J **33**(7): 829-837, 837a-837d.

Francisco, L. M., V. H. Salinas, K. E. Brown, V. K. Vanguri, G. J. Freeman, V. K. Kuchroo and A. H. Sharpe (2009). "PD-L1 regulates the development, maintenance, and function of induced regulatory T cells." J Exp Med **206**(13): 3015-3029.

Freeman, G. J., A. J. Long, Y. Iwai, K. Bourque, T. Chernova, H. Nishimura, L. J. Fitz, N. Malenkovich, T. Okazaki, M. C. Byrne, H. F. Horton, L. Fouser, L. Carter, V. Ling, M. R. Bowman, B. M. Carreno, M. Collins, C. R. Wood and T. Honjo (2000). "Engagement of the PD-1 immunoinhibitory receptor by a novel B7 family member leads to negative regulation of lymphocyte activation." J Exp Med **192**(7): 1027-1034.

Gao, X., Y. Zhu, G. Li, H. Huang, G. Zhang, F. Wang, J. Sun, Q. Yang, X. Zhang and B. Lu (2012). "TIM-3 expression characterizes regulatory T cells in tumor tissues and is associated with lung cancer progression." PLoS One **7**(2): e30676.

Goncalves, R., X. Zhang, H. Cohen, A. Debrabant and D. M. Mosser (2011). "Platelet activation attracts a subpopulation of effector monocytes to sites of Leishmania major infection." J Exp Med **208**(6): 1253-1265.

Green, S. J., R. M. Crawford, J. T. Hockmeyer, M. S. Meltzer and C. A. Nacy (1990). "Leishmania major amastigotes initiate the L-arginine-dependent killing mechanism in IFN-gamma-stimulated macrophages by induction of tumor necrosis factor-alpha." J Immunol **145**(12): 4290-4297.

Guimarães-Costa, A. B., M. T. Nascimento, G. S. Froment, R. P. Soares, F. N. Morgado, F. Conceição-Silva and E. M. Saraiva (2009). "Leishmania amazonensis promastigotes induce and are killed by neutrophil extracellular traps." Proc Natl Acad Sci U S A **106**(16): 6748-6753.

Guimaraes-Costa, A. B., J. P. Shannon, I. Waclawiak, J. Oliveira, C. Meneses, W. de Castro, X. Wen, J. Brzostowski, T. D. Serafim, J. F. Andersen, H. D. Hickman, S. Kamhawi, J. G. Valenzuela and F. Oliveira (2021). "A sand fly salivary protein acts as a neutrophil chemoattractant." Nat Commun **12**(1): 3213.

Habuchi, S., H. Tsutsui, A. B. Kochaniak, A. Miyawaki and A. M. van Oijen (2008). "mKikGR, a monomeric photoswitchable fluorescent protein." PLoS One **3**(12): e3944.

Haby, C., F. Lisovoski, D. Aunis and J. Zwiller (1994). "Stimulation of the cyclic GMP pathway by NO induces expression of the immediate early genes c-fos and junB in PC12 cells." J Neurochem **62**(2): 496-501.

Hall, L. R. and R. G. Titus (1995). "Sand fly vector saliva selectively modulates macrophage functions that inhibit killing of Leishmania major and nitric oxide production." J Immunol **155**(7): 3501-3506.

Harari, O. and J. K. Liao (2004). "Inhibition of MHC II gene transcription by nitric oxide and antioxidants." Curr Pharm Des **10**(8): 893-898.

Harding, F. A., J. G. McArthur, J. A. Gross, D. H. Raulet and J. P. Allison (1992). "CD28-mediated signalling co-stimulates murine T cells and prevents induction of anergy in T-cell clones." Nature **356**(6370): 607-609.

Herter, J. and A. Zarbock (2013). "Integrin Regulation during Leukocyte Recruitment." J Immunol **190**(9): 4451-4457.

Heyde, S., L. Philipsen, P. Formaglio, Y. Fu, I. Baars, G. Hobbel, C. L. Kleinholz, E. A. Seiss, J. Stettin, P. Gintschel, A. Dudeck, P. Bousso, B. Schraven and A. J. Muller (2018). "CD11c-expressing Ly6C+CCR2+ monocytes constitute a reservoir for efficient Leishmania proliferation and cell-to-cell transmission." PLoS Pathog **14**(10): e1007374.

Hierholzer, C., B. Harbrecht, J. M. Menezes, J. Kane, J. MacMicking, C. F. Nathan, A. B. Peitzman, T. R. Billiar and D. J. Tweardy (1998). "Essential role of induced nitric oxide in the initiation of the inflammatory response after hemorrhagic shock." J Exp Med **187**(6): 917-928.

Hoffman, R. A., J. M. Langrehr, T. R. Billiar, R. D. Curran and R. L. Simmons (1990). "Alloantigen-induced activation of rat splenocytes is regulated by the oxidative metabolism of L-arginine." J Immunol **145**(7): 2220-2226.

Hohman, L. S. and N. C. Peters (2019). "CD4(+) T Cell-Mediated Immunity against the Phagosomal Pathogen Leishmania: Implications for Vaccination." Trends Parasitol **35**(6): 423-435.

Hung, K., R. Hayashi, A. Lafond-Walker, C. Lowenstein, D. Pardoll and H. Levitsky (1998). "The central role of CD4(+) T cells in the antitumor immune response." J Exp Med **188**(12): 2357-2368.

Hurdayal, R., N. E. Nieuwenhuizen, R. Khutlang and F. Brombacher (2019). "Inflammatory Dendritic Cells, Regulated by IL-4 Receptor Alpha Signaling, Control Replication, and Dissemination of Leishmania major in Mice." Front Cell Infect Microbiol **9**: 479.

Hurrell, B. P., M. Beaumann, S. Heyde, I. B. Regli, A. J. Müller and F. Tacchini-Cottier (2017). "Frontline Science: Leishmania mexicana amastigotes can replicate within neutrophils." J Leukoc Biol **102**(5): 1187-1198.

Hurrell, B. P., S. Schuster, E. Grün, M. Coutaz, R. A. Williams, W. Held, B. Malissen, M. Malissen, S. Yousefi, H. U. Simon, A. J. Müller and F. Tacchini-Cottier (2015). "Rapid Sequestration of Leishmania mexicana by Neutrophils Contributes to the Development of Chronic Lesion." PLoS Pathog **11**(5): e1004929.

Joshi, T., S. Rodriguez, V. Perovic, I. A. Cockburn and S. Stäger (2009). "B7-H1 blockade increases survival of dysfunctional CD8(+) T cells and confers protection against Leishmania donovani infections." PLoS Pathog **5**(5): e1000431.

Kamphorst, A. O., A. Wieland, T. Nasti, S. Yang, R. Zhang, D. L. Barber, B. T. Konieczny, C. Z. Daugherty, L. Koenig, K. Yu, G. L. Sica, A. H. Sharpe, G. J. Freeman, B. R. Blazar, L. A. Turka, T. K. Owonikoko, R. N. Pillai, S. S. Ramalingam, K. Araki and R. Ahmed (2017). "Rescue of exhausted CD8 T cells by PD-1-targeted therapies is CD28-dependent." Science **355**(6332): 1423-1427.

Karkamo, V., A. Kaistinen, A. Näreaho, K. Dillard, K. Vainio-Siukola, G. Vidgrén, N. Tuoresmäki and M. Anttila (2014). "The first report of autochthonous non-vector-borne transmission of canine leishmaniosis in the Nordic countries." Acta Vet Scand **56**(1): 84.

Kaye, P. and P. Scott (2011). "Leishmaniasis: complexity at the host-pathogen interface." Nat Rev Microbiol **9**(8): 604-615.

Kelly, B. and L. A. O'Neill (2015). "Metabolic reprogramming in macrophages and dendritic cells in innate immunity." Cell Res **25**(7): 771-784.

Kerr, A., R. S. Dawe, D. Nathwani, A. T. Evans and J. Ferguson (2009). "Presentation of leishmaniasis (Leishmania infantum) in the skin of a patient with severe atopic dermatitis." Br J Dermatol **161**(1): 202-203.

Kim, Y. M., R. V. Talanian, J. Li and T. R. Billiar (1998). "Nitric oxide prevents IL-1beta and IFN-gamma-inducing factor (IL-18) release from macrophages by inhibiting caspase-1 (IL-1beta-converting enzyme)." J Immunol **161**(8): 4122-4128.

Klimov, V. V. (2019). From Basic to Clinical Immunology, springer.

Kloehn, J., E. C. Saunders, S. O'Callaghan, M. J. Dagley and M. J. McConville (2015). "Characterization of metabolically quiescent Leishmania parasites in murine lesions using heavy water labeling." PLoS Pathog **11**(2): e1004683.

Kobayashi, Y. (2010). "The regulatory role of nitric oxide in proinflammatory cytokine expression during the induction and resolution of inflammation." J Leukoc Biol **88**(6): 1157-1162.

Krummel, M. F. and J. P. Allison (1995). "CD28 and CTLA-4 have opposing effects on the response of T cells to stimulation." J Exp Med **182**(2): 459-465.

Kubes, P., E. Sihota and M. J. Hickey (1997). "Endogenous but not exogenous nitric oxide decreases TNF-alpha-induced leukocyte rolling." Am J Physiol **273**(3 Pt 1): G628-635.

Kubes, P., M. Suzuki and D. N. Granger (1991). "Nitric oxide: an endogenous modulator of leukocyte adhesion." Proc Natl Acad Sci U S A **88**(11): 4651-4655.

Kumar, A. (2013). Leishmania and Leishmaniasis, springer.

Lee, S. H., M. Charmoy, A. Romano, A. Paun, M. M. Chaves, F. O. Cope, D. A. Ralph and D. L. Sacks (2018). "Mannose receptor high, M2 dermal macrophages mediate nonhealing Leishmania major infection in a Th1 immune environment." J Exp Med **215**(1): 357-375.

León, B., M. López-Bravo and C. Ardavín (2007). "Monocyte-derived dendritic cells formed at the infection site control the induction of protective T helper 1 responses against Leishmania." Immunity **26**(4): 519-531.

Ley, K., C. Laudanna, M. I. Cybulsky and S. Nourshargh (2007). "Getting to the site of inflammation: the leukocyte adhesion cascade updated." Nat Rev Immunol **7**(9): 678-689.

Liew, F. Y., Y. Li, D. Moss, C. Parkinson, M. V. Rogers and S. Moncada (1991). "Resistance to Leishmania major infection correlates with the induction of nitric oxide synthase in murine macrophages." Eur J Immunol **21**(12): 3009-3014.

Littringer, K., C. Moresi, N. Rakebrandt, X. Zhou, M. Schorer, T. Dolowschiak, F. Kirchner, F. Rost, C. W. Keller, D. McHugh, S. LeibundGut-Landmann, M. D. Robinson and N. Joller (2018). "Common Features of Regulatory T Cell Specialization During Th1 Responses." Front Immunol **9**: 1344.

Liu, D. and J. E. Uzonna (2012). "The early interaction of Leishmania with macrophages and dendritic cells and its influence on the host immune response." Front Cell Infect Microbiol **2**: 83.

Lopez Kostka, S., S. Dinges, K. Griewank, Y. Iwakura, M. C. Udey and E. von Stebut (2009). "IL-17 promotes progression of cutaneous leishmaniasis in susceptible mice." J Immunol **182**(5): 3039-3046.

Luckheeram, R. V., R. Zhou, A. D. Verma and B. Xia (2012). "$CD4^+$T cells: differentiation and functions." Clin Dev Immunol **2012**: 925135.

MacMicking, J. D. (2012). "Interferon-inducible effector mechanisms in cell-autonomous immunity." Nat Rev Immunol **12**(5): 367-382.

Mandell, M. A. and S. M. Beverley (2017). "Continual renewal and replication of persistent Leishmania major parasites in concomitantly immune hosts." Proc Natl Acad Sci U S A **114**(5): E801-e810.

Matthews, J. R., C. H. Botting, M. Panico, H. R. Morris and R. T. Hay (1996). "Inhibition of NF-kappaB DNA binding by nitric oxide." Nucleic Acids Res **24**(12): 2236-2242.

Melikian, N., M. D. Seddon, B. Casadei, P. J. Chowienczyk and A. M. Shah (2009). "Neuronal nitric oxide synthase and human vascular regulation." Trends Cardiovasc Med **19**(8): 256-262.

Mishra, B. B., R. R. Lovewell, A. J. Olive, G. Zhang, W. Wang, E. Eugenin, C. M. Smith, J. Y. Phuah, J. E. Long, M. L. Dubuke, S. G. Palace, J. D. Goguen, R. E. Baker, S. Nambi, R. Mishra, M. G. Booty, C. E. Baer, S. A. Shaffer, V. Dartois, B. A. McCormick, X. Chen and C. M. Sassetti (2017). "Nitric oxide prevents a pathogen-permissive granulocytic inflammation during tuberculosis." Nat Microbiol **2**: 17072.

Mishra, B. B., V. A. Rathinam, G. W. Martens, A. J. Martinot, H. Kornfeld, K. A. Fitzgerald and C. M. Sassetti (2013). "Nitric oxide controls the immunopathology of tuberculosis by inhibiting NLRP3 inflammasome-dependent processing of IL-1β." Nat Immunol **14**(1): 52-60.

Monack, D. M., A. Mueller and S. Falkow (2004). "Persistent bacterial infections: the interface of the pathogen and the host immune system." Nat Rev Microbiol **2**(9): 747-765.

Moreau, H. D., F. Lemaître, E. Terriac, G. Azar, M. Piel, A. M. Lennon-Dumenil and P. Bousso (2012). "Dynamic in situ cytometry uncovers T cell receptor signaling during immunological synapses and kinapses in vivo." Immunity **37**(2): 351-363.

Mou, Z., H. M. Muleme, D. Liu, P. Jia, I. B. Okwor, S. M. Kuriakose, S. M. Beverley and J. E. Uzonna (2013). "Parasite-derived arginase influences secondary anti-Leishmania immunity by regulating programmed cell death-1-mediated CD4+ T cell exhaustion." J Immunol **190**(7): 3380-3389.

Mougneau, E., F. Bihl and N. Glaichenhaus (2011). "Cell biology and immunology of Leishmania." Immunol Rev **240**(1): 286-296.

Mourao-Sa, D., S. Roy and J. M. Blander (2013). "Vita-PAMPs: signatures of microbial viability." Adv Exp Med Biol **785**: 1-8.

Müller, A. J., S. Aeschlimann, R. Olekhnovitch, M. Dacher, G. F. Späth and P. Bousso (2013). "Photoconvertible pathogen labeling reveals nitric oxide control of Leishmania major infection in vivo via dampening of parasite metabolism." Cell Host Microbe **14**(4): 460-467.

Müller, A. J., O. Filipe-Santos, G. Eberl, T. Aebischer, G. F. Späth and P. Bousso (2012). "CD4+ T cells rely on a cytokine gradient to control intracellular pathogens beyond sites of antigen presentation." Immunity **37**(1): 147-157.

Murphy, M. L., S. E. Cotterell, P. M. Gorak, C. R. Engwerda and P. M. Kaye (1998). "Blockade of CTLA-4 enhances host resistance to the intracellular pathogen, Leishmania donovani." J Immunol **161**(8): 4153-4160.

Nash, A. A., R. G. Dalziel and J. R. Fitzgerald (2015). Chapter 8 - Mechanisms of Cell and Tissue Damage. Mims' Pathogenesis of Infectious Disease (Sixth Edition). A. A.

Nash, R. G. Dalziel and J. R. Fitzgerald. Boston, Academic Press**:** 171-231.
Nathan, C. (2012). "Fresh approaches to anti-infective therapies." Sci Transl Med **4**(140): 140sr142.

Noël, W., G. Raes, G. Hassanzadeh Ghassabeh, P. De Baetselier and A. Beschin (2004). "Alternatively activated macrophages during parasite infections." Trends Parasitol **20**(3): 126-133.

Novais, F. O., B. T. Nguyen, D. P. Beiting, L. P. Carvalho, N. D. Glennie, S. Passos, E. M. Carvalho and P. Scott (2014). "Human classical monocytes control the intracellular stage of Leishmania braziliensis by reactive oxygen species." J Infect Dis **209**(8): 1288-1296.

Nylén, S. and D. Sacks (2007). "Interleukin-10 and the pathogenesis of human visceral leishmaniasis." Trends Immunol **28**(9): 378-384.

Olekhnovitch, R. and P. Bousso (2015). "Induction, Propagation, and Activity of Host Nitric Oxide: Lessons from Leishmania Infection." Trends Parasitol **31**(12): 653-664.

Olekhnovitch, R., B. Ryffel, A. J. Müller and P. Bousso (2014). "Collective nitric oxide production provides tissue-wide immunity during Leishmania infection." J Clin Invest **124**(4): 1711-1722.

Orman, M. A. and M. P. Brynildsen (2015). "Inhibition of stationary phase respiration impairs persister formation in E. coli." Nat Commun **6**: 7983.

Pace, D. (2014). "Leishmaniasis." J Infect **69 Suppl 1**: S10-18.

Pardoll, D. M. (2012). "The blockade of immune checkpoints in cancer immunotherapy." Nat Rev Cancer **12**(4): 252-264.

Pautz, A., J. Art, S. Hahn, S. Nowag, C. Voss and H. Kleinert (2010). "Regulation of the expression of inducible nitric oxide synthase." Nitric Oxide **23**(2): 75-93.

Pearce, E. J. and B. Everts (2015). "Dendritic cell metabolism." Nat Rev Immunol **15**(1): 18-29.

Peng, K., P. Broz, J. Jones, L. M. Joubert and D. Monack (2011). "Elevated AIM2-mediated pyroptosis triggered by hypercytotoxic Francisella mutant strains is attributed to increased intracellular bacteriolysis." Cell Microbiol **13**(10): 1586-1600.

Peters, N. C., J. G. Egen, N. Secundino, A. Debrabant, N. Kimblin, S. Kamhawi, P. Lawyer, M. P. Fay, R. N. Germain and D. Sacks (2008). "In vivo imaging reveals an essential role for neutrophils in leishmaniasis transmitted by sand flies." Science **321**(5891): 970-974.

Picelli, S., O. R. Faridani, A. K. Björklund, G. Winberg, S. Sagasser and R. Sandberg (2014). "Full-length RNA-seq from single cells using Smart-seq2." Nat Protoc **9**(1): 171-181.

Postat, J., R. Olekhnovitch, F. Lemaître and P. Bousso (2018). "A Metabolism-Based Quorum Sensing Mechanism Contributes to Termination of Inflammatory Responses." Immunity **49**(4): 654-665.e655.

Rab, M. A., M. Hassan, D. Bux, M. T. Mahmood and D. A. Evans (1992). "The isolation and cultivation of Leishmania infantum from apparently normal skin of visceral leishmaniasis patients in northern Pakistan." Trans R Soc Trop Med Hyg **86**(6): 620-621.

Robert, P. A., H. Jönsson and M. Meyer-Hermann (2018). "MoonFit, a minimal interface for fitting ODE dynamical models, bridging simulation by experimentalists and customization by C++ programmers." bioRxiv: 281188.

Romano, A., M. B. H. Carneiro, N. A. Doria, E. H. Roma, F. L. Ribeiro-Gomes, E. Inbar, S. H. Lee, J. Mendez, A. Paun, D. L. Sacks and N. C. Peters (2017). "Divergent roles for Ly6C+CCR2+CX3CR1+ inflammatory monocytes during primary or secondary infection of the skin with the intra-phagosomal pathogen Leishmania major." PLoS Pathog **13**(6): e1006479.

Ronet, C., Y. Hauyon-La Torre, M. Revaz-Breton, B. Mastelic, F. Tacchini-Cottier, J. Louis and P. Launois (2010). "Regulatory B cells shape the development of Th2 immune responses in BALB/c mice infected with Leishmania major through IL-10 production." J Immunol **184**(2): 886-894.

Sacks, D. and N. Noben-Trauth (2002). "The immunology of susceptibility and resistance to Leishmania major in mice." Nat Rev Immunol **2**(11): 845-858.

Sarathy, J., V. Dartois, T. Dick and M. Gengenbacher (2013). "Reduced drug uptake in phenotypically resistant nutrient-starved nonreplicating Mycobacterium tuberculosis." Antimicrob Agents Chemother **57**(4): 1648-1653.

Sasidharan Nair, V. and E. Elkord (2018). "Immune checkpoint inhibitors in cancer therapy: a focus on T-regulatory cells." Immunol Cell Biol **96**(1): 21-33.

Schenkel, A. R., Z. Mamdouh and W. A. Muller (2004). "Locomotion of monocytes on endothelium is a critical step during extravasation." Nat Immunol **5**(4): 393-400.

Scott, P., P. Natovitz and A. Sher (1986). "B lymphocytes are required for the generation of T cells that mediate healing of cutaneous leishmaniasis." J Immunol **137**(3): 1017-1021.

Segovia-Juarez, J. L., S. Ganguli and D. Kirschner (2004). "Identifying control mechanisms of granuloma formation during M. tuberculosis infection using an agent-based model." J Theor Biol **231**(3): 357-376.

Shaik, J. S., D. E. Dobson, D. L. Sacks and S. M. Beverley (2021). "Leishmania Sexual Reproductive Strategies as Resolved through Computational Methods Designed for Aneuploid Genomes." Genes (Basel) **12**(2).

Shimada, T., B. G. Park, A. J. Wolf, C. Brikos, H. S. Goodridge, C. A. Becker, C. N. Reyes, E. A. Miao, A. Aderem, F. Götz, G. Y. Liu and D. M. Underhill (2010). "Staphylococcus aureus evades lysozyme-based peptidoglycan digestion that links phagocytosis, inflammasome activation, and IL-1beta secretion." Cell Host Microbe **7**(1): 38-49.

Stecher, B., R. Robbiani, A. W. Walker, A. M. Westendorf, M. Barthel, M. Kremer, S. Chaffron, A. J. Macpherson, J. Buer, J. Parkhill, G. Dougan, C. von Mering and W. D. Hardt (2007). "Salmonella enterica serovar typhimurium exploits inflammation to compete with the intestinal microbiota." PLoS Biol **5**(10): 2177-2189.

Stenger, S., N. Donhauser, H. Thüring, M. Röllinghoff and C. Bogdan (1996). "Reactivation of latent leishmaniasis by inhibition of inducible nitric oxide synthase." J Exp Med **183**(4): 1501-1514.

Stenger, S., H. Thuring, M. Rollinghoff, P. Manning and C. Bogdan (1995). "L-N6-(1-iminoethyl)-lysine potently inhibits inducible nitric oxide synthase and is superior to NG-monomethyl-arginine in vitro and in vivo." Eur J Pharmacol **294**(2-3): 703-712.

Stuehr, D. J., J. Tejero and M. M. Haque (2009). "Structural and mechanistic aspects of flavoproteins: electron transfer through the nitric oxide synthase flavoprotein domain." Febs j **276**(15): 3959-3974.

Suresh, R. and D. M. Mosser (2013). "Pattern recognition receptors in innate immunity, host defense, and immunopathology." Adv Physiol Educ **37**(4): 284-291.

Syed Khaja, A. S., S. M. Toor, H. El Salhat, I. Faour, N. Ul Haq, B. R. Ali and E. Elkord (2017). "Preferential accumulation of regulatory T cells with highly immunosuppressive characteristics in breast tumor microenvironment." Oncotarget **8**(20): 33159-33171.

Terrazas, C., S. Varikuti, S. Oghumu, H. M. Steinkamp, N. Ardic, J. Kimble, H. Nakhasi and A. R. Satoskar (2017). "Ly6C(hi) inflammatory monocytes promote susceptibility to Leishmania donovani infection." Sci Rep **7**(1): 14693.

Thomas, D. D., X. Liu, S. P. Kantrow and J. R. Lancaster, Jr. (2001). "The biological lifetime of nitric oxide: implications for the perivascular dynamics of NO and O2." Proc Natl Acad Sci U S A **98**(1): 355-360.

Van den Bossche, J., J. Baardman, N. A. Otto, S. van der Velden, A. E. Neele, S. M. van den Berg, R. Luque-Martin, H. J. Chen, M. C. Boshuizen, M. Ahmed, M. A. Hoeksema, A. F. de Vos and M. P. de Winther (2016). "Mitochondrial Dysfunction Prevents Repolarization of Inflammatory Macrophages." Cell Rep **17**(3): 684-696.

Wei, X. Q., I. G. Charles, A. Smith, J. Ure, G. J. Feng, F. P. Huang, D. Xu, W. Muller, S. Moncada and F. Y. Liew (1995). "Altered immune responses in mice lacking inducible nitric oxide synthase." Nature **375**(6530): 408-411.

Woelbing, F., S. L. Kostka, K. Moelle, Y. Belkaid, C. Sunderkoetter, S. Verbeek, A. Waisman, A. P. Nigg, J. Knop, M. C. Udey and E. von Stebut (2006). "Uptake of Leishmania major by dendritic cells is mediated by Fcgamma receptors and facilitates acquisition of protective immunity." J Exp Med **203**(1): 177-188.

Wykes, M. N. and S. R. Lewin (2018). "Immune checkpoint blockade in infectious diseases." Nat Rev Immunol **18**(2): 91-104.

Xie, K., Z. Dong and I. J. Fidler (1996). "Activation of nitric oxide synthase gene for inhibition of cancer metastasis." J Leukoc Biol **59**(6): 797-803.

Zhang, B., S. Chikuma, S. Hori, S. Fagarasan and T. Honjo (2016). "Nonoverlapping roles of PD-1 and FoxP3 in maintaining immune tolerance in a novel autoimmune pancreatitis mouse model." Proc Natl Acad Sci U S A **113**(30): 8490-8495.

Zhao, G., D. Wirth, I. Schmitz and M. Meyer-Hermann (2017). "A mathematical model of the impact of insulin secretion dynamics on selective hepatic insulin resistance." Nat Commun **8**(1): 1362.

Zhu, C., A. C. Anderson, A. Schubart, H. Xiong, J. Imitola, S. J. Khoury, X. X. Zheng, T. B. Strom and V. K. Kuchroo (2005). "The Tim-3 ligand galectin-9 negatively regulates T helper type 1 immunity." Nat Immunol **6**(12): 1245-1252.

Declaration of Honour

“I hereby declare that I prepared this thesis without the impermissible help of third parties and that none other than the aids indicated have been used; all sources of information are clearly marked, including my own publications.
In particular I have not consciously:
• fabricated data or rejected undesirable results,
• misused statistical methods with the aim of drawing other conclusions than those warranted by the available data,
• plagiarized external data or publications,
• presented the results of other researchers in a distorted way.

I am aware that violations of copyright may lead to injunction and damage claims by the author and also to prosecution by law enforcement authorities.
I hereby agree that the thesis may be electronically reviewed with the aim of identifying plagiarism.
This work has not been submitted as a doctoral thesis in the same or a similar form in Germany, nor in any other country. It has not yet been published as a whole.”